INFORMATION TO USERS

This manuscript has been reproduced from the microfilm master. UMI films the text directly from the original or copy submitted. Thus, some thesis and dissertation copies are in typewriter face, while others may be from any type of computer printer.

The quality of this reproduction is dependent upon the quality of the copy submitted. Broken or indistinct print, colored or poor quality illustrations and photographs, print bleedthrough, substandard margins, and improper alignment can adversely affect reproduction.

In the unlikely event that the author did not send UMI a complete manuscript and there are missing pages, these will be noted. Also, if unauthorized copyright material had to be removed, a note will indicate the deletion.

Oversize materials (e.g., maps, drawings, charts) are reproduced by sectioning the original, beginning at the upper left-hand corner and continuing from left to right in equal sections with small overlaps. Each original is also photographed in one exposure and is included in reduced form at the back of the book.

Photographs included in the original manuscript have been reproduced xerographically in this copy. Higher quality 6" x 9" black and white photographic prints are available for any photographs or illustrations appearing in this copy for an additional charge. Contact UMI directly to order.

UMI

A Bell & Howell Information Company
300 North Zeeb Road, Ann Arbor MI 48106-1346 USA
313/761-4700 800/521-0600

University of Oklahoma

Graduate College

Novel Catalytic Materials For Carbon Dioxide Reforming Of Methane Under Severely Deactivating Conditions

A Dissertation

SUBMITTED TO THE GRADUATE FACULTY

in partial fulfillment of the requirements for the

degree of

Doctor of Philosophy

By

Susan Michelle Stagg-Williams

Norman, Oklahoma

1999

NOVEL CATALYTIC MATERIALS FOR CARBON DIOXIDE REFORMING OF METHANE UNDER SEVERELY DEACTIVATING CONDITIONS

A Dissertation APPROVED FOR THE
DEPARTMENT OF CHEMICAL ENGINEERING AND MATERIALS SCIENCE

BY

Daniel Resasco

R. Sundaram

K. M. Nicholas

Lance Lobban

J. A. Harwell

To

My parents

With love, admiration, and gratitude.

Many of life's experiences cultivate unforgettable lessons and rewards.

ACKNOWLEDGMENTS

I gratefully acknowledge the Donors of the Petroleum Research Fund administered by the American Chemical Society and the National Science Foundation-CONICET International Program (INT-9415590) for their generous support. I would also like to thank the National Science Foundation for a Traineeship, which provided for travel to many conferences and countries for the advancement of this research. I appreciate the collaborative effort and support of Walter Alavarez, Adriana Pisanu, Carlos Querini, Armando Bornga, Christina Padro, Eva Romeo, and Enrique Romero. Their expertise and contribution to this project has been invaluable.

I would like to thank all of the Chemical Engineering Faculty and Staff at the University of Oklahoma for the knowledge and friendship they have shared with me. I would especially like to thank Dr. Jeffery Harwell, Dr. Lance Lobban, Dr. Richard Mallinson, and Dr. Ken Nicholas for their participation on my dissertation committee. It is with tremendous appreciation and gratitude that I acknowledge Dr. Daniel Resasco for the countless hours of support, advice, guidance, friendship, and laughter we have shared. He is the reason that I attended the University of Oklahoma and has been an integral part of the enjoyment and success that I have experienced here. I will be forever grateful.

I would like to thank my friends at the University of Oklahoma for the wonderful moments we have spent together including time at Pepe's and

"Red Lobsta". You have helped to make me a better person, and I thank God everyday for blessing me with such incredible friends. I would also like to thank my family for all of the love, encouragement, and support they have given me throughout my academic endeavors and my life. You have given me the courage to try, the will to persist, and the strength to succeed. For these, I thank you. Finally, I would like to thank my husband, Michael. You are and always will be the best thing to ever happen to me. Thank you for your never-ending patience, encouragement, and love.

TABLE OF CONTENTS

LIST OF TABLES

LIST OF FIGURES

APPENDIX A

ABSTRACT

In recent years, the utilization of carbon dioxide for the reforming of methane (dry reforming) has attracted significant interest due to the industrial advantages over conventional steam reforming. The major obstacle preventing commercialization of this process is the lack of a catalyst capable of operating at the high temperatures and pressures required by industry. Studies have shown that Pt/ZrO_2 catalysts exhibit high activity and stability at moderate temperatures, 650°C, but the catalysts experience deactivation due to carbon deposition at 800°C.

This thesis reports the study of the dry reforming reaction over SiO_2 and ZrO_2 supported Pt catalysts. It was found that the Pt/ZrO_2 catalyst had much higher activity and stability than the Pt/SiO_2 catalyst due to the ability of the ZrO_2 to adsorb CO_2 near the metal particle, facilitating its dissociation. The decomposition of CH_4 and the dissociation of CO_2 occur via two independent pathways. CH_4 decomposition occurs on the metal particle resulting in the formation of H_2 and carbon deposition. When Pt is supported on ZrO_2, the carbon formed during the decomposition of CH_4 can reduce the support to form CO, creating oxygen vacancies in the support lattice near the metal particle. The adsorption and dissociation of CO_2 occurs at the vacancies, forming CO and replenishing the oxygen in the support lattice. This redox mechanism results in a cleaning of the metal particle by oxygen provided by the support. The long-term activity of the catalyst is dependent

upon the balance between the rate of CH_4 decomposition and the rate of dissociation of CO_2.

Promoters were added to both the metallic phase and to the support to improve the stability of the catalyst by decreasing carbon deposition. The co-impregnation of Sn and Pt on the ZrO_2 resulted in lower activity and stability than the monometallic catalysts. Under oxidizing conditions, segregation of the Pt-Sn alloys occurred, resulting in the formation of tin oxide inhibiting the role of the ZrO_2. Surface reduction deposition and other preparation methods resulted in the controlled placement of Sn on the Pt particle, minimizing the promoter-support interaction. These catalysts exhibited higher activity and stability than the monometallic catalyst under severely deactivating conditions, 800°C and a 3:1 ratio of CH_4:CO_2.

Promotion of the ZrO_2 support with cerium and lanthanum, prior to the addition of the Pt, resulted in increased activity and stability of the catalyst. The improved performance of the promoted catalyst can be attributed to multiple effects including stabilizing the surface area for high temperature operation, increasing the density of CO_2 adsorption sites near the metal particle, and retarding particle growth under reaction conditions. Detailed characterization of the catalysts has been performed using temperature programmed techniques (TPO, TPD, and TPR), transmission electron microscopy (TEM), chemisorption, physisorption, diffuse reflectance infrared Fourier transform spectroscopy (DRIFTS), X-ray absorption spectroscopy, X-ray diffraction (XRD), and isotopically labeled studies.

CHAPTER 1

INTRODUCTION

1.1 Overview

The production of synthesis gas, a mixture of H_2 and CO, is of great industrial significance and has been extensively studied for many decades because it is the first step in a series of reactions to convert natural gas into hydrocarbons and higher value products [1]. Synthesis gas is primarily used in the production of ammonia, methanol, polycarbonates, and oxygenated alcohols. Furthermore, when used in Fischer-Tropsch (FT) processes, the products produced from synthesis gas can be used for a variety of applications. For example, during low temperature FT processing, the synthesis gas is converted to a syncrude that contains a large fraction of heavy, waxy hydrocarbons. These heavy hydrocarbons can then be refined to make specialty waxes or can be hydrocracked and/or isomerized to produce high quality diesel, base stock for lube oils, and a feedstock naptha for cracking to light olefins. High temperature FT processing produces compounds that can be refined to produce olefins, diesel, solvents, and environmentally friendly gasolines [2,3] due to the absence of sulfur and aromatics.

The production of synthesis gas can be achieved using processes that involve both catalytic and noncatalytic means of reacting natural gas, coal, or petroleum residua. The conversion of coal to synthesis gas is done through gasification, or the burning of the hydrocarbon in the presence of steam.

Even though this process is more expensive and complex than starting with natural gas, it is still used commercially in South Africa [2]. Other processes involving the conversion of Naptha were popular from 1940 through 1960 when natural gas was not readily available. However, with the subsequent availability and abundance of natural gas, the interest in these processes has decreased, and emphasis on reacting natural gas has dramatically increased [4].

Several technologies currently exist to produce synthesis gas from natural gas including partial oxidation (1-1), steam reforming (1-2), CO_2 reforming (1-3), or a combination of the reactions (autothermal reforming).

$$CH_4 + 1/2\ O_2 \rightarrow CO + 2\ H_2 \qquad \Delta H=-35.6\ kJ/mol \qquad (1\text{-}1)$$

$$CH_4 + H_2O \rightarrow CO + 3\ H_2 \qquad \Delta H=206.3\ kJ/mol \qquad (1\text{-}2)$$

$$CH_4 + CO_2 \rightarrow 2\ CO + 2\ H_2 \qquad \Delta H=246.9\ kJ/mol \qquad (1\text{-}3)$$

FT processing requires approximately a 2:1 ratio of H_2:CO. Therefore, partial oxidation is the preferred reaction for the production of synthesis gas. However, the cost of building and operating a partial oxidation plant is very expensive, primarily due to the costs associated with obtaining the oxygen. If air is used in the partial oxidation plant, capital and operating costs are greatly increased due to the amount of nitrogen that is carried throughout the

process. Furthermore, downstream processing requirements cannot tolerate nitrogen, which makes recycling with cryogenic separation necessary [5]. If air separation plants are used to separate the oxygen and nitrogen, the cost of the oxygen purification amounts to 50% of the total cost of the synthesis gas production plant [6].

The most commonly used process for the production of synthesis gas is the conversion of methane via steam reforming [7]. This reaction, although widely accepted, has several disadvantages. The first disadvantage is poor selectivity to carbon monoxide as seen in the high H_2:CO product ratio of 3:1. Second, the steam reforming reaction often results in a high percentage of impurities, primarily unreacted methane, which can cause problems in the downstream production of polycarbonates [8]. Third, the steam reforming reaction is very endothermic, which requires the reaction to be performed at high temperatures. These conditions are conducive to carbon formation, and the catalyst deactivates due to carbon deposition on the metal. To prevent deactivation and to have reasonable reaction cycles, a high steam to hydrocarbon ratio is used. This high ratio is very expensive, making the process less attractive in terms of cost efficiency [9].

Methane reforming using carbon dioxide (dry reforming) has been of interest for a long time [10-12], but in recent years that interest has experienced a rapid increase both for environmental and commercial reasons. It was originally thought that replacing the steam with CO_2 would be more beneficial because the reaction would then consume CH_4 and CO_2, the

two most abundant greenhouse gases [13-16]. However, the reduction of CO_2 emissions would only occur if the synthesis gas produced by the reaction was used to make chemicals and products other than fuels, and if the heat supplied to the highly endothermic reforming reaction was not provided by combustion [8,17-18]. One advantage of dry reforming that would have a large impact on the industrial sector, is the 1:1 ratio of H_2:CO that is produced. The lower product ratio (compared to steam reforming and partial oxidation) is preferred for the production of oxygenated compounds [17,19], and it also introduces the possibility of combining the steam reforming, partial oxidation, and dry reforming reactions to get the desired H_2:CO ratio for the downstream processes using the synthesis gas produced [20-22]. Furthermore, the utilization of CO_2 provides a source of clean oxygen, which eliminates the need for costly separation plants, that are necessary for partial oxidation. Another driving force behind the research into dry reforming is the development of Chemical Energy Transmission and Storage (CETS) systems [23] used to provide energy to geographical regions that are energy deficient. The idea behind this process is to run a highly endothermic reaction to equilibrium using fossil, nuclear, or solar energy. The products of the reaction, which now store the incident energy, can be transported through pipelines to a location where the reverse reaction, now exothermic, releases the energy. Dry reforming is the preferred thermochemical reaction for this process due to the endothermic nature of the reaction and the products formed. The final, and perhaps most important advantage of dry reforming is

the simultaneous availability and low cost of the reactants [24]. CO_2 and CH_4 are the cheapest and most abundant carbon containing materials, which provides for a tremendous return on investment for the efficient production of higher value commodities. Furthermore, natural gas reservoirs contain primarily CH_4, but some reservoirs also have a large fraction of CO_2 [13,25,26]. Many of these reservoirs are located in remote regions and have quantities of natural gas that are too small to make production economical [27]. The capability to efficiently convert the natural gas in these reservoirs to higher value products could increase the cost effectiveness of remotely located reservoirs. This capability, along with the other advantages, makes the dry reforming reaction very desirable for commercialization.

The major obstacle preventing commercialization of this process is that, due to the high endothermic nature of the process, temperatures near 800°C are required to reach 100% conversion. Independently, CH_4 and CO_2 undergo dissociation at much lower temperatures, but the decomposition products are C, O, and CO, which terminate all reactions by covering active sites. The presence of both CH_4 and CO_2 is believed to accelerate the decomposition of both species by H_2 assisted adsorption of CO_2 and activation of CH_4 by the oxygen formed during the decomposition of CO_2 [12]. Under these conditions, the majority of catalysts investigated experience rapid deactivation due to carbon deposition via the Boudouard reaction (1-4) and the decomposition of CH_4 (1-5) [28].

$$2\,CO \rightarrow C + CO_2 \qquad (1\text{-}4)$$

$$CH_4 \rightarrow C + 2\,H_2 \qquad (1\text{-}5)$$

Two processes have been commercially developed which overcome the problem of carbon deposition during the reforming reaction. The first process, known as the CALCOR process, was developed with the intention of producing high purity CO from natural gas or LPG [29]. To reduce carbon deposition the process operates under the dry reforming conditions in an excess of CO_2. Furthermore, several different catalysts are used throughout the reactor to aid in the reduction of coke formation. Although specific details of the catalyst are proprietary, it has been reported that the CO produced contains less than 0.1% of methane, and after purification, the CO purity is greater than 90%.

The second process is the SPARG (sulfur passivated reforming) process which was first commercialized in 1987 by Sterling Chemical Inc., Texas [30]. The process operates using a partially sulfur poisoned nickel catalyst which reduces carbon deposition under conditions where coke formation is favored. Operating temperatures are between 1188-1218K, which reduces the amount of unreacted methane leaving the reactor. As previously mentioned, high levels of methane or other impurities in the CO can cause problems in the downstream processing of polycarbonates, leading to materials with inferior mechanical properties.

Although the problems related to carbon deposition are minimized with the SPARG process, the problem of trace levels of sulfur in the synthesis gas requires additional cleaning steps and higher cost. Thus, a catalyst that can operate without substantial carbon deposition at high temperatures is preferred. Current research efforts have focused on developing such catalysts that show high activity and stability at the high operating temperatures required to make the dry reforming process industrially feasible.

1.2 Current Catalyst Technology

1.2.1 Effect of Metal

In 1817 H. Davy observed that it was possible to carry out the oxidation of hydrogen by air over Pt metal. Since this time, the majority of surface catalytic processes involve the use of transition metals and their compounds (oxides, sulfides and carbides). Transition metal catalysts tend to be unique in their activity, which is often ascribed to the importance of the *d*-electrons to the bonding of atoms and molecules on the surface [31]. Some of the most important functions of the transition metals is to chemisorb molecules, facilitate in the breaking of the molecular bonds, and then supply the atoms to atoms or molecules on the surface. Traditionally, these metals have the highest activity for the activation of hydrocarbons.

In the late 1920's, Fischer and Tropsch demonstrated the activity of transition metals for the CO_2 reforming reaction [10]. Since this time, most of the dry reforming research has focussed on Group VIII metals on a variety of

supports [32]. The primary transition metals that have been investigated are Rh, Ru, and Ni [12,13,22,33-36]. Some studies have also been performed on Pt, Ir, and Pd [8,25,37-38]. Of the many combinations studied, Rh has emerged as the most active and results in the least amount of carbon deposition. However, this metal is limited in supply, and its fluctuations in the market reduce the commercial feasibility [22,39-41]. The Ni catalysts, which are less expensive and more abundant, have also received a great deal of attention, but the Ni catalysts experience severe deactivation due to carbon deposition [22,23,32,42-43]. Ni is known to form filamentous carbon or "whiskers" which can result in blockage of the reactor bed, leading to large pressure drops [44-46]. This deactivation results in short operating times and long regeneration/catalyst replacement procedures, which are not economically desirable. Pt also exhibited high activity for the CO_2 reforming reaction but deactivated due to carbon deposition [25, 32, 37]. However, the carbon that forms on the Pt catalyst is not filamentous, eliminating the problems of reactor plugging that the Ni catalysts have. Thus, from an economic view, if the problem of coke formation could be reduced on the Pt catalysts, Pt would be the more commercially feasible metal for the dry reforming reaction.

1.2.2 Effect of the Support

Several papers have been published on the role of the support in the dry reforming reaction. Variations in the catalytic properties are expected with

changes in the support due to the support affecting the degree of metal dispersion and the metal-support interactions [39]. Masai *et al.* [38] observed an increase in the activity with an increase in Pd dispersion, which he attributed to increases in acidity of the support. In contrast, when MgO or CaO were physically mixed with SiO_2, a decrease in the deactivation of the Rh catalyst was observed [33]. The authors suggest that increasing the basicity of the support increases the CO_2 adsorption, which shifts the equilibrium of the coking reaction to the left. Thus, the activity of the catalyst increases with increasing basicity of the support due to decreases in carbon formation.

Erdohelyi *et al.* [12], when studying Rh, reported that Al_2O_3 was more active than SiO_2 and MgO for the decomposition of CH_4, but the activity of the high temperature reforming reaction was independent of the support. However, others have shown that Al_2O_3 can be up to 35 times more active for the reforming reaction, and physical mixtures of Al_2O_3 and SiO_2 result in increased activity and stability over SiO_2 supported catalysts [34,35]. The increased activity is ascribed to the metal oxide promoting the dissociation of CO_2 by increasing the concentration of CO_2 near the Rh particle and trapping the CO_2 as formate on the surface.

Several groups have focused on TiO_2 and ZrO_2. These groups have found that, on the studied supports, Pt reaches much higher conversions than when supported on SiO_2 and Al_2O_3. Bradford and Vannice have performed an extensive study of Pt/TiO_2 and model TiO_x/Pt catalysts [47,48]. The

results from the model catalyst studies indicate that the activity of the catalyst increases with increasing TiO_x coverage. They attribute this increase to the formation of new metal-support interfacial sites and propose that these sites promote the dissociation of CH_4, the dissociation and reduction of CO_2, and the decomposition of CH_xO [48]. Also, the formation of TiO_x overlayers on the Pt/TiO_2 catalyst was proposed to increase stability due to suppression of carbon deposition via an ensemble effect [47]. Lercher *et al.* [49,50] have also studied TiO_2 as a support, as well as ZrO_2 and Al_2O_3. They found that, among these three supports, ZrO_2 was the most effective, resulting in a stable catalyst at 600°C and a 1:1 CH_4:CO_2 feed ratio.

1.2.3 Reaction Mechanism

Several theories on the reaction mechanism exist in the literature. The first is an Eley Rideal type mechanism, in which CH_4 is activated on the metal, decomposes to form H_2 and adsorbed carbon. The adsorbed carbon reacts directly with the CO_2 from the gas phase to yield CO [12,51-52].

An alternative [22-23,25,32,47,48,53] is that the methane decomposes on the metal to form a CH_x species. The CO_2 adsorbs and dissociates to form CO and an adsorbed O species. This adsorbed O is then free to react with the CH_x species on the metal to form H_2 and CO. The details of this mechanism are still unclear, and there is an ongoing debate about the activation of the CO_2. Many suggest that on Rh and Ni, the dissociation occurs on the metal, and the support has no major contribution [22,53].

Others [47,48] have suggested that the CO_2 dissociates to form CO and an OH group, which can then react to form CH_xO species. These species then subsequently decompose to form H_2 and CO.

1.2.4 Addition of Promoters

A promoter is generally thought of as a material, that when added in small amounts to the catalyst during the preparation, imparts better activity, selectivity, and stability [4]. This increased performance is greater than that attributed to the promoter acting independently, which often has little or no activity by itself towards the reaction. Promoters can have many effects on the catalyst such as altering the physical and/or chemical state of the metal or support. Textural promotion arises from the ability of the promoter to alter the physical properties of the catalyst without modifying the chemical state. Often times these materials are found in the form of inert, highly dispersed particles which help to prevent sintering or agglomeration of the active metal species. In the case of an oxide support, promotion of the support may result in the stabilization of a specific phase. This phase stabilization can result in increased thermal stability.

Alternatively, structural promoters alter the chemical state of the catalyst. Some effects of structural promoters might include alteration of the adsorption properties of the catalyst, the creation of basic sites, the neutralization of acid sites, or the formation of alloys. All of which may have a different activity for the reaction. In addition, many other promoters exist

which improve the catalytic performance by both structural and textural methods, and it is often times difficult to distinguish between the two because the promoters will exhibit characteristics of both classes. However, in either case, promoters offer the ability to greatly improve the activity, selectivity, or stability of a catalyst.

Some studies have been done on the promotion of Ni catalysts for the dry reforming reaction in an attempt to reduce carbon deposition [54-57]. The results have shown that the promoters can influence the nickel particle morphology and size distribution, which in turn alters the origin kinetics and the reactivity of the carbon deposited during the reaction. More specifically the addition of basic metal oxides to the support reduced the carbon deposition and increased the catalytic performance for the reforming reaction [56]. Little work has been done on the promotion of the supported Pt catalysts for the dry reforming reaction, but it is logical that similar effects would be observed regarding suppression of carbon deposition.

1.3 Objectives of Research

As discussed above, the major factor preventing commercialization of the CO_2 reforming of CH_4 is the inability to find a catalyst capable of operating at high temperatures without substantial deactivation due to carbon deposition. Furthermore, many questions remain about the mechanism and the role of the support in the reaction. The aim of this work was to study the reaction mechanism over supported Pt catalysts and then increase the

catalyst activity and stability by reducing carbon deposition. In an attempt to achieve the reduction in carbonaceous deposits, promoters were added to both the metallic phase and to the support to inhibit the decomposition of CH_4 and to facilitate the dissociation of CO_2, respectively.

1.4 Structure of Dissertation

The following chapter outlines all of the experimental procedures and preparation methods that were employed for the experiments discussed in this work. Chapter 3 discusses the mechanism for the reforming reaction over supported Pt catalysts, and the role of the support in this mechanism. It will be shown that Pt/ZrO_2 catalysts are promising catalysts for the reforming reaction but experience deactivation due to carbon deposition at high temperatures, 800°C. The problem of carbon deposition was attacked in two ways, both of which are described in Chapters 4 and 5. The first method to suppress carbon deposition involved promotion of the metallic phase. The results of this work and the effects of the promoter on the role of the support are discussed in Chapter 4. The second method was to use promoters to enhance the role of the support in the dry reforming reaction. Chapter 5 gives a detailed description of this work. It will be shown that the addition of promoters to the support can enhance the role of the ZrO_2 in the suppression of carbon deposition. These catalysts exhibit high activity and stability under severely deactivating conditions.

1.5 References

1. Fischer, F., and Tropsch, H., German Patent 484337 (1925).
2. Jager, B., *Stud. Surf. Sci. Catal.*, **119**, 25 (1998).
3. De Jong, K. P., Post, M. F. M., and Knoester, A., *Stud. Surf. Sci. Catal.*, **119**, 119 (1998).
4. Satterfield, C. N., "Heterogeneous Catalysis in Industrial Practice", 2nd edition, McGraw-Hill, New York, 1991, Chapter 10.
5. Balachandran, U., Dusek, J. T., Sweeney, S. M., Poeppel, R. B., Mieville, R. L., Maiya, P. S., Kleefisch, M. S., Pei, S., Kobylinski, T. P., and Udovich, C. A., *American Ceramic Society Bulletin*, **74 (1)**, 71 (1995).
6. Maiya, P. S., Balachandran, U., Dusek, J. T., Mieville, R. L., Kleefisch, M. S., and Udovich, C. A., *Solid State Ionics*, **99**, 1 (1997).
7. Rostrup-Nielsen, J. R., *Catal. & Sci. Tech.*, **5**, 3 (1984).
8. Seshan, K., ten Barge, H. W., Hally, W., van Keulen, A. N. J., and Ross, J. R. H., *Stud. Surf. Sci. Catal.*, **81**, 285 (1994).
9. Pena, M. A., Gomez, J. P., and Fierro, J. L. G., *Appl. Catal. A*, **144**, 7 (1996).
10. Fischer, V. F., and Tropsch, H., *Brennst.-Chem.*, **3(9)**, 39 (1928).
11. Gadalla, A. M., and Sommer, M. E., *Chem. Eng. Sci.*, **44(12)**, 2825 (1989).
12. Erdohelyi, A., Cserenyi, J., and Solymosi, F., *J. Catal.*, **141**, 287 (1993).
13. Takano, A., Tagawa, T., and Goto, S., *J. Chem. Eng. Japan*, **27**, 727 (1994).
14. Osaki, T., Horiuchi, T., Suzuki, K., and Mori, T., *Catal. Lett.*, **35**, 39 (1995).
15. Takayasu, O., Soman, C., Takegahara, Y., and Matsuura, I., *Stud. Surf. Sci. Catal.*, **88**, 281 (1994).
16. Rostrup-Nielsen, J. R., *Stud. Surf. Sci. Catal.*, **81**, 25 (1994).
17. Ross, J. R. H., van Keulen, A. N. J., Hegarty, M. E. S., and Seshan, K., *Catal. Today*, **30**, 193 (1996).
18. van Keulen, A. N. J., Seshan, K., Hoebink, J. H. B. J., and Ross, J. R. H., *J. Catal.*, **166**, 306 (1997).
19. Wang, S. B., and Lu, G. Q., *Energy & Fuels*, **10**, 896 (1996).
20. Choudhary, V. R., and Rajput, A. M., *Ind. Eng. Chem. Res.*, **35**, 3934 (1996).
21. Xiaoding, X., and Moulijn, J. A., *Energy & Fuels*, **10**, 305 (1996).
22. Qin, D., and Lapszewicz, J., *Catal. Today*, **21**, 551 (1994).
23. Richardson, J. T., and Paripatyadar, S. A., *Appl. Catal.*, **61**, 293 (1990).
24. Zhang, Z. L., Verykios, X. E., *Appl. Catal.* A, **138**, 109 (1996).
25. Solymosi, F., Kustan, G., and Erdohelyi, A., *Catal. Lett.*, **11**, 149 (1991).

26. Zhang, Z. L., Tsipouriari, V. A., Efstathiou, A. M., and Verykios, X. E., *J. Catal.*, **158**, 51 (1996).
27. The Shell Review, Shell International Petroleum Company Limited (1994).
28. Bhat, R. N., and Sachtler, W. M. H., *Appl. Catal. A*, **150**, 279 (1997).
29. Teuner, S., *Hydrocarbon Processing*, **64**, 106 (1985).
30. Udengaard, N. R., Hansen, J. B., Hanson, D. C., and Stal, J., A., *Oil & Gas Journal.*, **62**, 9 (1992).
31. Somorjai, G., "Introduction to Surface Chemistry and Catalysis", John Wiley & Sons, New York 1994.
32. Rostrup-Nielsen, J. R., and Bak Hansen, J-H., *J. Catal.*, **144**, 38 (1993).
33. Tang, S. B., Qiu, F. L., and Lu, S. J., *Catal. Today*, **24**, 253 (1995).
34. Nakamura, J., Aikawa, K., Sato, K., and Uchijima, T., *Stud. Surf. Sci. Catal.*, Amsterdam, NY, Elsevier, **90**, 495 (1994).
35. Uchijima, T., Nakamura, J., Sato, K., Aikawa, K., Kubushiro, K., and Kunimori, K., *Natural Gas Conversion II*, Curry-Hyde, H. E. and Howe, R. F. (editors), Elsevier Science, 325 (1994).
36. Qin, D., Lapszewicz, J., and Jiang, X., *J. Catal.*, **159**, 140 (1996).
37. Solymosi, F., Erodohelyi, A., and Cserenyi, J., *Catal. Lett.*, **16**, 399 (1992).
38. Masai, K., Kado, H., Miyake, A., Nishiyama, S., and Tsuruya, S., *Methane Conversion*, **67** (1988).
39. Edwards, J. H., and Maitra, A. M., *Fuel Processing Tech.*, **42**, 269 (1995).
40. Tsipouriari, V. A., Efstathiou, A. M., Zhang, Z. L., and Verykios, X. E., *Catal. Today*, **21**, 579 (1994).
41. Sakai, Y., Saito, H., Sodesawa, T., and Nozaki, F., *React. Kinet. Catal. Lett.*, **24**, 253 (1984).
42. Hally, W., Bitter, J. H., Seshan, K., Lercher, J. A., and Ross, J. R. H., *Stud. Surf. Sci. Catal.*, **88**, 167 (1994).
43. Kroll, V. C. H., Swaan, H. M., and Mirodatos, C., *J. Catal.*, **161**, 409 (1996).
44. Bradford, C. J., and Vannice, M. A., *Appl. Catal. A*, **142** 73 (1996).
45. Chang, J., Park, S., and Chon, H., *Appl. Catal. A*, **145** 111 (1996).
46. Vernon, P. D. F., Green, M. L. H., Cheetam, A. K., and Ashcroft A. T., *Catal. Today*, **13**, 417 (1992).
47. Bradford, M., Vannice, M. A., *J. Catal.*, **173**, 157 (1998).
48. Bradford, M., Vannice, M. A., *Catal. Lett.*, *48*, 31 (1997).
49. Lercher, J. A., Bitter, J. H., Hally, W., Niessen, W., and Seshan, K., *Stud. Surf. Sci. Catal.*, **101**, 463 (1996).
50. Bitter, J. H., Seshan, K., and Lercher, J. A., *J. Catal.*, **171**, 279 (1997).
51. Mark, M. F., Maier, W. F., *Agnew. Chem. Int. Ed. Engl.*, **15-16**, 33 (1994).
52. Mark, M. F., Maier, W. F., *J. Catal.*, **164**, 122 (1996).

53. Bodrov, I. M., Apel'baum, L. O., *Kinetic. Katal.*, **8**, 379 (1967).
54. Chen, Y. G., Yamazaki, O., Tomishige, K., and Fujimoto, K., *Catal. Lett.*, **39**, 91 (1996).
55. Cheng, Z., Wu, Q., Li, J., and Zhu, Q., *Catal. Today*, **30**,147 (1996).
56. Horiuchi, T., Sakuma, K., Fukui, T., Kubo, Y., Osaki, T., and Mori, T., *Appl. Catal. A*, **144**, 111 (1996).
57. Goula, M. A., Lemonidou, A. A., and Efstathiou, A. M., *J. Catal.*, **161**, 626 (1996).

CHAPTER 2

EXPERIMENTAL

2.1 Materials

2.1.1 Gases

The majority of the gases used for activity and characterization experiments were obtained from Sooner Airgas and used as received. These gases include ultra high purity (UHP) hydrogen, UHP helium, UHP argon, UHP oxygen, zero grade air, instrument grade carbon dioxide, CP grade carbon monoxide, CP grade methane, CP grade ethylene, 5% hydrogen in argon, and 5% oxygen in helium. Several isotopically labeled studies were also performed using $^{13}CH_4$ with 99 atom % ^{13}C obtained from MSD isotopes. The specific information about the gas flow rates used will be given in the appropriate section describing the technique.

2.1.2 Supports

Several supports were used in this investigation, and the properties of these supports are listed in Table 2.1. The SiO_2 (Silica Grade Gel 923) was obtained from W. R. Grace & Co. with a measured surface area of 470 m^2/g and a pore volume of 0.35 cm^3/g. The ZrO_2 was obtained by calcination of $Zr(OH)_4$ (obtained from Magnesium Elektron Inc. (MEI)) at 800°C for 4 hours in stagnant air. The surface area and pore volume of the ZrO_2 was 35 m^2/g and 0.2 cm^3/g, respectively. Two additional supports were prepared by adding Ce^{4+} and La^{3+} as promoters to the $Zr(OH)_4$. The lanthanum-doped

ZrO_2 was obtained from MEI and had a La content of 5% by weight in the final support. The cerium-doped ZrO_2 was made by aqueous impregnation of cerium nitrate to the zirconium hydroxide. The incipient wetness of the $Zr(OH)_4$ was 0.2 cm^3/g and the weight percent of Ce in the final material was 5%. After impregnation of the cerium, the material was dried overnight at 110°C, and then calcined at 800°C for 4 hours in stagnant air.

Support	Weight % of Promoter	Pretreatment of support prior to impregnation of Pt	BET (m^2/g)	Pore Volume cm^3/g
SiO_2	—	Dried at 110C	470	0.35
ZrO_2	—	Dried at 110C, calcined at 800C for 4 hours	35	0.20
La-ZrO_2	5.0%	Dried at 110C, calcined at 800C for 4 hours	55	0.10
Ce-ZrO_2	5.0%	Dried at 110C, calcined at 800C for 4 hours	41	0.18
Ce-La-ZrO_2	Ce - 17.0% La - 5.0%	Dried at 110C, calcined at 800C for 4 hours	49	0.30

Table 2.1: Characteristics of supports investigated.

2.1.3 Metallic Precursors

Two Pt precursors were used to make the catalysts. The precursor for the catalysts which were prepared by sequential impregnation of Pt and Sn was $Pt(NH_3)_4(NO_3)_2$. All of the other catalysts were prepared using $H_2PtCl_6 \bullet 6H_2O$ as the Pt salt. The Sn was added to the catalysts using $SnCl_2 \bullet 2H_2O$. All of the metallic salts were obtained from Johnson Mathey.

2.1.4 Catalyst Preparation

The primary method of catalyst preparation used in this investigation was incipient wetness impregnation. In this technique, the salt was placed into a measured amount of solution, which corresponded to the volume of solution required to fill the pores of the catalyst. By filling the pores of the catalyst, the metal precursor was dispersed throughout the pores increasing the surface area available for the deposition of the active species. The incipient wetness liquid/solid ratio of the SiO_2 was determined for each preparation and varied from 0.5 to 0.75 cm^3/g. The unpromoted ZrO_2 had an incipient wetness ratio that ranged from 0.3 to 0.5 cm^3/g. The addition of the promoters changed the incipient wetness ratio of the ZrO_2, lowering it to 0.15 cm^3/g and 0.2 cm^3/g for the La and Ce promoted catalysts, respectively. Three solvents were used during the impregnation preparations in this study, water, acetone, and hydrochloric acid. Table 2.2 lists the catalyst nomenclature as well as the characteristics of the catalysts investigated.

2.1.4.1 SiO_2 Supported Catalysts

Two monometallic catalysts were prepared on SiO_2 using impregnation. The first catalyst had a Pt loading of 1.0 wt % and the solvent used was HCl. The second catalyst was prepared using aqueous impregnation with a final Pt loading of 1.5 wt %. These catalysts will be referred to throughout this contribution as Pt (1.0) and Pt (1.5), respectively.

Catalyst	Pt Wt %	Molar Ratio Pt:Sn	Preparation Technique	Solvent	Precursor	Catalyst Nomenclature
Pt/SiO_2	1.0	1:0	Impregnation	HCl	H_2PtCl_6	Pt (1.0)
Pt/SiO_2	1.5	1:0	Impregnation	Water	H_2PtCl_6	Pt (1.5)
$Pt\text{-}Sn/SiO_2$	1.5	1:1	Co-impregnation	Water	H_2PtCl_6 - $SnCl_2$	Pt-Sn (CI)
$Pt\text{-}Sn/SiO_2$	1.0	1:1.65	Co-impregnation	HCl	H_2PtCl_6 - $SnCl_2$	Pt-Sn (CIC)
$Pt\text{-}Sn/SiO_2$	0.3	1:1.65	Sequential impregnation	Acetone	$Pt(NH_3)_4(NO_3)_2$	Pt-Sn (SI0.3)
$Pt\text{-}Sn/SiO_2$	1.0	1:1.65	Sequential impregnation	Acetone	$Pt(NH_3)_4(NO_3)_2$	Pt-Sn (SI)
Pt/ZrO_2	1.5	1:0	Impregnation	Water	H_2PtCl_6	Pt/ZrO_2
$Pt\text{-}Sn/ZrO_2$	1.5	1:1	Co-impregnation	Water	H_2PtCl_6 - $SnCl_2$	$Pt\text{-}Sn/ZrO_2$
$Pt\text{-}Sn/ZrO_2$	2.5	2.5:1	Co-impregnation	Water	H_2PtCl_6 - $SnCl_2$	Pt-Sn/Pt
$Pt\text{-}Sn/ZrO_2$	1.0	1:0.05	Surface Reduction Deposition	n-hexane	H_2PtCl_6 - $Sn(C_4H_9)_4$	Pt-Sn (SR)
$Pt/Ce\text{-}ZrO_2$	1.5	1:0	Impregnation	Water	H_2PtCl_6	$Pt/Ce\text{-}ZrO_2$
$Pt/La\text{-}ZrO_2$	1.5	1:0	Impregnation	Water	H_2PtCl_6	$Pt/La\text{-}ZrO_2$
$Pt/Ce\text{-}La\text{-}ZrO_2$	1.5	1:0	Impregnation	Water	H_2PtCl_6	$Pt/Ce\text{-}La\text{-}ZrO_2$

Table 2-2: Characteristics of the catalysts investigated.

Two bimetallic Pt-Sn samples were supported on SiO_2 using co-impregnation. During the preparation, both the Pt and Sn salts are combined in the solvent prior to impregnation of the support. It has been shown that the preparation method employed for the addition of Pt and Sn to the support can strongly influence the degree of Pt-Sn interaction and the catalytic performance [Appendix A]. The first catalyst was prepared by aqueous impregnation with a Pt loading of 1.5 wt % and a 1:1 molar ratio of Pt:Sn. The second catalyst was prepared using HCl as the solvent and had a final Pt loading of 1.0 wt % and a 1:1.65 molar ratio of Pt:Sn. This preparation method has been previously used, and it has been shown [1] that, in the presence of HCl, a bimetallic complex $PtCl_2(SnCl_3)_2^{2-}$ is formed in solution and a higher degree of metal-metal interaction should result. These catalysts will be referred to as Pt-Sn (Cl) and Pt-Sn (ClC), respectively. Two additional bimetallic catalysts were prepared using SiO_2 as a support. These two samples were made by sequential impregnation of the nitrate metallic precursors. In both cases the Pt salt was added first followed by the Sn. This preparation method involved the use of two solvents. The Pt salt was dissolved in water, while acetone was the solvent used for the Sn precursor. The molar ratio of Pt:Sn was the same for both samples at 1:1.65. The weight percent of the Pt for the catalysts was 0.3 and 1.0, and these catalysts will be referred to as Pt-Sn (Sl0.3) and Pt-Sn (Sl), respectively. All of the catalysts were dried overnight at 110°C, calcined in air (30 cm^3/min) at 400°C

for 2 hours, and then reduced *in situ* for 1 hour in H_2 (30 cm^3/min) at 500°C prior to reaction.

2.1.4.2 ZrO_2 Supported Catalysts

The Pt loading used on the monometallic and bimetallic ZrO_2, Ce-ZrO_2, and La-ZrO_2 catalysts prepared by aqueous impregnation was 1.5 wt %, with a 1:1 molar ratio of Pt:Sn. The bimetallic catalyst was prepared using co-impregnation of the hexachloroplatinic salt and the tin chloride and will be referred to as Pt-Sn/ZrO_2. Two additional bimetallic catalysts were prepared by special techniques. The first involved the co-impregnation of a 1.0 wt % Pt and Sn (1:1 molar ratio) onto a precalcined 1.5 wt % Pt/ZrO_2 catalyst prepared as described above. This catalyst will be referred to as Pt-Sn/Pt. The other preparation method used was surface reduction deposition. Details about this technique, which is intended to selectively deposit Sn on Pt, can be found elsewhere [2]. The catalyst was prepared in a solution of *n*-hexane and $Sn(C_4H_9)_4$ at room temperature in He. Prior to the addition of Sn, the 1.0 wt % Pt/ZrO_2 used as a base was reduced *in situ* at 250°C for 1 hour and cooled to room temperature in H_2. This step results in adsorbed H on Pt, which is responsible for the reduction of the $Sn(C_4H_9)_4$. After the introduction of the Sn solution, the catalyst was washed in clean *n*-hexane and then heated to 60°C in a low flow of He. Finally, the catalyst was dried for 1 hour in He at 150°C. This catalyst (Pt:Sn molar ratio of 1:0.5) was reduced *in situ* by heating to 300°C in H_2 (30 cm^2/min) prior to any reaction or characterization, and will be

referred to as Pt-Sn (SR). All catalysts, except the Pt-Sn (SR) were dried overnight at 110°C, calcined in air (30 cm^3/min) at 400°C for 2 hours, and then reduced *in situ* for 1 hour in H_2 (30 cm^3/min) at 500°C prior to reaction. Any variations in the catalyst pretreatment will be clearly stated in the section describing the experiment or the results.

2.2 Catalyst Activity

The catalyst activity studies were carried out in a flow reactor consisting of a quartz tube with an inner diameter of 0.4 cm and an outer diameter of 0.6 cm. A schematic of the reactor system and the analysis equipment is shown in Figure 2.1.

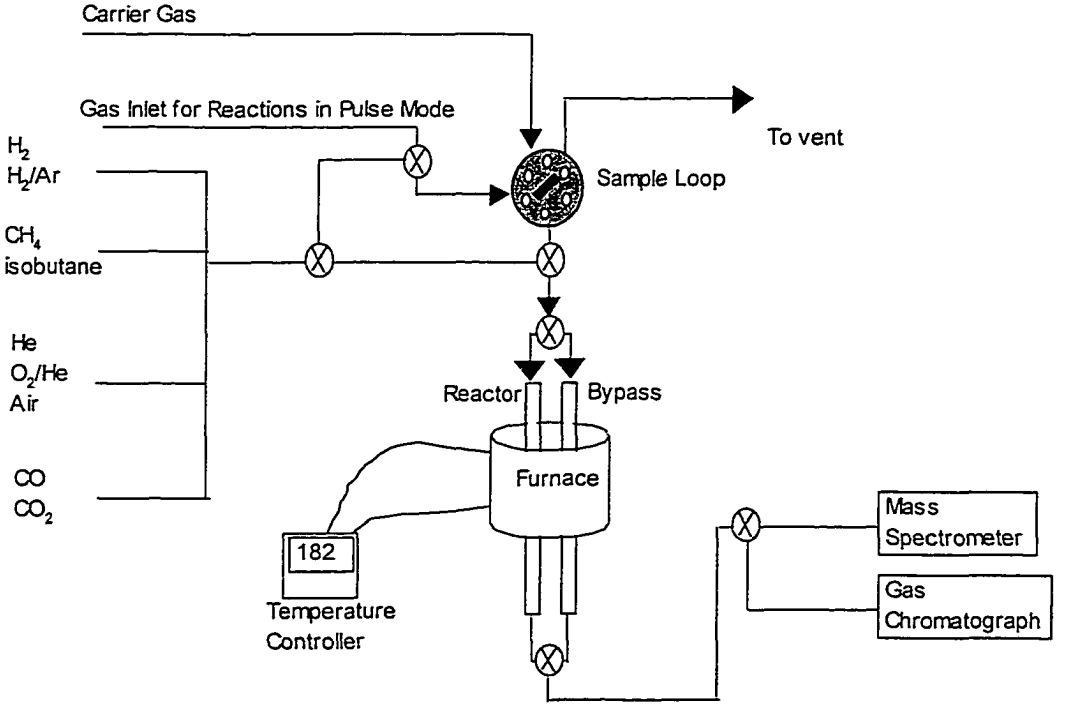

Figure 2.1: Schematic of microcatalytic reactor

The gases went through a zeolite trap to eliminate water before entering mass flow controllers (Porter model #201), which regulated flow to the reactor. The catalyst was suspended in the quartz tube using two small plugs of quartz wool. Each sample was diluted with either SiO_2 or ZrO_2 to minimize heat and mass transfer limitations. A thermocouple was placed directly in contact with the bottom of the catalyst bed during the reaction. An additional thermocouple was placed at the side of the bed on the outside of the quartz tube and was used to control the temperature of the furnace. The Weisz-Prater criteria for internal diffusion was calculated and the results showed that mass transfer limitations were not present during any of the experiments.

Reactions were performed at either 650°C or 800°C and at CH_4:CO_2 ratio of 1:1, 2:1 and 3:1. The flow rates used for each experiment varied between 75 cm^3/min and 150 cm^3/min resulting in space velocities between 90,000 GHSV and 700,000 GHSV. The exit gases were analyzed using a gas chromatograph (Hewlett Packard HP5890) equipped with a thermal conductivity detector and a Supelco Carboxen 1006 PLOT fused capillary column (30 m, 0.53 mm ID), which allowed for separation of H_2, CO,CH_4 and CO_2. The carrier gas used was Ar. The samples were reduced *in situ*, and then heated to the reaction temperature in He or Ar (30 cm^3/min). Calibration of the GC using varying ratios of the reactants and products resulted in a mole/area ratio for each gas. Quantification of H_2O was not attempted; however, equilibrium data shows that water production is minimal at high

operating temperatures (800°C). The conversion of CH_4 and CO_2 was calculated using the following equations:

Methane conversion: $$X_{CH4} = \frac{CH_{4in} - CH_{4out}}{CH_{4in}} * 100\% \quad (2\text{-}1)$$

Carbon dioxide conversion : $$X_{CO2} = \frac{CO_{2in} - CO_{2out}}{CO_{2in}} * 100\% \quad (2\text{-}2)$$

where CH_{4in} and CO_{2in} was the average peak area of the CH_4 and CO_2 through the by-pass, prior to reaction. The value of the CH_{4out} and CO_{2out} was the peak area for each reactant during the reaction.

2.3 Catalyst Characterization

Due to the many variations in the experimental conditions for each sample and each study, only the general procedure is described for each of the following characterization techniques. Further information about the specific catalyst pretreatment will be provided in the section or chapter that describes the results of the experiment.

2.3.1 Temperature Programmed Oxidation (TPO)

TPO experiments of carbonaceous deposits were used to determine the amount of carbon that was deposited under reaction conditions. After exposure to reaction conditions, the samples were cooled to room temperature in He. Once at room temperature, the sample was heated at a

rate of 8°C/min in O_2 (30 cm^3/min) or in a 5% O_2/He mixture (30 cm^3/min) up to 800°C. The exit gases were analyzed using a quadrupole residual gas analyzer from MKS (PPT 4.24). In order to normalize the pressure data, 200μL of CO_2 was injected multiple times after the system reached 800°C and the average peak area for the injections was determined. The amount of coke formed on the catalysts under the various conditions was determined using the calculated area for the known moles of CO_2 as a calibration. The TPO experiments were also used to provide information about the type of carbon that was formed. For example, the more structured graphitic forms of carbon are harder to remove and therefore, typically require higher temperatures for removal, while more amorphous carbon is burned at lower temperatures.

2.3.2 Temperature Programmed Desorption (TPD)

TPD experiments of CO_2 were performed in the same reactor system described in the catalyst activity section above. The samples were heated to 300°C in air (30 cm^3/min) to remove any surface contaminants. After the cleaning stage, the samples were cooled to room temperature in He (15 cm^3/min) and then exposed to ten 50μL pulses of CO_2. After flushing in He (15 cm^3/min) at room temperature for 30 minutes, the samples were then heated in He (15 cm^3/min) to 800°C at a rate of 8°C/minute. The exit gases were analyzed using a quadrupole residual gas analyzer from MKS (PPT 4.24). In order to normalize the pressure data, 50μL of CO_2 was injected

multiple times after the system reached 800°C and the average peak area for the injections was determined. The amount of CO_2 desorbed was calculated using the known moles of CO_2 injected and the area of the injections.

2.3.3 Temperature Programmed Reduction (TPR)

TPR experiments were performed by Carlos Querini at INCAPE, Santa Fe, Argentina, using an OKHURA TP-2002s system. The sample weights used varied from 0.25 to 0.34 g; therefore, all signals were normalized on a per gram basis. During the TPR, the samples were exposed to a flow of 5% H_2/Ar (45 cm^3/min), while heating to 800°C using a heating rate of 10°C/minute. The H_2/Ar mixture was passed through a zeolite trap before coming into contact with the catalyst to eliminate water. The exit gases were analyzed using a thermal conductivity detector (TCD) with Ar as the reference gas. H_2 consumption was measured as a function of temperature.

2.3.4 Pulse experiments and Carbon Quantification

Pulse experiments using CH_4 and CO_2 were performed in the same reactor system as previously described in the catalytic activity section. The samples were heated to 500°C in hydrogen (30 cm^3/min) and reduced *in situ* for 1 hour. After reduction, the samples were then heated to 800°C in He (15 cm^3/min) and, while in He, exposed to pulses of CH_4, CO_2, or mixtures of the reactants (50 μL pulses, 10-15 minutes apart). During each pulse the exit gases were analyzed using the quadrupole residual gas analyzer. The area

of each pulse was converted to moles using a conversion factor that was determined from a calibrated injection prior to the experiments.

Quantification of carbonaceous deposits was also performed using pulses of O_2 (50 μL pulses, 10-15 minutes apart). After reaction, the sample was flushed in He (15 cm^3/min) for 15 minutes and, while in He, exposed to pulses of O_2 to burn the carbon that was deposited during the reaction. The exit gases, primarily CO_2, CO, and unreacted O_2 were monitored using the residual quadrupole gas analyzer. The area of each pulse was converted to moles using a conversion factor that was determined from calibrated injections prior to the experiments. The quantification reaction continued until no CO_2 production or O_2 consumption was detected. The amount of carbon deposited on the catalyst was determined from the amount of CO_2 produced, and verified by the total consumption of O_2. All quantification experiments were verified to within reasonable experimental error.

2.3.5 Isotopically Labeled Studies

Pulse experiments using ^{13}C-labeled CH_4 were performed in the same reactor system previously described in the catalytic activity section. The samples were heated to 500°C in H_2 (30 cm^3/min) and reduced *in situ* for 1 hour. After reduction, the samples were then heated to 800°C in He (15 cm^3/min) and, while in He, exposed to four pulses of $^{13}CH_4$ (50 μL pulses, 10-15 minutes apart). During each pulse, the exit gases were analyzed using the quadrupole residual gas analyzer. After the $^{13}CH_4$ pulses, the system was

flushed for 15 minutes in He (15 cm^3/min) at 800°C and then exposed to pulses of $^{12}CO_2$. The area of each pulse was converted to moles using a conversion factor that was determined from a calibrated injection prior to the experiments.

2.3.6 Probe Reactions

The Methylcyclopentane ring opening (MCP-RO) reaction was used as a test reaction to study the amount of exposed metal surface available for reaction. Adriana Pisanu performed the experiments in our laboratory. The reactor setup consisted of a microreactor in which 0.050 grams of catalyst were loaded into a Pyrex reactor. The samples were reduced *in situ* at temperatures ranging from 200°C to 500°C and then exposed to reaction at temperatures ranging from 200°C to 380°C. For the reaction, the sample was exposed to three consecutive 100 μL pulses, containing 6.46 x 10^{-7} moles of MCP. The products were analyzed using a Hewlett Packard 5890 Gas Chromatograph equipped with a FID detector and a 30% DC200-Chromosorb 60/80 P AW packed column from Altech. In all experiments hydrogen was used as the carrier gas, and the only products detected were 2MP, 3MP, and hexane.

The dehydrogenation of isobutane was also used as a probe reaction for the degree of interaction between Pt and Sn in a bimetallic catalyst. The reactor system was a microreactor consisting of a quartz reactor, similar to the reactor configuration shown in Figure 2.1. Samples consisting of 0.015

grams of catalyst were reduced *in situ* at 500°C for 1 hour prior to exposure to reaction. The majority of the runs were conducted in the absence of H_2, using a 2:1 feed ratio of isobutane:He, at a flow rate of 36 cm^3/min (248 WHSV). The exit gases were analyzed using a Hewlett Packard GCD (Model #G1800A) equipped with a quadrupole mass analyzer which identified all species generated during the reaction. The conversion was calculated from the area of the isobutene peak divided by the sum of the areas of all of the peaks detected. The selectivity to isobutene was calculated from the area of the isobutene peak divided by the sum of the areas of all of the products.

To ensure that no heat transport problems occurred, several experiments were performed with a thermocouple in contact with both the top and the bottom of the catalyst bed. During these experiments, the maximum temperature drop reported across the bed was less than 2°C. For a typical activation energy of 20 kcal/mol, this difference, measured at a conversion of 35%, represents a maximum error of ± 1% conversion. This is less than the typical experimental variations in activity due to any of the effects that we have considered in this research. Similarly, the Weisz-Prater criteria for internal diffusion was calculated and the results showed that mass transfer limitations were not present during any of the experiments.

2.3.7 Diffuse Reflectance Infrared Fourier Transform Spectroscopy (DRIFTS)

Infrared Spectroscopy of adsorbed CO were obtained by Adriana Pisanu on a Bio-Rad FTS-40 spectrometer, equipped with a MCT detector.

All of the experiments were conducted in a diffuse reflectance cell from Harrick Scientific, type HVC-DR2 with ZnSe windows. This setup allowed for *in situ* oxidation and reduction. Each IR spectrum consisted of 128 scans added together which were taken at a resolution of 8 cm^{-1}. Before each spectrum, the samples were exposed to cycles of oxidation in air at 300°C followed by reduction in hydrogen at 300°C to remove any impurities on the catalyst. Following this pretreatment, the samples were exposed to CO_2 at 300°C. The IR spectra were recorded while the sample was in the CO_2 atmosphere.

Several experiments were also performed using ethylene to simulate impurities on the support. For these experiments the catalyst was oxidized and reduced as described above and then cooled to room temp while under a flow of He. Subsequently, the sample was exposed to a 1.0 % ethylene in He mixture at room temperature. After this pretreatment, the sample was flushed in Ar, and then heated up to 300°C in Ar while collecting data. After reaching 300°C the sample was flushed in Ar until no change in signal was observed. The sample was then exposed to a series of treatments involving exposure to CO_2, purging in Ar, and then exposure to CO_2. Spectra were recorded during all of the treatments, with primary emphasis being placed on the area in which CO adsorbed on the metal appears.

2.3.8 X-ray Diffraction

X-ray diffraction experiments were carried out using a Rigaku Automatic Difractometer (Model D-MAX A) with a curved crystal monochromator and system setting of 40kV and 30 mA. Data was collected in the angle range of 5.0 to 70.0 degrees with a step size of 0.05 degrees and a count time of 1.0 second. The samples were finely ground and then placed on the glass slide using a smear mount technique.

2.3.9 Transmission Electron Microscopy (TEM)

TEM was performed by Greg Strout at the Samuel Roberts Noble Electron Microscopy Laboratory at the University of Oklahoma on a JEOL 2000FX TEM. After the catalyst was exposed to the specific pretreatment, reduction, or reaction, the sample was then ground into a fine powder and suspended in isopropyl alcohol. One drop of solution was placed on a 0.3 mm diameter Lacey carbon grid (Electron Microscopy Sciences) and allowed to dry.

2.3.10 Chemisorption/Physisorption

Volumetric H_2 chemisorption measurements were performed using two techniques. The first involved the use of a Micromeritics ASAP 2000 system. For each measurement, 0.6 grams of each sample was loaded into the chemisorption cell. The sample was reduced *in situ* at 500°C for 1 hour, evacuated to 10^{-6} Torr at 500°C, and then cooled to 35°C at which the adsorption of H_2 was performed.

The second technique involved the use of a static volumetric adsorption Pyrex system built by Gary Jacobs, equipped with a high capacity, high vacuum station that provided vacuum of the order of 10^{-9} Torr. The catalysts were reduced *in situ*, followed by evacuation at the reduction temperature, and then cooled to 35°C at which the adsorption was performed. Walter Alvarez performed the chemisorption experiments on this system.

The physical properties of the materials were obtained using a Micromeritics ASAP 2010 adsorption apparatus. All of the samples were degassed for approximately 20 hours before starting the experiments.

2.3.11 X-ray Absorption Spectroscopy

Extended X-ray Absorption Fine Structure (EXAFS) and X-ray Absorption Near Edge Spectroscopy (XANES) were performed on beamline X-18B and X-23A2 at the National Synchrotron Light Source at Brookhaven National Laboratory, Upton, New York. The ring energy was 2.5 GeV with a ring current of 80-220 mA. A Si(111) and Si(100) crystal monochromator was used to vary the photon energy incident to the sample. The spectra were recorded near the L_{III}-edge of Pt (11,564 eV) and the K-edge for Sn (29,200 eV) ranging from 50eV below the edge to at least 1000eV past the edge.

For each sample, the optimum mixture of catalyst and diluent (SiO_2/ZrO_2) was determined, thoroughly mixed, and then pressed into pellets. Some EXAFS and XANES experiments were performed on samples that had been prepared in the laboratory at the University of Oklahoma. After

exposure to reaction at 800°C, the pellets were then transferred to a glove bag filled with He, and sealed into holders with Kapton tape, without exposure to air. The samples were then placed into a stainless steel cell, which could be cooled to liquid nitrogen temperatures. Some additional EXAFS and XANES experiments were performed in a stainless steel cell that could be heated to 650°C or cooled to liquid nitrogen temperatures. During these experiments, reductions, and reactions were performed *in situ*. The XANES data collected for these experiments were done under reaction because the high temperatures do not alter the spectra. In contrast, all EXAFS spectra on the reduced samples and those samples exposed to reaction conditions were recorded at liquid nitrogen temperatures.

Data for the SiO_2 supported catalysts was taken in transmission mode. However, the best spectra for the ZrO_2 supported catalysts were obtained in fluorescence mode due to the high absorbency of the ZrO_2. Multiple scans were recorded for each sample, and then added together to minimize any noise in the data. The pre-edge background was subtracted using power series curves, while the post edge subtraction was done with a spline function. All of the spectra were normalized to the height of the adsorption edge. During the analysis of the Pt spectra, the χ data was k^3-weighted to avoid over-emphasizing the low energy region [3], and the range that was utilized in k-space was 3.0 -15.0 A^{-1}.

Theoretical references for Pt-Pt, Pt-Sn, Pt_3-Sn, Sn-0 bonds were obtained by using the FEFF program from the University of Washington [4-6].

The FEFFIT fitting routine was employed by Armando Borgna, to obtain the structural parameters of the Pt and PtSn clusters after the various pretreatments and reactions. The variables that were used in the fitting included the Debye Waller factor (σ), the edge energy difference (ΔE_o), the coordination number (N), and the difference in the bond distances (ΔR) with respect to the theoretical bond distance.

2.4 References

1. De Miguel, S. R., Baronetti, G. T., Castro, A. A., and Scelza, O. A., Appl. Catal., **45**, 61 (1988).
2. Margifalvi, J., Hegedus, M., Gobolos, S., Kern-Talas, E., Szedlacsek, P., Szabo, S., Nagy, F., *in* "Proceedings, 8th Inter, Cong. Catal., Berlin, 1984," Vol. IV, p. 903. Dechema, Frankfurt-am-Main, 1984.
3. D. E. Sayers, B. A. Bunker, "X-ray Absorption: Principles, Applications, Techniques of EXAFS, SEXAFS, and XANES", (D. Koningsberger and R. Prins, editors), Wiley, 1988, P. 211.
4. J. J. Rehr, S. I. Zabinsky, R. C. Albers, *Phys. Rev. Lett.*, **69** (1992) 3397.
4. J. J. Rehr, J. Mustre de Leon, S. I. Zabinsky, R. C. Albers, *J. Amer. Chem. Soc.*, **113** (1991) 5135.
6. J. Mustre de Leon, J. J. Rehr, S. I. Zabinsky, R. C. Albers, *Phys. Rev. B*, **44** (1991) 4146.

CHAPTER 3

SUPPORTED Pt CATALYSTS

ROLE OF THE SUPPORT

3.1 Introduction

As mentioned in Chapter 1, the major obstacle preventing the commercialization of the dry reforming process is the ability of a catalyst to operate at the conditions required by industry. Because the reaction is highly endothermic, high temperatures are required to reach high conversions. These conditions are conducive to carbon deposition via the Boudouard reaction and the decomposition of CH_4 [1]; however, a catalyst capable of operating at such severely deactivating conditions has not been found. Most of the dry reforming research performed thus far has focused on Group VIII metals on a variety of supports [2]. Of the many combinations studied, Rh has emerged as the most active with the least amount of carbon deposition. However, this metal is not commercially feasible due to economic market fluctuations [3-6]. The Ni catalysts, which are less expensive and more abundant, have also received a great deal of attention, but they experience severe deactivation due to carbon deposition [7,8].

Supported Pt catalysts have emerged with a high potential for industrial application [9-15]. Several groups have focused on TiO_2 and ZrO_2 and have found that, on these supports, Pt reaches much higher conversions than when supported on SiO_2 and Al_2O_3. Bradford and Vannice have performed an extensive study of Pt/TiO_2 and model TiO_x/Pt catalysts [14,15].

The results from the model catalyst studies indicate that the activity of the catalyst increases with increasing TiO_x coverage. They attribute this increase to the formation of new metal-support interfacial sites and propose that these sites promote the dissociation of CH_4, the dissociation and reduction of CO_2, and the decomposition of CH_xO [15]. Also, the formation of TiO_x overlayers on the Pt/TiO_2 catalyst was proposed to increase stability due to suppression of carbon deposition via an ensemble effect [14]. Lercher *et al.* [11,13] have also studied TiO_2 as a support, as well as ZrO_2 and Al_2O_3. They have found that, among these three supports, ZrO_2 was the most effective, which resulted in a stable catalyst at 600°C and 1:1 CH_4:CO_2 feed ratio.

One hypothesis about the role of the support that has received significant attention involves the participation of two independent reaction paths [9,11,13]. According to this mechanism, CH_4 decomposition would take place on the metal, resulting in the production of H_2 and the formation of carbonaceous deposits. The role of the support would be to adsorb CO_2 and facilitate dissociation at the metal support interface. In this case, the CO_2 dissociation would result in CO and adsorbed O. The adsorbed O could then react with carbon deposited on the metal to produce additional CO.

The majority of the previous work on Pt/ZrO_2 catalysts has shown that these catalysts exhibit minimal carbon deposition when operating at relatively moderate temperatures (550°C-650°C) and with CH_4:CO_2 ratios less than or equal to unity [9,14,11]. However, the equilibrium conversion of the dry reforming reaction under these conditions is relatively low, i.e., approximately

50%. Furthermore, at low temperatures and low CH_4:CO_2 ratios, a fraction of the H_2 produced is converted to H_2O via the reverse water gas shift reaction (3-1) resulting in a H_2/CO product ratio less than one.

$$H_2 + CO_2 \rightarrow CO + H_2O \qquad \Delta H=40 \text{ kJ/mol} \qquad (3\text{-}1)$$

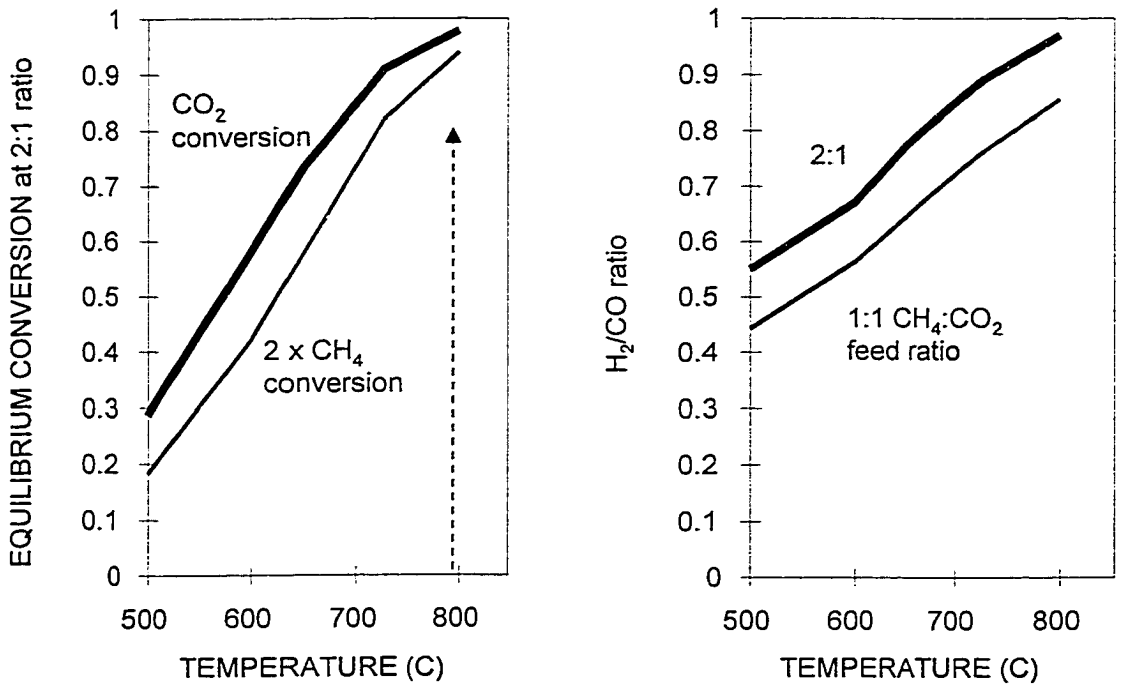

Figure 3.1: Equilibrium conversion and H_2/CO product ratio for CO_2 reforming of CH_4.

Considering the reforming reaction and the reverse water gas shift reaction, high conversions and a product ratio near unity can only be achieved near 800°C [4,5] (Figure 3.1).

Most of the concepts developed from the studies conducted at lower temperatures are not valid for the dry reforming reaction at 800°C. It has been shown [16] that hydroxyl groups remain on the surface of the zirconia up

to 700°C. These OH groups strongly interact with CO_2, which can generate formate and bicarbonate intermediates. However, under industrially relevant conditions (i.e. T>800°C), these species may not play a role. Therefore, detailed studies of the reforming reaction at high temperatures are needed.

This chapter focuses on the investigated ZrO_2-supported catalysts at 800°C, using CH_4:CO_2 ratios of 2:1 and 3:1. These high CH_4:CO_2 ratios accelerate deactivation by favoring carbon formation. These conditions have allowed us to investigate the role of the support in the suppression of carbon formation over relatively short reaction periods.

3.2 Experimental

A combination of the characterization techniques described in the experimental chapter along with catalytic activity measurements have been employed to study Pt/SiO_2 and Pt/ZrO_2 catalysts. Specific details about the preparation method and characterization techniques can be found in Chapter 2.

3.3 Results

3.3.1 Catalytic Activity for Pt/SiO_2 and Pt/ZrO_2

Figure 3.2 shows the CH_4 and CO_2 conversions for the Pt/ZrO_2 and Pt/SiO_2 catalysts at 650°C. The initial conversions of CH_4 and CO_2 were extremely low on the SiO_2-supported catalyst, and they decreased to almost zero after 30 minutes on stream. By contrast, the ZrO_2-supported catalyst

was much more active and did not deactivate during the 2 hour period. The Pt/ZrO_2 sample had a constant H_2:CO ratio of approximately 0.6 throughout the reaction period, while the ratio for the SiO_2-supported catalyst continuously decreased.

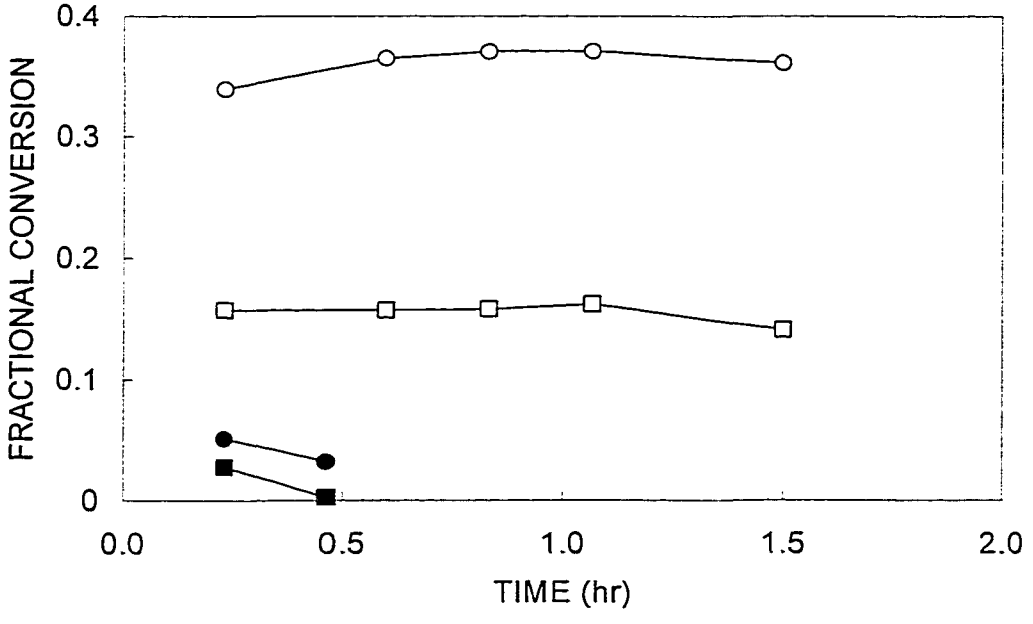

Figure 3.2: Fractional Conversions of CH_4 (squares) and CO_2 (circles) for Pt/SiO_2 (filled) and Pt/ZrO_2 (open) during reaction at 650°C with a CH_4:CO_2 ratio of 2:1.

A more drastic deactivation was observed when the same experiment was performed at 800°C. Figure 3.3 shows the conversion of CH_4 and CO_2 for the Pt/ZrO_2 catalyst during 20 hours of reaction at 800°C with a 2:1 CH_4:CO_2 feed ratio. Initially, the conversion of both CO_2 and CH_4 decreased rapidly, but the decay of the latter was significantly faster. After 4 hours on stream, the rate of deactivation decreased with only a slight drop in activity

over the next 16 hours. The H_2:CO product ratio was initially 1.0 and decreased to approximately 0.5 by the end of the run. The $X_{(CH4)}/X_{(CO2)}$ conversion ratio, which according to the feed composition and stoichiometry of the reforming reaction, should be 0.5, but, was in fact, greater than that at the beginning of the run but decreased to 0.32 with time on stream. Under similar conditions, the Pt/SiO_2 catalysts showed no activity.

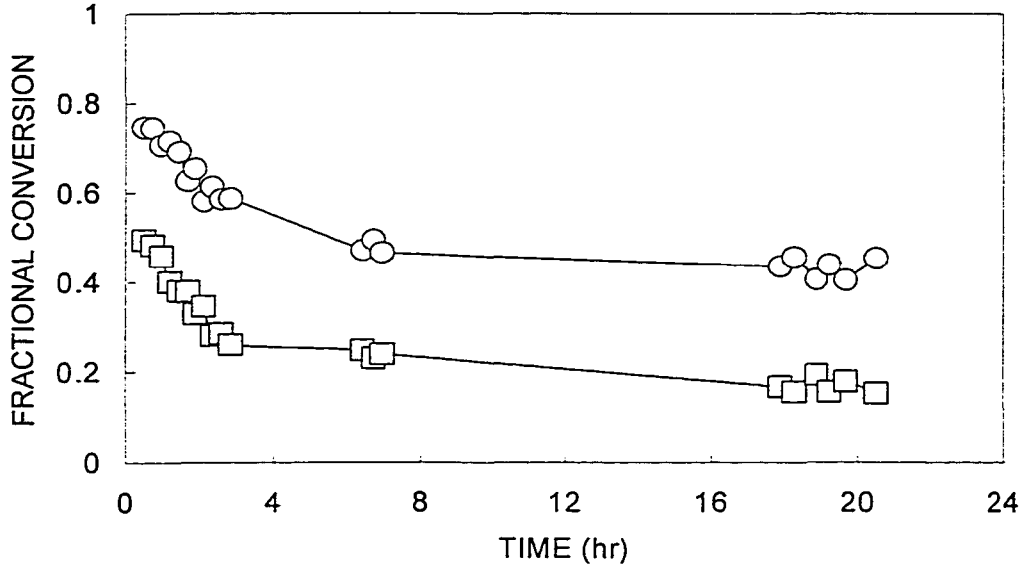

Figure 3.3: Fractional conversions of CH_4 (squares) and CO_2 (circles) for Pt/ZrO_2 during reaction at 800°C with a 2:1 ratio of CH_4:CO_2.

The low activity observed on the Pt/SiO_2 catalyst could be due to sintering of the Pt particles and subsequent carbon formation on the large Pt agglomerates. It is also possible that the morphology of the support can be greatly altered at high temperatures, causing a large reduction of surface area, which would explain the large activity loss observed.

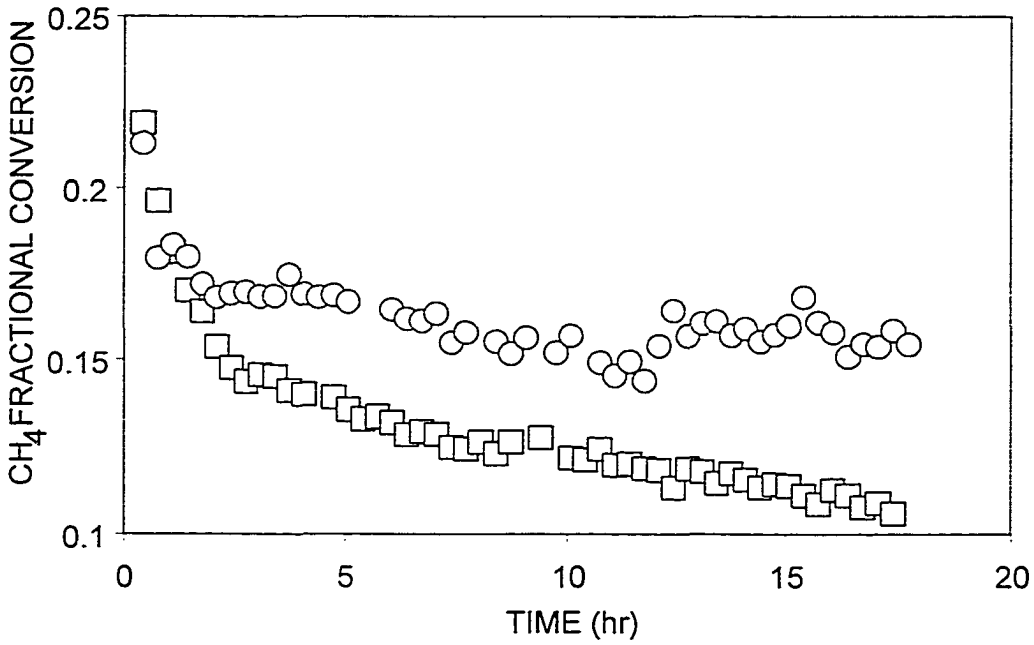

Figure 3.4: Fractional conversion of CH_4 for Pt/ZrO_2 during reaction at 800°C with a 2:1 ratio of CH_4:CO_2 after reduction at 200°C (circles) and 500°C (squares)

Activity studies were also performed on the Pt/ZrO_2 catalyst following calcination at 400°C and reduction at either 200°C or 500°C. These studies were done to probe the extent of metal-support interaction and the effect of this interaction on the activity and stability of the catalyst. It has been suggested [14] that, in some cases, reduction at high temperature leads to partial encapsulation of the metal by the support and the formation of new interfacial sites. The belief is that these new sites stem from the formation of a reduced oxide species that is decorating the particle and is responsible for the improved catalytic performance. Figure 3.4 shows the data for the CH_4 conversion as a function of time on stream for the two reduction temperatures. Both of the catalysts had an initial conversion near 22%.

However, a large difference in the long-term activity was observed with a CH_4 conversion after 18 hours of 10% and 16% for the sample reduced at 500°C and 200°C, respectively.

3.3.2 $^{13}CH_4$ and $^{12}CO_2$ Pulse Experiments

Although a substantial amount of work has been done on the dry reforming reaction, significant debate still exists concerning the reaction mechanism and the role of the metal and support. Isotopically labeled studies afford the opportunity to track the carbon that comes from both the CH_4 and the CO_2, which can provide valuable information about the reaction mechanism. We employed this technique to determine information about the carbon species responsible for deactivation and to determine if the support was participating in the removal of carbon from the metal, as has been previously suggested. Figure 3.5 shows the results of exposing the Pt/ZrO_2 catalyst to pulses of ^{13}C-labeled methane at 800°C. As expected, H_2 was the primary product for both catalysts. However, ^{13}CO and a small amount of $^{13}CO_2$ were also observed. Since the only possible source of oxygen in this experiment was the support, this result suggests that some of the carbon produced from the decomposition of $^{13}CH_4$ was able to partially reduce the oxide support near the perimeter of the particle. Each subsequent pulse resulted in an increase in the amount of unreacted $^{13}CH_4$ and a decrease in the H_2 and ^{13}CO production.

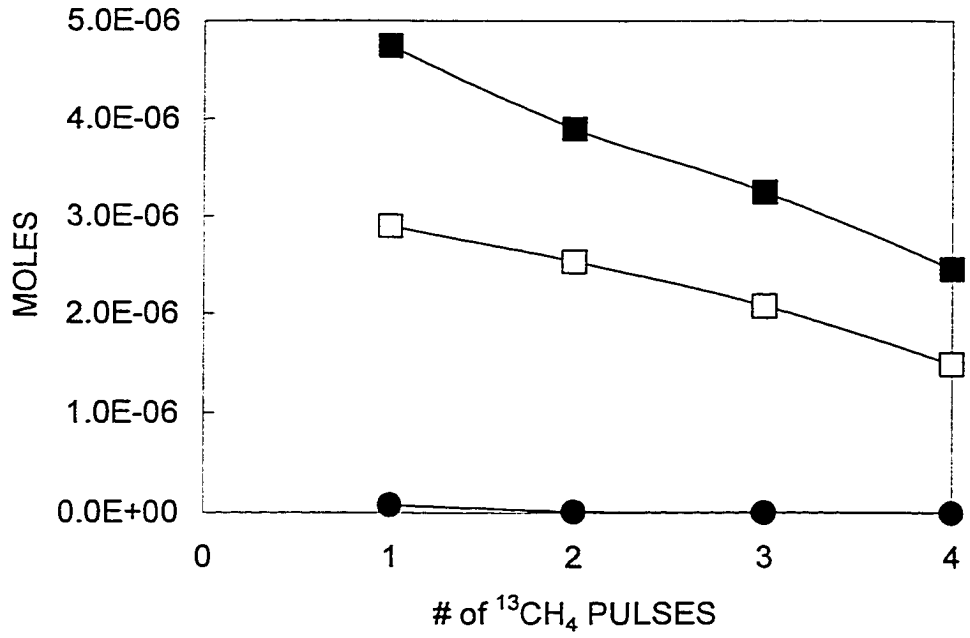

Figure 3.5: Moles of H_2 (■), ^{13}CO (□), and $^{13}CO_2$ (●) produced during $^{13}CH_4$ pulses at 800°C over Pt/ZrO_2.

Following the series of $^{13}CH_4$ pulses, the sample was exposed to 11 pulses of $^{12}CO_2$ (Figure 3.6). For the Pt/ZrO_2 catalyst, the first two pulses resulted in total conversion of $^{12}CO_2$ into ^{13}CO and ^{12}CO. The ^{13}CO comes from the oxidation of ^{13}C-deposited on the metal during the previous $^{13}CH_4$ pulses, while the ^{12}CO comes from the dissociation of $^{12}CO_2$. However, the formation of ^{13}CO and ^{12}CO rapidly dropped after each subsequent pulse, while the amount of unreacted $^{12}CO_2$ increased. No CO_2 dissociation was observed after the sixth pulse. One explanation for the inability to dissociate CO_2 could be oxidation of the Pt metal by the O formed during the dissociation. However, x-ray absorption studies that will be shown later do not indicate any oxidation of the Pt metal. These results suggest that there

are other factors that influence the catalyst's ability to dissociate CO_2.

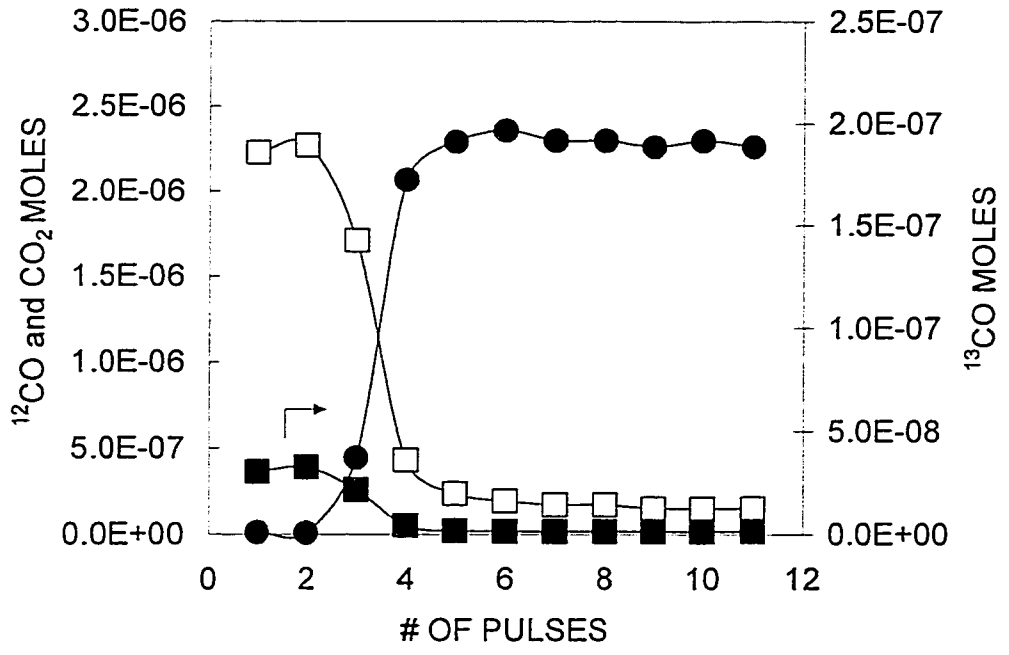

Figure 3.6: Moles of ^{13}CO (■), ^{12}CO (□), and $^{12}CO_2$ (●) produced during $^{12}CO_2$ pulses at 800°C after pulses of $^{13}CH_4$ over Pt/ZrO_2.

3.3.3 XANES and EXAFS

X-ray absorption studies were performed to determine whether the state of Pt was altered during the reaction due to interaction with the support. Analysis of the spectra can be broken into two regions, the near-edge (XANES) and the extended structure (EXAFS). The XANES region contains a first peak, which for Pt and other transition metals, represents the excitation of electrons from filled *p* states to unoccupied *d* states in the absorbing atoms. The size of the first peak (commonly called white line) is an indication of the number of unoccupied *d* states. The EXAFS region consists of fine

structure which appears as oscillations in the absorption spectra. These oscillations arise from the presence of neighbors surrounding the absorbing atom and are a result of the constructive and destructive interference of the outgoing and back-scattered electron. Analysis of the fine structure provides information about the number and type of neighbors surrounding the absorbing atom, as well as the distance between the atom and those neighbors. A more detailed explanation and examples of common transition metals spectra can be found elsewhere [17,18].

Before exposure to reaction, the XANES spectrum of the Pt/ZrO_2 sample (Figure 3.7) looked very similar to that of the Pt foil. The intensity of the first peak (white line) was the same, with only a minor dampening of the second and third oscillations due to the lower coordination of Pt in the catalyst compared to the foil. A slight increase in the intensity of the white line was observed after exposure to reaction at 650°C with a 2:1 feed ratio of CH_4:CO_2. However, the intensity was still much smaller than the white line of an oxidized Pt sample (not shown).

Figure 3.8 makes a comparison of the EXAFS data for the reduced and spent Pt/ZrO_2 catalysts in comparison to the Pt foil. The main peak corresponds to the Pt-Pt bond distance (2.68 Å before correction, 2.77 Å after correcting for phase and amplitude) with the typical satellite peak at approximately 2-2.1 Å. An increase in the magnitude of the Fourier transform was observed after exposure to reaction.

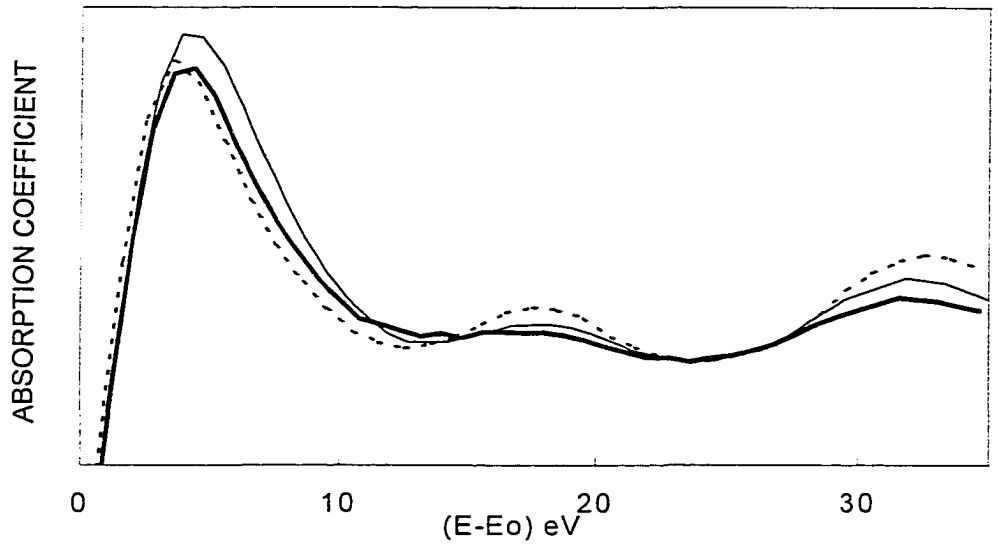

Figure 3.7: XANES spectra of Pt foil (- -), Pt/ZrO_2 before reaction (–), and Pt/ZrO_2 during reaction at 650°C and a 2:1 CH_4:CO_2 ratio (–).

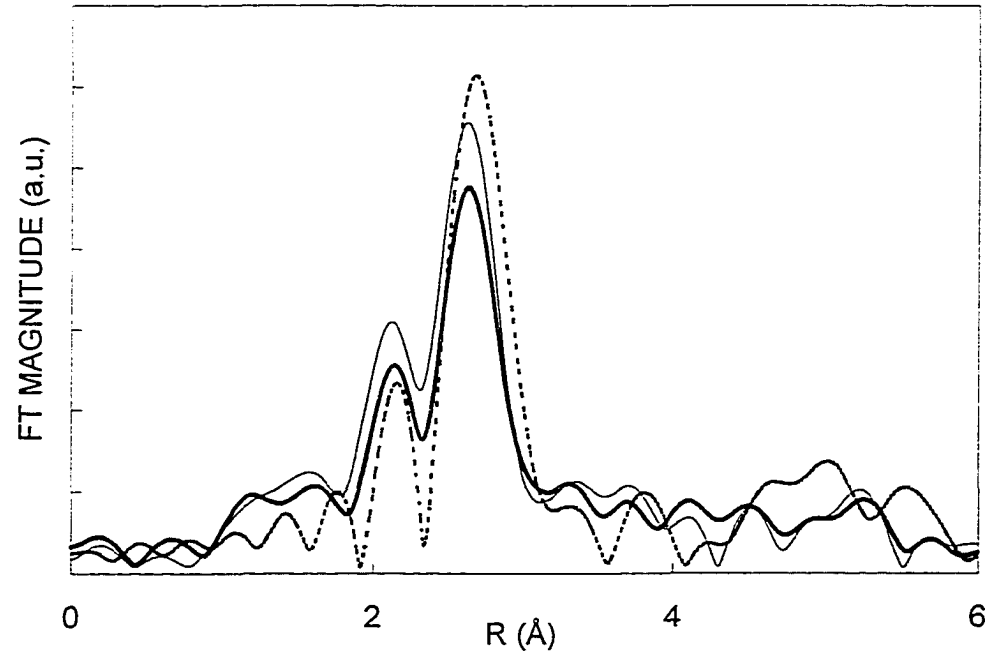

Figure 3.8: EXAFS spectra of Pt foil (- -), Pt/ZrO_2 before reaction (–), and Pt/ZrO_2 after reaction at 650°C and a 2:1 CH_4:CO_2 ratio (–).

Using the FEFFIT program discussed in Chapter 2 and Pt foil (coordination number of 12) as a reference, the average coordination number of the Pt in the Pt/ZrO_2 catalyst under reaction conditions was calculated to be 8.5±0.5.

Figure 3.9 shows the EXAFS spectra for the Pt/ZrO_2 catalyst after reduction at 200°C and 500°C, followed by heating to 800°C in helium. The magnitude of the peak characteristic to the Pt-Pt bond distance is the same for both catalysts after heating to 800°C. This indicates that after heating to 800°C, the size of the Pt particles is approximately the same for the catalysts regardless of the reduction temperature.

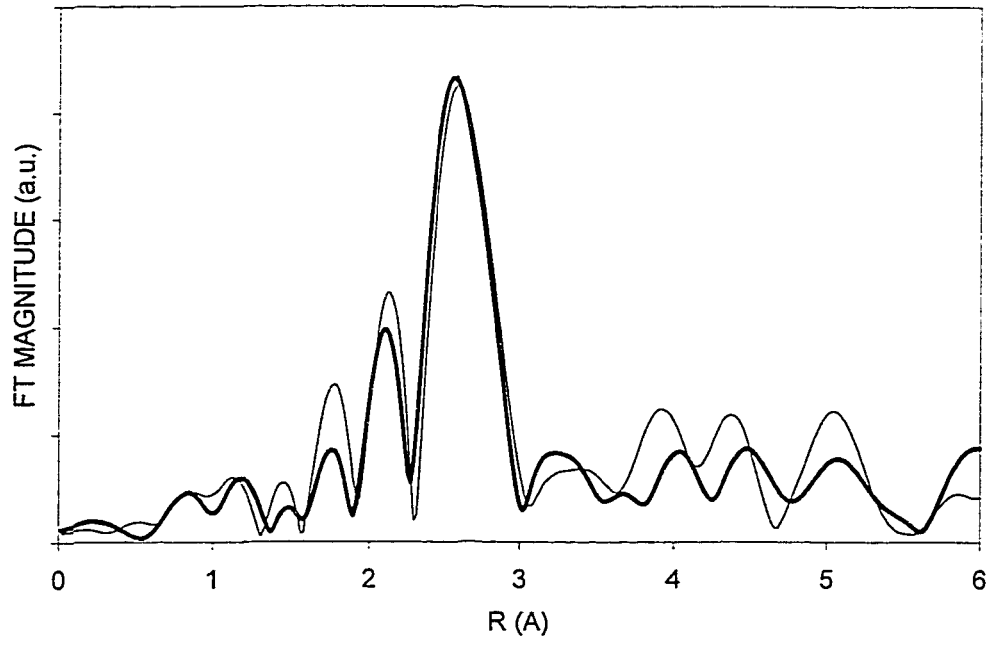

Figure 3.9: EXAFS spectra of Pt/ZrO_2 after reduction at 200°C (–) and reduction at 500°C (–) followed by heating to 800°C in helium.

3.3.4 DRIFTS

Infrared spectroscopy is a valuable technique that can be used to obtain information about the interaction between CO_2 and the metal or support. We employed this technique to study the role of the support in facilitating the dissociation of CO_2. DRIFTS experiments were performed on a Pt/ZrO_2 catalyst which had been previously oxidized at 300°C followed by reduction at 300°C. The oxidation at 300°C prior to reduction was for the purpose of removing any impurities, which may have adsorbed on the support while exposed to air. After flushing in Ar for 30 minutes, the sample was exposed to CO_2 at 300°C. Only gas phase CO_2 was observed with no adsorbed CO being detected. Thus, CO_2 dissociation did not occur on the reduced catalyst.

The same sample was then cooled to room temperature and, while at room temperature, exposed to a mixture of 1.0 % ethylene in He for 30 minutes. The ethylene was adsorbed on the surface to induce carbon impurities on the metal and support. After flushing in Ar, the system was linearly heated to 300°C in an Ar atmosphere. Figure 3.10 shows the spectrum obtained during the temperature ramp. The band near 2070 cm^{-1} that appears during the heating is indicative of CO that is linearly adsorbed on reduced Pt. Since the oxide support was the only source of oxygen in the system for this part of the experiment, the formation of CO can only be formed as a result of the decomposition of ethylene and subsequent reduction

of the oxide support. As the temperature reached 300°C in Ar, the band at 2070 cm^{-1} disappeared indicating the removal of the CO from the metal.

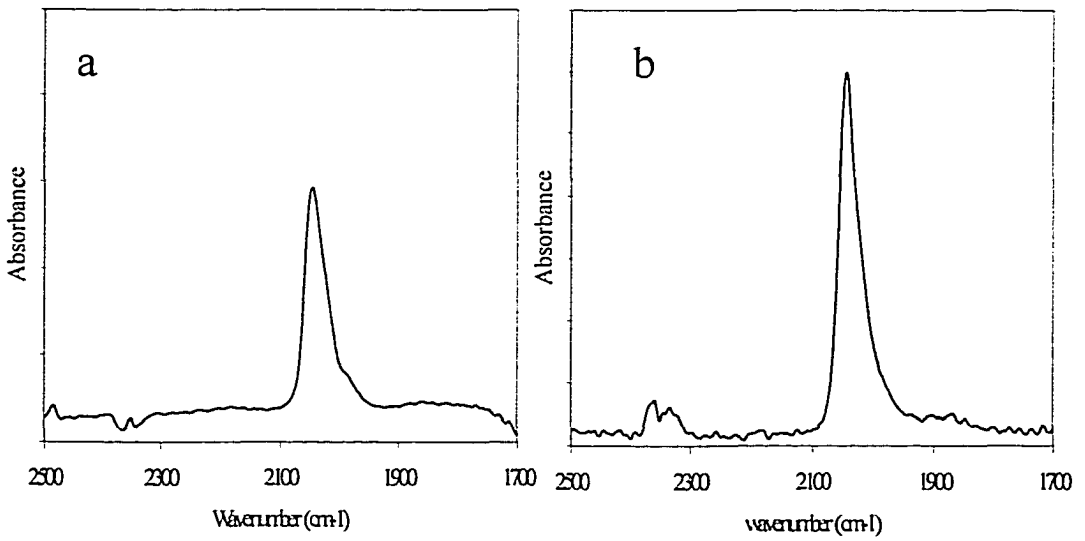

Figure 3.10: DRIFTS spectra of (a) Pt/ZrO_2 while heating to 300°C in Ar after exposure to ethylene at room temperature, and (b) subsequent exposure to CO_2 at 300°C.

After flushing in Ar for 15 minutes at 300°C, the sample was again exposed to CO_2. Unlike the reduced catalyst, Figure 3.10 also shows that exposure to CO_2 after the support had been reduced resulted in the appearance of the band near 2070 cm^{-1}. Thus, after the support had been reduced, linear CO was observed on the metal, as a result of the dissociation of CO_2. The small band at 2350 cm^{-1} is a result of the presence of gas phase CO_2. Subsequently, the sample was flushed in Ar for 30 minutes, and the CO band disappeared with the removal of the adsorbed species from the metal.

Finally, the sample was then re-exposed to CO_2. Only gas phase CO_2 was observed. Therefore, in the absence of the reduced support, no dissociation occurred. These results present strong evidence that the oxygen vacancies play an important role in the reaction mechanism.

3.3.5 Reaction Pulses

Figure 3.11 shows the moles of H_2 and CO produced while exposing the Pt/ZrO_2 catalyst to pulses of CH_4:CO_2 at a 2:1 ratio, CH_4 alone, and CO_2 alone, at 800°C. This experiment was performed in order to observe how exposing the catalyst to only one of the reactants would affect the activity. The first nine pulses contained the reaction mixture, labeled (A) in Figure 3.11. The production of CO and H_2 was approximately 1:1 for the first pulse, but then decreased with each subsequent pulse. The subsequent series of CO_2 pulses (B) produced no H_2. However, the amount of CO produced during the first CO_2 pulse was substantial, equaling the amount produced during the last pulse of the reaction mixture. The last five pulses of CO_2 resulted in minimal CO production.

The next set of pulses (C) that were sent to the reactor again contained the reaction mixture. The amount of CO and H_2 produced from the first pulse of reaction after the pulses of CO_2 was greater than the amount observed during the final pulse of the initial reaction series (A). The observed activity was almost 50% of the initial activity. Again the amount of CO_2 and H_2 decreased during the subsequent reaction pulses.

The next series of pulses (D) sent to the reactor were of pure CH_4. The first pulse produced equal amounts of H_2 and CO. It should be noted that the time between individual pulses is 15 minutes, which is sufficient to flush any remaining oxygen out of the system. Each CH_4 pulse resulted in less H_2 and CO production then the previous pulse due to deactivation from coke deposition. After the CH_4 pulses, the third series of reaction pulses (E) was sent to the reactor. The initial H_2 and CO production was less than the final reaction pulse of the second series (C), but then increased with each pulse, approaching the steady state activity from the last series of reaction pulses (C).

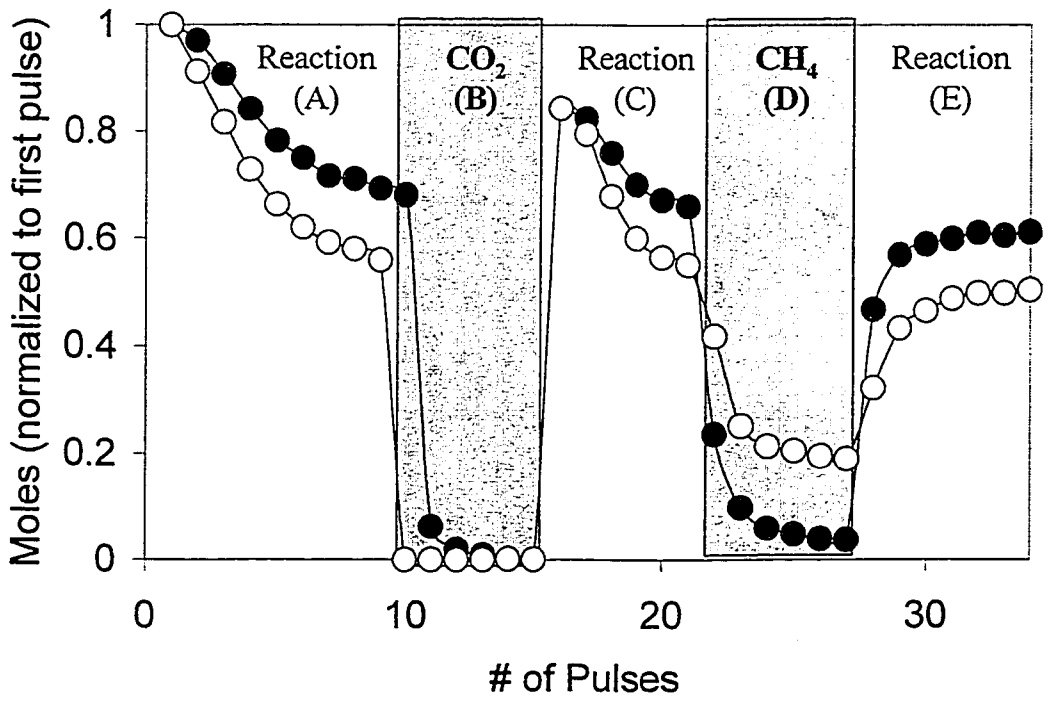

Figure 3.11: CO(●) and H_2 (○) production from pulses of reaction mixture (2:1 ratio of CH_4:CO_2), CH_4, or CO_2 over Pt/ZrO_2 at 800°C.

As will be further discussed in section 3.4, these pulse experiments provide a clear picture of the various steps (oxygen vacancy formation, cleaning mechanism, and CO_2 dissociation) involved in the reaction mechanism.

3.3.6 Chemisorption

Figure 3.12 shows the results of the chemisorption performed on the Pt/ZrO_2 catalyst. The H/Pt ratio obtained for the catalyst after low temperature reduction (200°C) and high temperature reduction (500°C) were very different at 0.66 and 0.05, respectively. After reduction at 500°C, the same sample was oxidized for 1 hour at 80°C and then reduced at 200°C. The treatment resulted in an increase in the H/Pt ratio to 0.18. Another oxidation/reduction cycle was performed with the oxidation temperature being increased to 200°C, followed by low temperature reduction. The H/Pt ratio increased even further to 0.41. Finally, the sample was exposed to oxidation at 500°C and low temperature reduction, which yielded the highest chemisorption value of 0.98. This increase in the chemisorption value after high temperature oxidation is commonly observed when re-dispersion of the metal has occurred. Re-dispersion often results in the formation of a highly dispersed material, with smaller particles than the original sample.

H_2 chemisorption was also performed on samples that had been reduced at either 200°C or 500°C and then heated to 800°C in He. These chemisorption values are better at indicating what the area of exposed metal

surface would be at the reaction temperatures. The H/Pt chemisorption values obtained for this experiment are also shown in Figure 3.12 and they are 0.17 and 0.09, for the catalyst reduced at 200°C and 500°C, respectively.

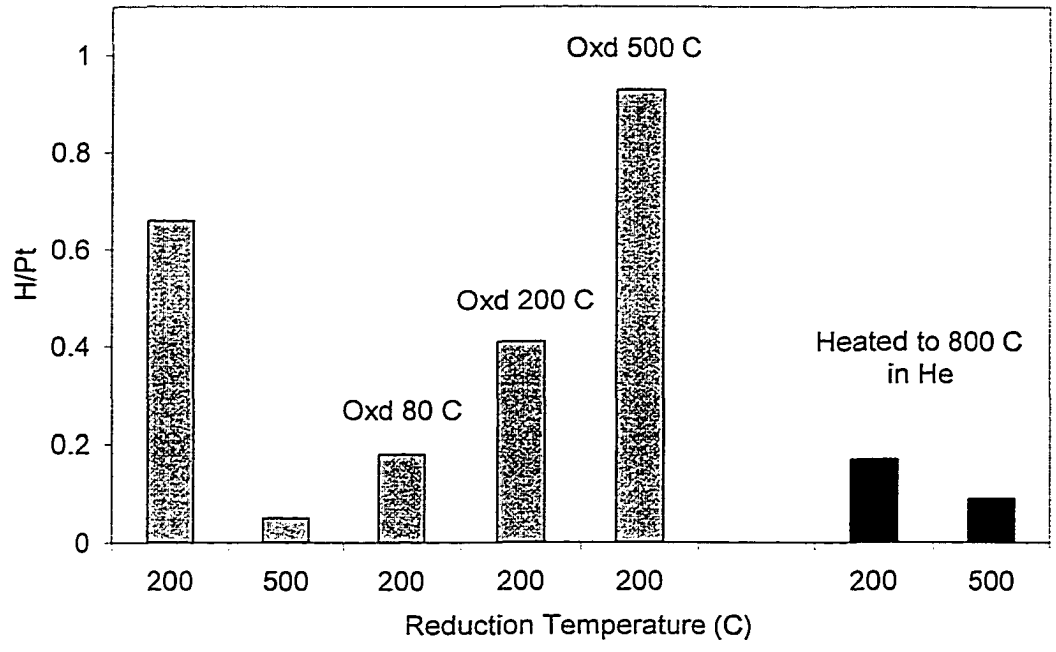

Figure 3.12: H/Pt ratio obtained from H_2 chemisorption on Pt/ZrO_2 after various pretreatments.

3.3.7 Methylcyclopentane Ring Opening Reaction (MCP-RO)

The MCP-RO experiment was performed on a Pt/ZrO_2 catalyst after reduction at various temperatures. The results of these experiments are shown in Figure 3.13. The conversion of MCP to 2MP, 3MP and hexane was held at 8.5% and the reaction temperature required to reach this conversion level was compared. After reduction at 200°C, the reaction temperature

needed to reach 8.5% conversion was 220°C, while after reduction at 500°C, similar conversions could only be obtained after increasing the reaction temperature to 380°C. This corresponds to a 160°C difference in the reaction temperature after reduction at 200°C and 500°C.

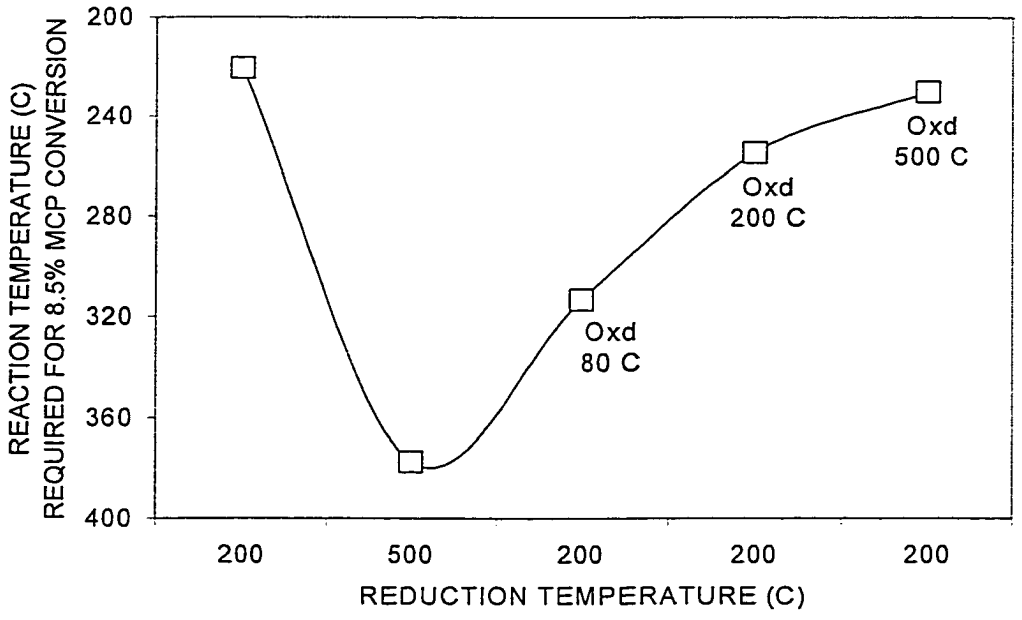

Figure 3.13: Reaction temperature required to obtain 8.5% conversion for the MCP-RO reaction over Pt/ZrO_2 after various pretreatments.

Similar to the chemisorption experiments described in the previous section, after reduction at 500°C the catalyst was exposed to cycles of oxidation and reduction, followed by the MCP-RO reaction. Figure 3.13 clearly shows that with each increase in oxidation temperature, the temperature required to reach the desired conversion decreased. After oxidation at 500°C followed by reduction at 200°C, 8.5% conversion was

achieved at a reaction temperature of 230°C. This is only 10°C above the temperature required for the catalyst reduced at 200°C with no pretreatment.

3.4 Discussion

3.4.1 Role of the Support

The results of this work show that, in agreement with results from previous authors, the support plays a decisive role, by having a strong effect on the activity and the stability of the catalyst. When the Pt/ZrO_2 catalyst was exposed to pulses of $^{13}CH_4$, formation of ^{13}CO, together with small amounts of $^{13}CO_2$, was observed (Figure 3.5). Since the only possible source of oxygen in this experiment was the support, this result suggests that some of the carbon produced from the decomposition of $^{13}CH_4$ was able to partially reduce the oxide support near the perimeter of the particle. The remaining ^{13}C produced from the decomposition of $^{13}CH_4$ was deposited on the Pt metal, possibly as $^{13}CH_x$ species, which explains the observed decrease in the production of H_2 and ^{13}CO with each consecutive pulse. When the same catalyst was subsequently exposed to $^{12}CO_2$ pulses, both ^{12}CO and ^{13}CO were observed. The formation of both ^{12}CO and ^{13}CO supports the idea that carbon is removed from the metal particles under reaction conditions. It must be noted that similar experiments performed on ZrO_2 alone showed that, in the absence of Pt, CO_2 dissociation does not occur. These results indicate that Pt is needed to catalyze the dissociation of CO_2. Consequently, either the dissociation takes place near the metal-support interface, or it occurs on

oxygen vacancies generated during the previous reduction of the support by the methane pulses. The high activity of the ZrO_2 supported catalyst could be due to the ability of the support to be reduced and facilitate in the dissociation of CO_2 and removal of carbon from the metal.

Another explanation that has been offered for the differences observed when comparing the activity of various supports is the ability of ZrO_2 to anchor the Pt particles [11]. Van Keulen and co-workers [19] have also proposed that ZrO_2 has an anchoring effect, but they explain it in terms of a formation of Pt-Zr surface alloys that help to maintain a high Pt dispersion. Analysis of the x-ray absorption data does not show any modification to the Pt by the presence of ZrO_2. If intermetallic compounds were formed, it would be reasonable to expect changes in the density of unoccupied *d* states for the Pt. These modifications would be observed as a change in the intensity of the white line of the Pt L_{III} spectrum. However, the data shows that the spectra for the Pt/ZrO_2 catalyst before and after reaction are very similar to that of the Pt foil. This indicates that the Pt is in an unmodified state and provides evidence against the formation of intermetallic compounds.

Others have suggested that the high activity of the ZrO_2 supported catalyst is due to new interfacial sites that are created during the pretreatment. It has been proposed that these sites stem from the formation of ZrO_x species that are decorating the Pt particle [14]. The results of the characterization using H_2 chemisorption, MCP-RO reaction, and TEM all show strong evidence for the partial encapsulation of the Pt particles by a

reduced ZrO_x species. A substantial decrease in the chemisorption capacity was observed after reduction at 500°C, compared to the sample reduced at 200°C. TEM studies have shown that minimal particle growth occurs after reduction at 500°C, and the loss of metal area due to sintering could not be solely responsible for the loss of chemisorption capacity. The MCP-RO reaction studies clearly show that the temperature required to reach the same conversion for the catalyst reduced at high temperatures is 160°C higher than the catalyst reduced at low temperatures.

The increase in the temperature required to achieve the same conversion is indicative of decoration of the metal by the support and has been previously observed for Rh/TiO_2, and attributed to the strong metal support interaction (SMSI) effect [20]. Stronger evidence for a decoration of the metal by the support is demonstrated by the increase in chemisorption capacity and the increase in the MCP-RO activity after cycles of oxidation and low temperature reduction. Oxidation resulted in a removal of the support from the metal particle, which is demonstrated by the increase in exposed metal area and subsequent reduction in the MCP-RO reaction temperature. This reversibility by oxidation is a fingerprint for partial encapsulation and has been previously observed when studying catalysts that are known to exhibit SMSI, such as Rh/TiO_2 [21], Ni/TiO_2 [22], and Ni/La_2O_3 [23].

The H/Pt ratio after heating to 800°C in He provides a more accurate measurement of the metal area exposed under reaction conditions. The

chemisorption capacity for the catalyst reduced at 200°C was significantly less after heating to 800°C. TEM and EXAFS studies have shown that the loss of Pt surface area is due to sintering of the metal. Similar studies have been performed on the catalyst reduced at 500°C. Again, TEM and EXAFS studies have shown that sintering of the Pt occurs while heating to 800°C, however, the chemisorption capacity increased slightly. These results suggest that while particle agglomeration is occurring which acts to decrease the exposed metal area, at the same time the ZrO_x species is being removed from the Pt to expose more metal area. The final amount of exposed Pt is then a result of the two processes. This hypothesis is supported by the x-ray absorption experiments. Comparison of the EXAFS data for the catalyst reduced at 200°C and 500°C shows that the average Pt particle size is very similar for the two catalysts. Thus, after heating to 800°C, some of the reduced oxide support must remain on the Pt particle, and the partial encapsulation is responsible for the small changes in the chemisorption capacity observed.

Activity studies show that high temperature reduction did not affect the initial activity but resulted in a decrease in the long-term activity of the catalyst. The percent loss of activity after 18 hours was approximately 55% and 28% for the catalysts reduced at 500°C and 200°C, respectively. It is possible that the difference in the stability can be ascribed to the differences in the ability of the support to facilitate the dissociation of CO_2 and the

subsequent cleaning of the carbon from the metal particle. Our studies have shown that the oxygen vacancies created in the support during the decomposition of CH_4 are necessary for the dissociation of CO_2. These vacancies play an important role in the long-term activity of the catalyst. If the reduced oxide species did not have the same capacity for CO_2 adsorption and dissociation, the cleaning mechanism would be inhibited and the stability of the catalyst negatively affected.

It is also possible that during the reaction, the reduced oxide species decorating the Pt particle is removed. During the removal of the species, carbon deposition is occurring on the metal particle. This carbon would then result in a rapid deactivation of the metal and lower long-term activity, because the rate of decomposition is much greater than the rate of cleaning. In either case, the results of our work suggest that partial encapsulation of the metal does occur after high temperature reduction but does not have a beneficial effect on the activity or stability of the catalyst at 800°C. The high activity and stability of the catalyst is not caused by decoration of the Pt by ZrO_x species but is more likely related to the ability of the support to facilitate the dissociation of CO_2.

3.4.2 Role of Metal

The results presented in this chapter support the theory of a two-path mechanism. During the first 4 hours of reaction, at 800°C and a CH_4:CO_2 feed ratio of 2:1, the Pt/ZrO_2 catalyst exhibited a $X_{(CH4)}/X_{(CO2)}$ conversion ratio

greater than 0.5. The rate of deactivation was also very high for this same period (Figure 3.3). This suggests that the rate of CH_4 decomposition is initially greater than the rate of CO_2 dissociation, and that the CH_4 decomposition is responsible for the deactivation of the catalyst. Reaction performed in the absence of the metal resulted in no conversion. These results indicate that the decomposition of CH_4 and the carbon formation both occur on the metal. As the reaction progressed, both the product ratio and conversion ratio decreased. This is a result of a more pronounced inhibition of the CH_4 decomposition compared to that of the CO_2 dissociation.

3.4.3 Cleaning Mechanism

The results of the $^{13}CH_4$ and $^{12}CO_2$ provide strong evidence for the cleaning mechanism being responsible for the long-term stability of the catalyst. The production of ^{13}CO during the $^{12}CO_2$ pulses clearly shows that carbon is being removed from the Pt surface. This removal of carbon results in increased activity as seen in the reaction pulse study shown in Figure 3.11.

One possible cleaning mechanism that has been previously proposed is that the dissociation of CO_2 results in the formation of CO and an adsorbed O, which can then react with the carbon on the metal to form an additional CO and clean the metal particle. Although we see evidence for the cleaning of the metal particle in the presence of CO_2, we do not see any evidence for an adsorbed O species. One might expect that if an O species were adsorbed on the surface, in the absence of carbon on the metal, oxidation of the Pt

metal might occur. This could explain why, during the $^{12}CO_2$ pulses following the $^{13}CH_4$ pulses (Figure 3.5 and Figure 3.6), the dissociation of CO_2 stopped after the sixth pulse. As previously mentioned, Pt is necessary to catalyze the dissociation of CO_2. Therefore, if the Pt metal were being oxidized, the dissociation of the CO_2 would be inhibited. However, our x-ray absorption work does not indicate any oxidation of the Pt metal. This is in good agreement with work done by Lercher and co-workers [11,13].

Another possible mechanism for the removal of carbon from the metal is that the oxygen is provided by the support. The results of the isotopically labeled studies have clearly shown that in the presence of CH_4, partial reduction of the ZrO_2 support occurs. This reduction was also observed during the DRIFTS studies performed on the catalyst. Linear CO was observed on the reduced Pt during the decomposition of ethylene. Since the sample was in an Ar atmosphere, the only source of oxygen was the support. These results support that reduction of the ZrO_2 can occur in the presence of a hydrocarbon. Several experiments have been performed on ZrO_2 alone which show that no reduction of the support occurs in the absence of the metal. This implies that the Pt catalyzes the reduction of the ZrO_2 and that the resultant oxygen vacancies are located near the perimeter of the metal particle.

3.4.4 Role of the Oxygen Vacancies

The role of the oxygen vacancies can be further explained by the

results of the isotopically labeled pulses and the DRIFTS experiments. During the pulses of CO_2 after the $^{13}CH_4$ pulses (Figure 3.6), the dissociation of CO_2 occurred during the first 6 pulses, while the cleaning stopped after the fourth pulse. The results of the DRIFTS experiment suggest that the oxygen vacancies are responsible for dissociation and that the dissociation stops due to the disappearance of these vacancies. When the pre-oxidized and pre-reduced catalyst was exposed to CO_2 at 300°C, no dissociation was observed. However, after exposure to ethylene and heating to 300°C, linear CO was observed on the metal when the catalyst was in a CO_2 atmosphere at 300°C. It is reasonable to conclude that the vacancies formed near the metal particle are facilitating the dissociation of CO_2. Previous results have shown that during the dissociation of CO_2, no oxidation of the Pt metal occurs. Instead, linear CO is adsorbed on the metal, and the remaining oxygen replenishes the vacancy in the support. With the vacancies filled, the dissociation is now inhibited, as seen with the subsequent flushing in Ar and exposure to CO_2. During this portion of the experiment, no dissociation is observed. Thus, the oxygen vacancies are necessary for CO_2 dissociation and are an important factor in the reaction mechanism.

3.4.5 Reaction Mechanism

Figure 3.14 shows a schematic of the two independent paths as well as a concerted mechanism. The first path involves the decomposition of CH_4 on the metal, resulting in a reduction of the support and H_2 production.

During the decomposition, carbon from the CH_4 reduces the ZrO_2 near the metal particle to produce CO. The second path is the dissociation of CO_2, which occurs at the oxygen vacancies formed near the metal particle during the decomposition of CH_4. The dissociation then results in the formation of CO and the replenishing of the oxygen vacancy.

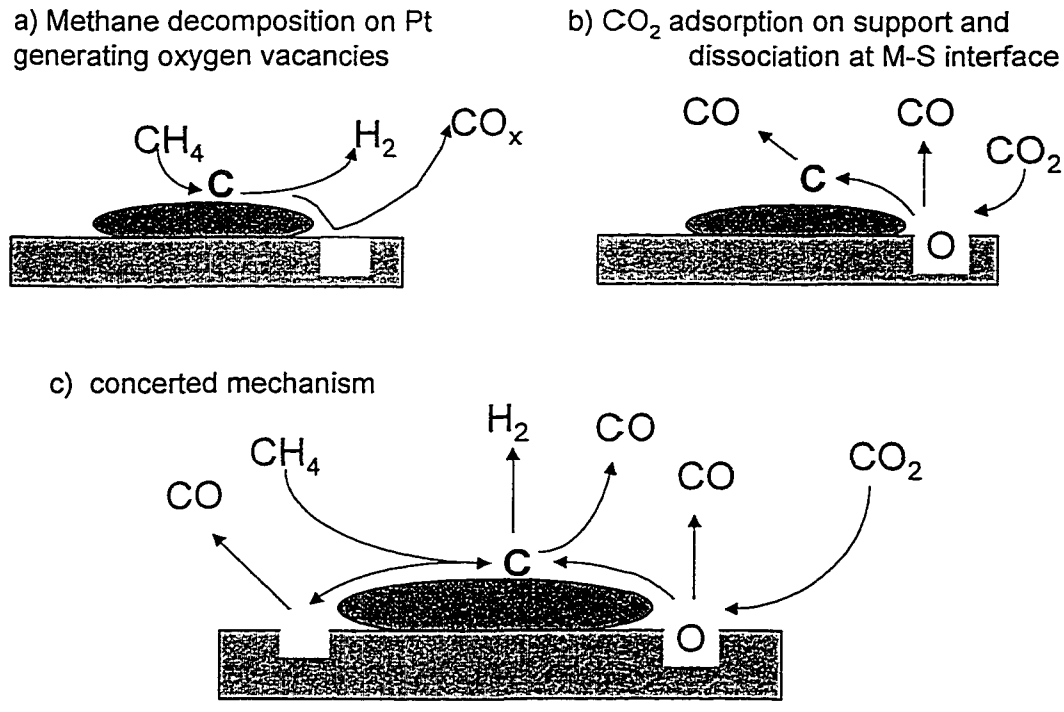

Figure 3.14: Schematic of two independent paths and concerted mechanism of CO_2 reforming of CH_4 at high temperatures over Pt/ZrO_2.

Although the two reaction paths are independent, the stability of the catalyst depends on the balance between the two paths. If the CH_4 decomposition is much faster than the rate of cleaning by CO_2 dissociation, carbon deposition occurs. As shown in the experiments with $^{13}CH_4$ pulses, in

the absence of CO_2, the CH_4 decomposition results in the formation of carbon species on the metal, which leads to rapid deactivation. By contrast, if the CH_4 decomposition becomes too slow, the CO_2 dissociation is inhibited. This effect has been observed during the pulses of CO_2 after the $^{13}CH_4$ pulses (Figure 3.6). The dissociation of CO_2 occurred during the first 6 pulses, while the cleaning stopped after the fourth pulse.

Further evidence for the balance between the rate of cleaning and the rate of deposition determining the long-term activity of the catalyst is provided by the reaction pulse experiments. During all three reaction pulse sets, the final activity of the catalyst approached the same value. More importantly, the production of H_2 and CO increases with each subsequent pulse in the last set of pulses. This can be explained by considering the state of the metal particle surface and the surrounding support after the pulses of CH_4 without any CO_2 present. The metal particle should have a large amount of carbon deposited on it, and the support near the perimeter of the particle will be almost completely reduced. The coke on the metal particle is now acting to inhibit the decomposition of methane, by physically blocking active metal sites. However, the support near the metal particle is sufficiently reduced to facilitate the adsorption and dissociation of CO_2. The dissociation helps replenish the oxygen vacancies, which then allows for the cleaning of the metal particle by the combination of carbon on the metal and oxygen from the support. Each pulse results in increased activity as the cleaning rate and the rate of CH_4 decomposition come into balance.

3.5 Conclusions

The support plays a significant role in determining the activity and stability of the catalyst by promoting the dissociation of CO_2. Supports that can adsorb CO_2 and maintain high surface area at high temperatures perform much better than those that cannot. ZrO_2 supported catalysts exhibit high activity and stability for the reforming reaction. On Pt/ZrO_2 catalysts the mechanism for the reforming reaction involves two independent paths. The first path is the decomposition of CH_4 on the metal resulting in the formation of H_2 and the reduction of the support near the metal particle. The second path involves the adsorption of CO_2 at the site of the oxygen vacancy, followed by dissociation, which produces CO and replenishes the oxygen of the support. The balance between the rate of CH_4 decomposition and the rate of CO_2 dissociation determines the overall stability of the catalyst.

3.6 References

1. Bhat, R. N., and Sachtler, W. M. H., *Appl. Catal. A,* **150**, 279 (1997).
2. Rostrup-Nielsen, J. R., and Bak Hansen, J-H., *J. Catal.*, **144**, 38 (1993).
3. Qin, D., and Lapszewicz, J., *Catal. Today,* **21**, 551 (1994).
4. Edwards, J. H., and Maitra, A. M., *Fuel Processing Tech.,* **42**, 269 (1995).
5. Tsipouriari, V. A., Efstathiou, A. M., Zhang, Z. L., and Verykios, X. E., *Catal. Today,* **21**, 579 (1994).
6. Sakai, Y., Saito, H., Sodesawa, T., and Nozaki, F., *React. Kinet. Catal. Lett.,* **24**, 253 (1984).
7. Hally, W., Bitter, J. H., Seshan, K., Lercher, J. A., and Ross, J. R. H., *Stud. Surf. Sci. Catal.,* **88**, 167 (1994).
8. Kroll, V. C. H., Swaan, H. M., and Mirodatos, C., *J. Catal,.* **161**, 409 (1996).

9. Ross, J. R. H., van Keulen, A. N. J., Hegarty, M. E. S., and Seshan, K., *Catal. Today,* **30**, 193 (1996).
10. Stagg, S. M., and Resasco, D. E., *Stud. Surf. Sci. Catal.,* **111**, 543 (1997).
11. Lercher, J. A., Bitter, J. H., Hally, W., Niessen, W., and Seshan, K., *Stud. Surf. Sci. Catal.,* **101**, 463 (1996).
12. Hally, W., Bitter, J. H., Seshan, K., Lercher, J. A., and Ross, J. R. H., *Stud. Surf. Sci. Catal.,*. **88**, 167 (1994).
13. Bitter, J. H., Seshan, K., and Lercher, J. A., *J. Catal.,* **171**, 279 (1997).
14. Bradford, M., Vannice, M. A., *J. Catal.,* **173**, 157 (1998).
15. Bradford, M., Vannice, M. A., *Catal. Lett., **48,*** 31 (1997).
16. Stoppek-Langner, K., Goldwasser, J., Houalla, M., and Hercules, D. M., *Catal. Lett.,* **32**, 263 (1995).
17. Niemantsverdriet, J.W., "Spectroscopy in Catalysis", VCH, New York, 1995.
18 . Thomas, J. M., and Thomas, W. J., "Principles and Practice of Heterogeneous Catalysis", VCH, New York, 1996.
19. van Keulen, A. N. J, Hegarty, M. E. S, Ross, J. R. H., and van den Oosterkamp, P. F., Natural Gas Conversion Meeting, South Africa Nov. 1995
20 Fenoglio, R. J., Nunez, G. M., and Resasco, D. E., *J. Catal.*, **121**, 77 (1990).
21. Haller, G. L., and Resasco, D. E., *Advances in Catalysis*, **36** 173 (1989).
22. Bradford, M. J. C., Vannice, M. A., *Appl. Catal.* **142**, 73,97 (1996).
23. Zhang, Z. and Verykios, X. E., *Appl. Catal. A:Gen.*, **138**, 109 (1996).

CHAPTER 4

PROMOTION OF THE METALLIC PHASE

4.1 Introduction

Chapter 3 discusses the role of the ZrO_2 in facilitating the cleaning of the metal particle, and emphasizes the two-path mechanism. As stated in the introduction, the goal of our work was to increase the stability of the catalyst by decreasing carbon deposition. One possible way to achieve this is to add a promoter to the metallic phase to inhibit the decomposition of CH_4. The ability of a promoter to alter the catalytic properties of supported transition metal catalysts has been known for decades [1]. The addition of Re, Sn, and Ir to Pt/Al_2O_3 reforming catalysts has a profound effect on the stability of the catalyst by substantially reducing carbon deposition [2-4]. More recently, the interest for bimetallic catalysts has grown further [5,6], especially for Pt catalysts promoted with Sn. These catalysts do not require complex activation procedures, which make them the preferred catalyst for continuous regeneration processes [7,8]. Promotion with Sn has also been shown to result in high activity for the dehydrogenation of lower alkanes [9-12]. Recent work has shown that on SiO_2-supported Pt catalysts, Sn could be effectively used as a promoter to reduce the carbon deposited during the dehydrogenation of isobutane [Appendix A]. The initial activity of the promoted catalyst was found to be lower than that for the unpromoted catalyst, but the stability and selectivity of the catalyst were greatly improved.

One explanation for the enhanced stability of the promoted catalysts is the formation of alloys between the Pt and the Sn, which reduces the size of Pt ensembles [5,13,14]. This reduction in the size of Pt ensembles results in a decrease in carbon formation and an increase in selectivity to the desired products. Reactions such as hydrogenolysis, isomerization, and coking reactions are structure sensitive reactions, which require large Pt ensembles to occur. The activity and selectivity of these reactions are highly dependent upon the structure around the metal atom [15]. The formation of Pt-Sn alloys can alter the structure around the Pt, reducing the number of Pt atoms exposed for reaction. This alteration can negatively affect the activity towards coking and other undesired side reactions. In contrast, dehydrogenation is a structure insensitive reaction, requiring very small ensembles of surface Pt [5]. The formation of Pt-Sn alloys does not modify the ensembles enough to alter the activity towards dehydrogenation. Because the undesired reactions are inhibited and the desired reaction in not affected an overall increase in the selectivity and stability of the catalyst is observed.

Another explanation that has been offered for the enhanced activity and stability of the bimetallic catalyst stems from the idea that the promoter is modifying the catalytic properties of the Pt by electronic or ligand effects [16,17]. X-ray absorption studies have shown that in the presence of a promoter, changes in the absorption spectra occur. These changes have been ascribed to a transfer of electrons from the Sn to the Pt reducing the number of unfilled *d* states of the Pt. It has more recently been suggested

that the intermetallic interactions occur through *sp* orbitals, and then, any effect on the *d* orbitals is only an indirect effect of the donation of *p* electrons from Sn to Pt [18]. In either case, these modifications to the electronic properties can be responsible for large changes in the heat of adsorption of different adsorbates participating in the reaction [19,20]. These changes in the heat of adsorption can have a large effect on the reactivity of species on the catalyst, which in turn, can alter the catalytic performance.

Both the alkane dehydrogenation and CO_2 reforming reactions are highly endothermic and are prone to deactivation from carbon deposition. Based on the success observed for the suppression of coke formation by the addition of Sn in the dehydrogenation studies [Appendix A], it is logical to suggest that the addition of Sn to the Pt/ZrO_2 catalyst might result in less carbon formation and higher stability for the reforming reaction. This chapter focuses on the addition of Sn to supported Pt catalysts for the reforming reaction at 650°C and 800°C, using CH_4:CO_2 ratios of 1:1, 2:1 and 3:1. Higher CH_4:CO_2 ratios accelerate deactivation by favoring carbon formation. These conditions have allowed us to investigate the role of the promoter in the suppression of carbon formation over relatively short reaction periods.

4.2 Experimental

A combination of the characterization techniques described in the experimental chapter along with catalytic activity measurements have been employed to study $Pt\text{-}Sn/SiO_2$ and $Pt\text{-}Sn/ZrO_2$ catalysts. Specific details

about the preparation method and characterization techniques can be found in Chapter 2.

4.3 Results

4.3.1 Catalytic Activity for Pt/SiO_2 and $Pt-Sn/SiO_2$

Figure 4.1 shows the CO_2 and CH_4 conversion for the Pt/SiO_2 and $Pt-Sn/SiO_2$ (Cl) catalysts at 650°C and a 1:1 feed ratio of CH_4:CO_2. The monometallic sample exhibited a high initial CO_2 conversion but, due to rapid deactivation, the conversion dropped below that of the bimetallic after only 25 minutes. The initial CH_4 conversion of the bimetallic catalyst was much lower than that of the monometallic catalyst, but both samples exhibited the same conversion after approximately 40 minutes of reaction.

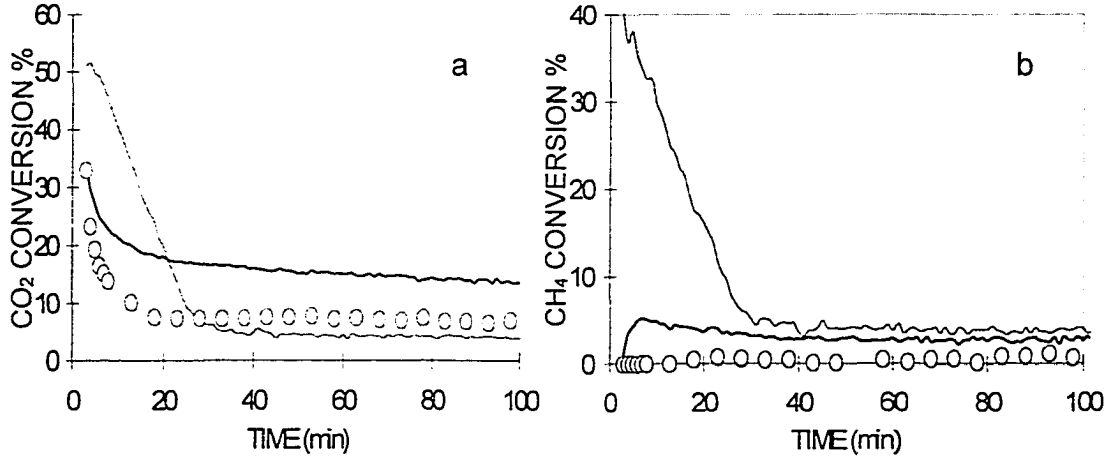

Figure 4.1: CO_2 (a) and CH_4 (b) conversion for reaction at 650°C with a 1:1 ratio of CH_4:CO_2 over Pt/SiO_2 (–), $Pt-Sn/SiO_2$ (Cl) (–) and $Pt-Sn/SiO_2$ (Cl) regenerated (O).

Figure 4.1 also shows the data for a Pt-Sn/SiO_2 (Cl) after regeneration. The regeneration treatment involved heating in a 5% O_2/He mixture to 650°C at a rate of 8°C/minute followed by treatment in pure air (30 cm^3/minute) at 650°C for 30 minutes. The sample was then reduced for 1 hour in H_2 at 500°C and exposed to reaction at 650°C. The same initial conversion was observed as for the fresh bimetallic sample, however, the conversion rapidly decreased to that of the monometallic sample. These results indicate that the promotional benefits of Sn are not maintained through the regeneration process.

4.3.2 Temperature Programmed Oxidation of Pt-Sn/SiO_2

Figure 4.2 shows the TPO of carbon deposits after reaction at 650°C. The carbon on the unpromoted Pt sample required higher temperatures for removal which is characteristic of carbon that is more graphitic. The Pt/SiO_2 also had a larger amount of carbon than the Pt-Sn/SiO_2 catalyst. The amount of carbon formed on the Pt and Pt-Sn catalysts were 6 and 1 mmol of C/gram of catalyst, respectively.

When the ratio of CH_4:CO_2 was varied, the amount of carbon changed significantly. The amount of carbon increased as the ratio of CH_4 to CO_2 increased. When no CO_2 was present in the feed, substantially more carbon was formed on both samples. In contrast, when no CH_4 was present, no carbon deposition was observed for either sample.

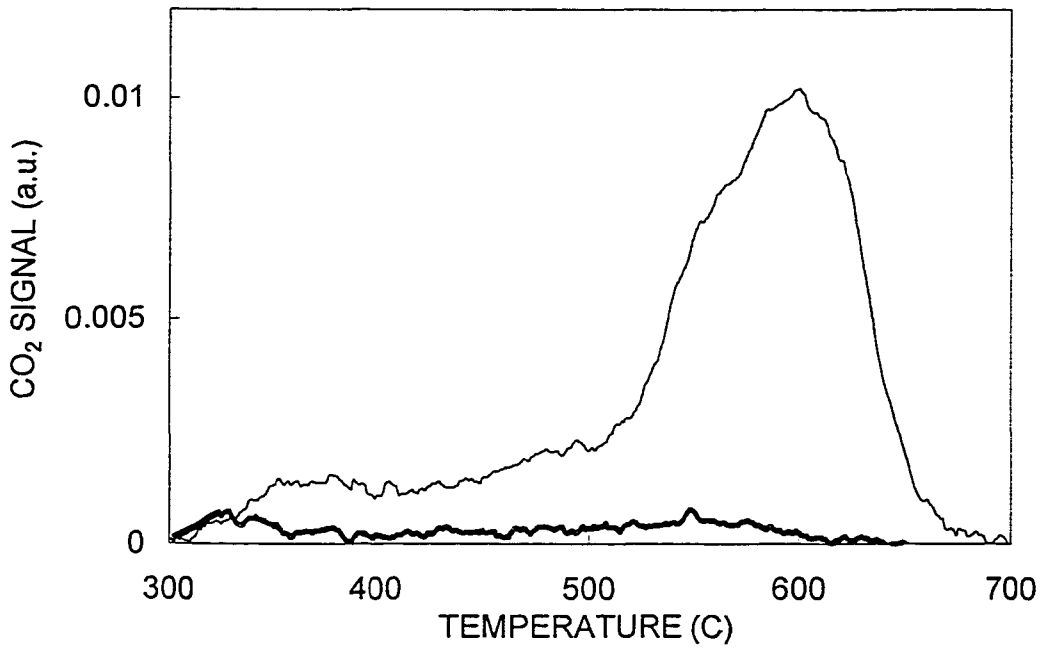

Figure 4.2: TPO spectra for Pt/SiO_2 and $Pt\text{-}Sn/SiO_2$ (Cl) after reaction at 650°C and a CH_4:CO_2 ratio of 1:1. CO_2 signal in arbitrary units.

4.3.3 Catalytic Activity for $Pt\text{-}Sn/ZrO_2$

As shown in Figure 4.3, the addition of Sn to the Pt/ZrO_2 catalyst by co-impregnation resulted in a decrease in both the CH_4 and CO_2 conversion when operating at 800°C and at a feed ratio of 2:1 CH_4:CO_2. Although the deactivation rate of the $Pt\text{-}Sn/ZrO_2$ (Cl) catalyst was slightly lower than that of the Pt/ZrO_2 catalyst, unlike the SiO_2 supported catalysts, the bimetallic ZrO_2 supported sample was less active than the monometallic sample even after 20 hours on stream (not shown).

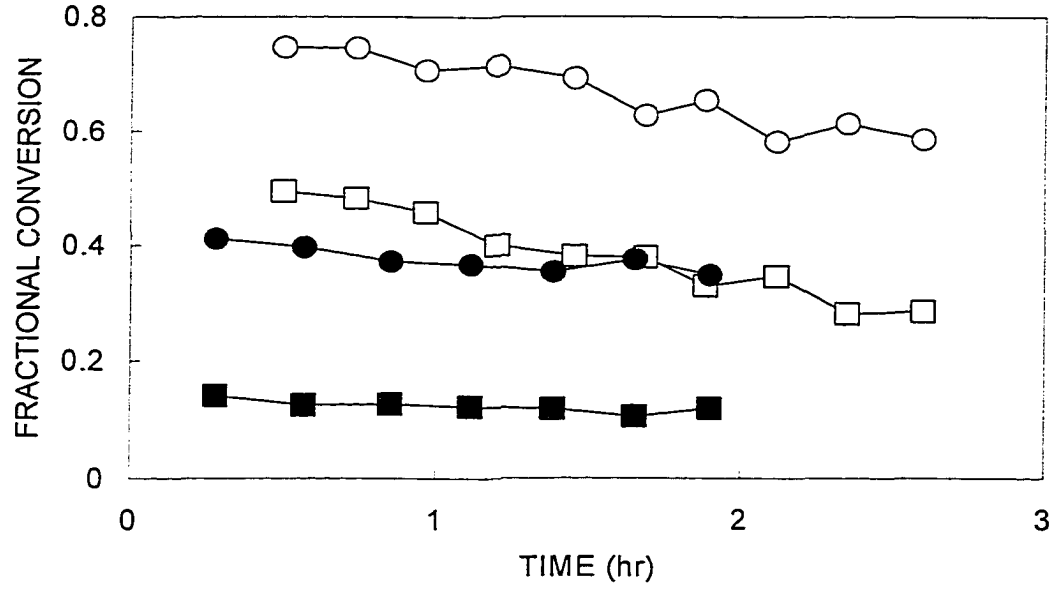

Figure 4.3: Fractional conversion of CH_4 (squares) and CO_2 (circles) for Pt-Sn/ZrO_2 (Cl) (filled) and Pt/ZrO_2 during reaction at 800°C with a CH_4:CO_2 ratio of 2:1.

Figure 4.4 shows the CO_2 conversion for the Pt-Sn/Pt and Pt-Sn (SR) catalysts compared to the Pt-Sn/ZrO_2 (Cl) at 800°C and a 2:1 CH_4:CO_2 feed ratio. The conversion of CO_2 was higher for the Pt-Sn/Pt and Pt-Sn (SR) preparations, approaching the conversion of the monometallic sample. Similar trends were observed for the CH_4 conversion. The H_2:CO ratio was measured for both the Pt-Sn (SR) and the Pt-Sn/Pt samples and, during the 20 hours of reaction, the values ranged from 0.9 to 0.65 and 0.75 to 0.5, respectively.

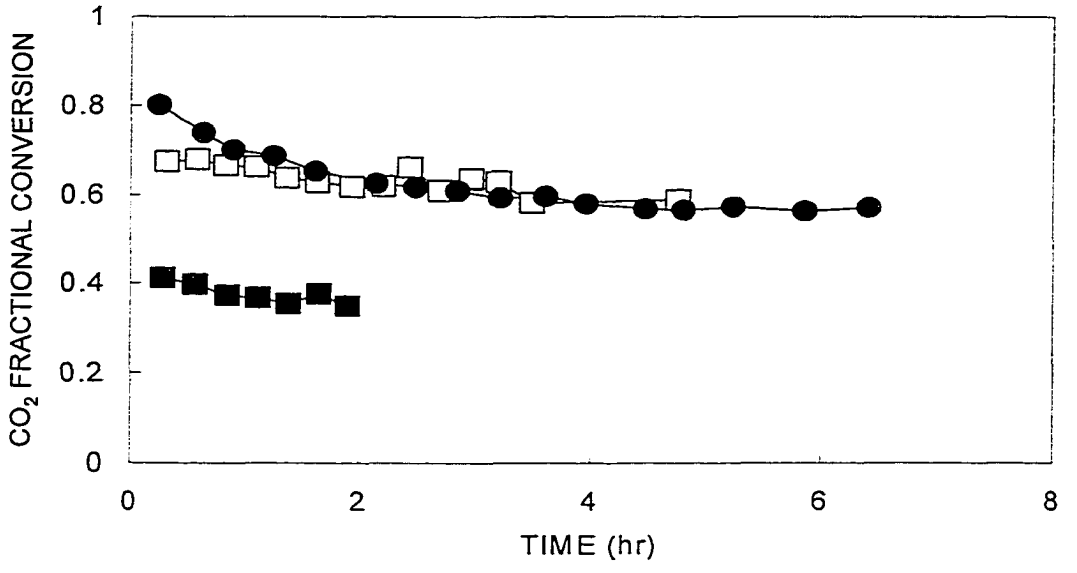

Figure 4.4: Fractional conversion of CO_2 for Pt-Sn/ZrO_2 (Cl) (■), Pt-Sn/Pt (□), and Pt-Sn (SR) (●) during reaction at 800°C with a CH_4:CO_2 ratio of 2:1.

When the CH_4:CO_2 feed ratio was increased to 3:1, larger differences were observed among the catalysts. Figure 4.5 compares the CO_2 conversion for all of the ZrO_2 supported samples discussed thus far at 800°C and the higher CH_4:CO_2 feed ratio. Under these conditions, the co-impregnated Pt-Sn/ZrO_2 exhibited the lowest conversion. On the other hand, the Pt-Sn/Pt and Pt-Sn (SR) catalysts showed much higher activity than both the co-impregnated bimetallic and the monometallic sample. The initial conversion of the Pt-Sn/Pt and Pt-Sn (SR) was 0.88, which was higher than the conversion (0.61) observed for the monometallic sample. The bimetallic Pt-Sn/Pt catalyst appeared to be the most stable under these severely deactivating conditions with a conversion after 4 hours of 0.75. The catalyst

prepared by surface reduction deposition Pt-Sn (SR) exhibited a greater rate of deactivation with a conversion after 4 hours of 0.68.

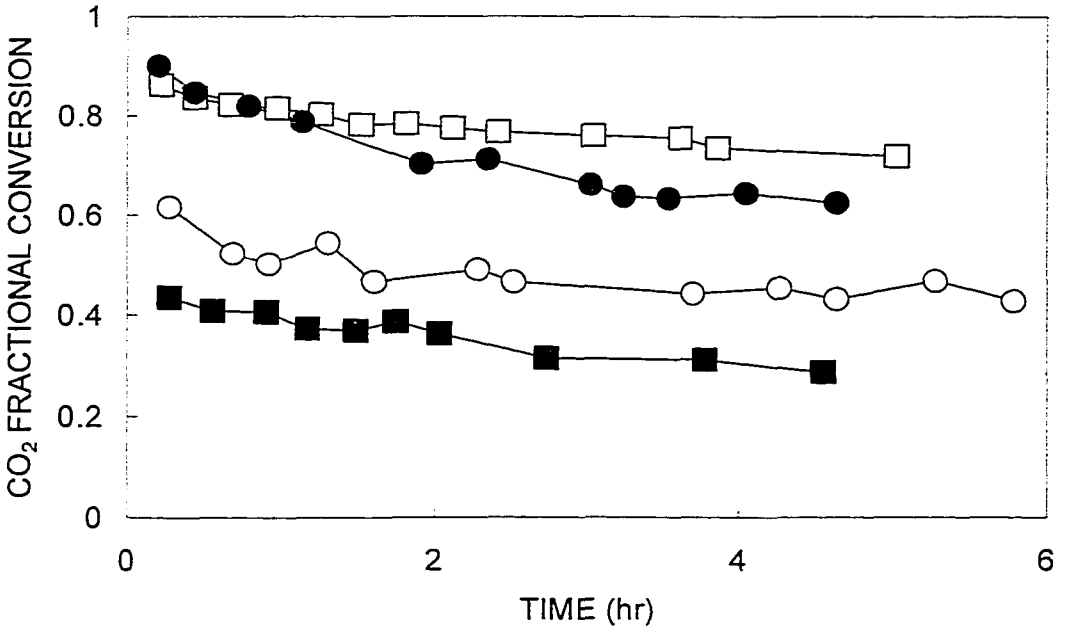

Figure 4.5: Fractional conversion of CO_2 for Pt/ZrO_2 (○), $Pt\text{-}Sn/ZrO_2$ (Cl) (■), Pt-Sn/Pt (□), and Pt-Sn (SR) (●) during reaction at 800°C with a CH_4:CO_2 ratio of 3:1.

Comparison of the two preparations shows that the Pt-Sn/Pt sample exhibited substantially less deactivation than the Pt-Sn (SR) sample. The conversion after 18 hours on stream (Figure 4.6) was 0.6 for the Pt-Sn/Pt, while the Pt-Sn (SR) had deactivated to approximately 0.3, near the conversion for the monometallic sample.

Figure 4.6 also shows how the activity of a deactivated catalyst was affected by temporarily stopping the flow of either CH_4 or CO_2 for the Pt-Sn/Pt and Pt-Sn (SR) samples after reaction at 800°C and a 3:1 CH_4:CO_2 ratio.

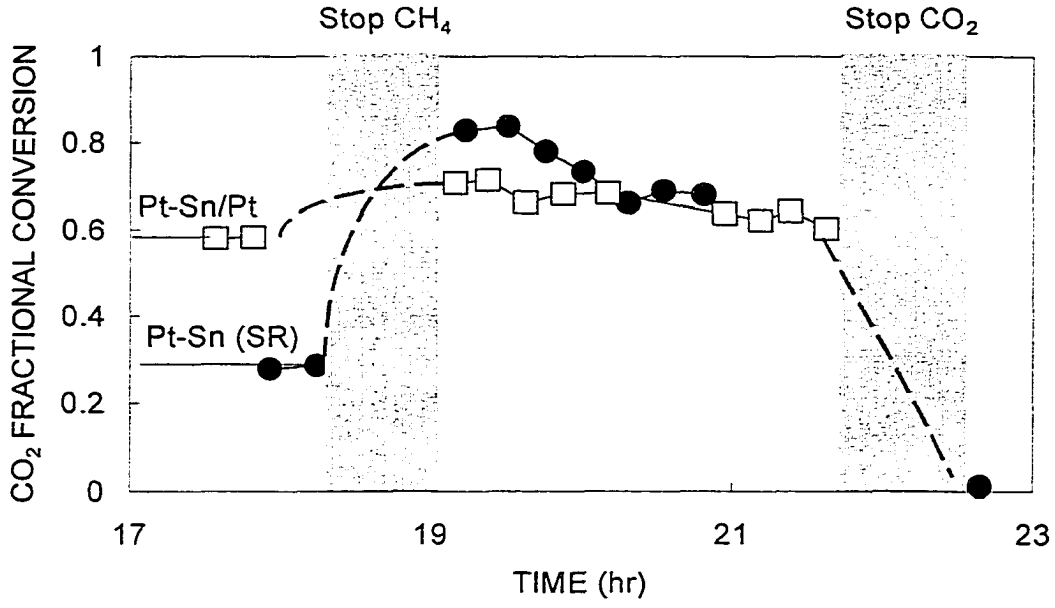

Figure 4.6: Effect of temporarily stopping the flow of one of the reactants on the CO_2 conversion for deactivated Pt-Sn/Pt (□) and Pt-Sn (SR) (●) samples after 18 hours of reaction at 800°C and a 3:1 ratio of CH_4:CO_2.

After 18 hours of reaction, the flow of CH_4 was stopped and only CO_2 was sent to the reactor. The flow of CH_4 was resumed after 45 minutes, and the catalyst was again exposed to the reaction mixture. The Pt-Sn (SR) sample showed the greatest increase in CO_2 conversion after stopping the flow of CH_4, reaching approximately 90% of the initial conversion, which as shown in Figure 4.7 was about 0.88. However, during the subsequent 2 hours of reaction, the activity of the Pt-Sn (SR) catalyst decreased to that of the Pt-Sn/Pt sample. The conversion for the Pt-Sn/Pt catalysts did not increase significantly after exposure to CO_2, but this catalyst experienced a lower extent of deactivation during the initial 18 hours on stream.

The increase in the activity after exposure to CO_2 indicates that some removal of the carbon from the metal particle has occurred. These results suggest that by varying the preparation method, it is possible to hinder the formation of carbon on the metal without inhibiting the role of the support.

After a subsequent 2 hour reaction period, the flow of CO_2 was stopped for 45 minutes and the catalyst was exposed to CH_4. As shown in Figure 4.6, no activity was observed on either catalyst when the flow of CO_2 was resumed. It is logical that the catalyst has been completely deactivated due to carbon deposition in the absence of CO_2.

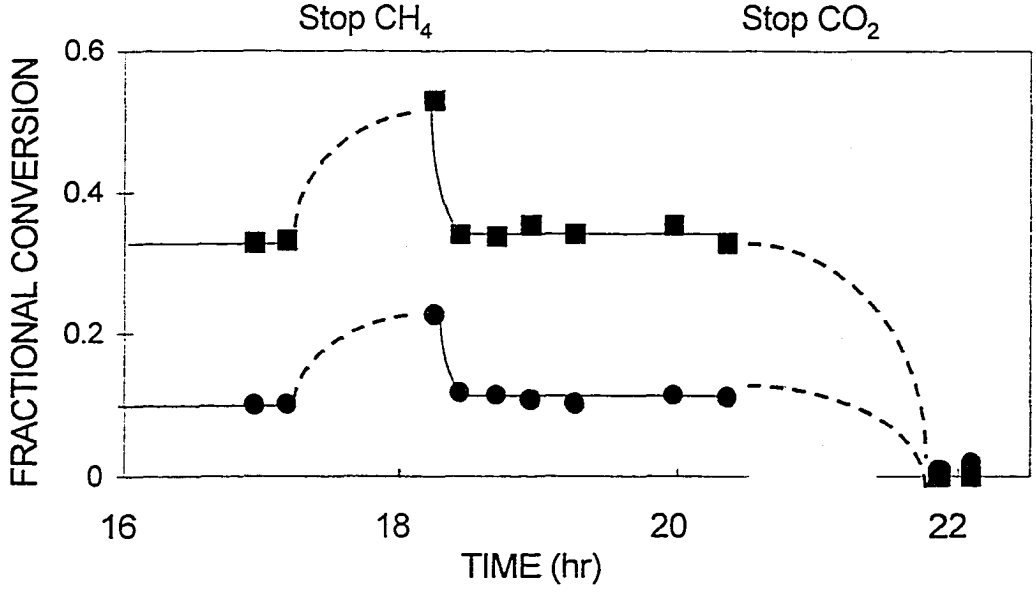

Figure 4.7: Effect of temporarily stopping the flow of one of the reactants on the CO_2 (■) and CH_4 (●) conversion for deactivated Pt/ZrO_2 catalyst after 18 hours of reaction at 800°C and a 3:1 ratio of CH_4:CO_2

When similar experiments were performed on the Pt/ZrO_2 (Figure 4.7) and $Pt\text{-}Sn/ZrO_2$ (Cl) (Figure 4.8) catalysts, they exhibited a very different

behavior. The deactivated Pt/ZrO_2 catalyst regained approximately 75% of its initial conversion after stopping the CH_4 flow for 45 min, but it rapidly dropped back to the same conversion. Finally, the deactivated $Pt\text{-}Sn/ZrO_2$ (Cl), unlike the monometallic or the other bimetallic catalysts, did not regain any activity after stopping the CH_4 flow and exposing it to pure CO_2.

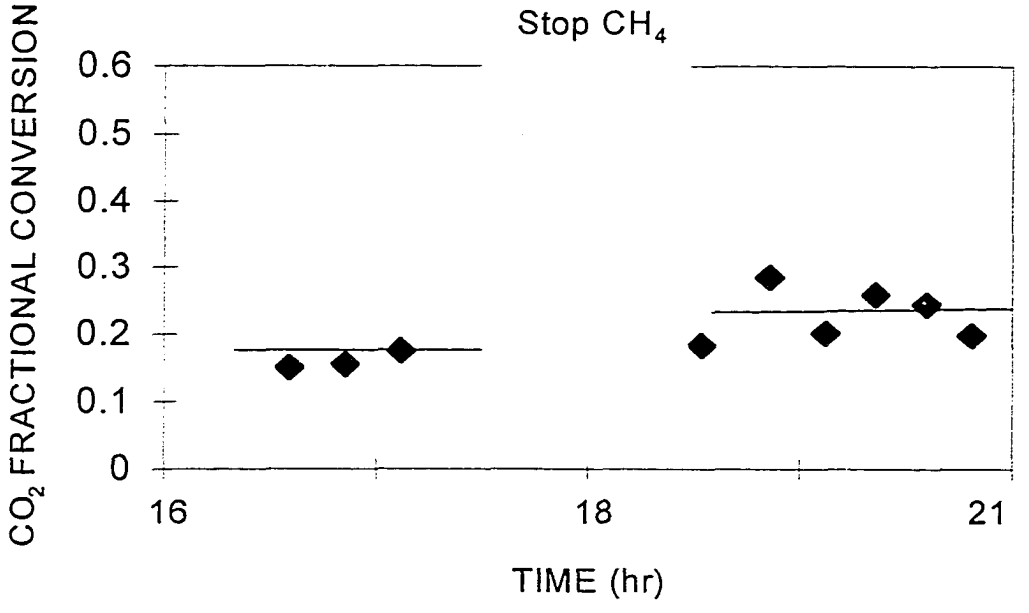

Figure 4.8: Effect of temporarily stopping the flow of one of the reactants on the CO_2 conversion for deactivated $Pt\text{-}Sn/ZrO_2$ (Cl) catalyst after 18 hours of reaction at 800°C and a 3:1 ratio of CH_4:CO_2.

4.3.4 Quantification of Carbon Deposits

Table 4.1 shows the quantification of carbon for the Pt/ZrO_2 and $Pt\text{-}Sn/ZrO_2$ (Cl) samples after two hours of reaction at 800°C with a CH_4:CO_2 feed ratio of 2:1. The addition of Sn did result in a decrease in the amount of

carbon deposited per mole of Pt. However, when the amount of carbon deposited is related to the amount of CH_4 converted, the Pt/ZrO_2 catalyst appears to be far superior to the Pt-Sn (Cl) catalyst.

Catalyst	Moles of C per mole of Pt	Moles of C per mole of CH_4 converted
Pt/ZrO_2	1.77	1.28E-04
$Pt\text{-}Sn/ZrO_2$ (Cl)	0.78	3.73E-04

Table 4.1: Quantification of carbon deposits for the Pt/ZrO_2 and $Pt\text{-}Sn/ZrO_2$ (Cl) catalysts after two hours of reaction at 800°C with a CH_4:CO_2 feed ratio of 2:1.

4.3.5 $^{13}CH_4$ and $^{12}CO_2$ Pulse Experiments

As stated in Chapter 3, isotopically labeled studies can be extremely valuable in determining the reaction mechanism. In these experiments we were specifically investigating the effect of the Sn on the cleaning mechanism. Figure 4.9a shows the results of exposing the $Pt\text{-}Sn/ZrO_2$ (Cl) catalyst to pulses of ^{13}C-labeled methane at 800°C. As expected, H_2 was the primary product. Similar to the isotopically labeled studies on Pt/ZrO_2 (Figure 4.9b), ^{13}CO and a small amount of $^{13}CO_2$ were also observed. However, the amount of ^{13}CO observed on the bimetallic catalyst was much less than that observed for the monometallic sample. This decrease in labeled CO indicates an inhibition of the reduction of the support by the presence of Sn. As previously observed on Pt/ZrO_2, each subsequent pulse resulted in an increase in the amount of unreacted $^{13}CH_4$ and a decrease in the H_2 and ^{13}CO production.

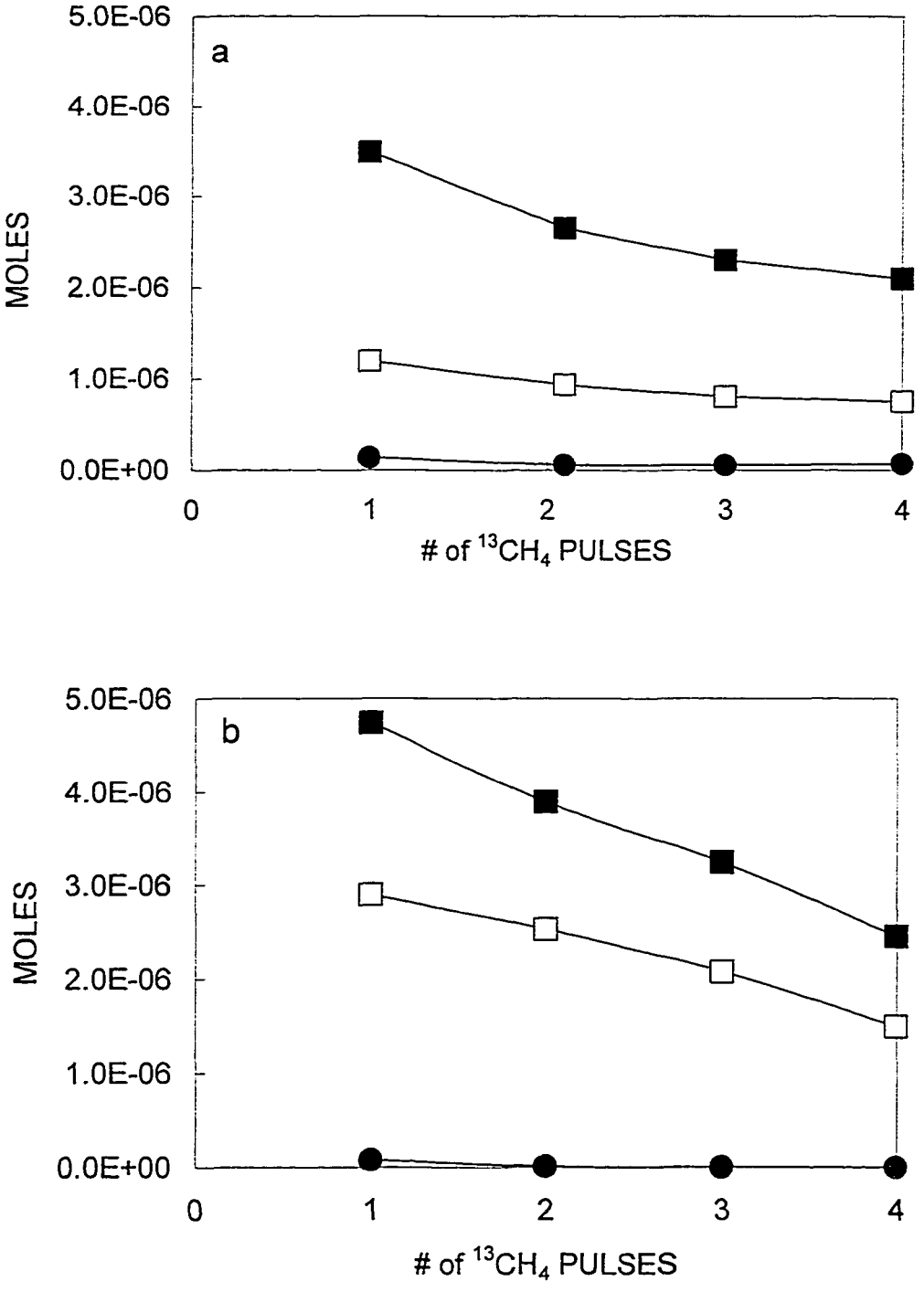

Figure 4.9: Moles of H_2 (■), ^{13}CO (□), and $^{13}CO_2$ (●) produced during $^{13}CH_4$ pulses at 800°C over (a) Pt-Sn/ZrO_2 (Cl) and (b) Pt/ZrO_2.

Following the series of $^{13}CH_4$ pulses, the catalyst was exposed to eleven pulses of $^{12}CO_2$ (Figure 4.10a). The conversion of the $^{12}CO_2$ pulses resulted in almost no ^{13}CO production and a much lower ^{12}CO production than on the Pt/ZrO_2 catalyst (Figure 4.10b). It might be expected that the amount of ^{13}CO formed should be less, due to the reduction in the amount of carbon deposited because of the promotion with Sn. However, the results presented in Chapter 3 showed that the dissociation of CO_2 occurs at the site of oxygen vacancies. Thus, the inability of the oxide support to be reduced on the bimetallic catalyst also results in a decrease in the ability to dissociate CO_2 and a less efficient cleaning mechanism.

A similar set of experiments was conducted on the Pt-Sn/Pt catalysts (not shown). During the $^{13}CH_4$ pulses, the production of H_2 was less than that observed for both the monometallic and the $Pt\text{-}Sn/ZrO_2$ (Cl) catalysts. However, the amount of ^{13}CO produced was less than that on the monometallic, but more than that on the $Pt\text{-}Sn/ZrO_2$ (Cl). Similarly, during the subsequent series of $^{12}CO_2$ pulses the amount of ^{13}CO and ^{12}CO observed was in the order of Pt/ZrO_2 > Pt-Sn/Pt > $Pt\text{-}Sn/ZrO_2$ (Cl). This result supports the idea that the Pt-Sn/Pt preparation results in suppression of carbon deposition without significant hindering of the role of the support.

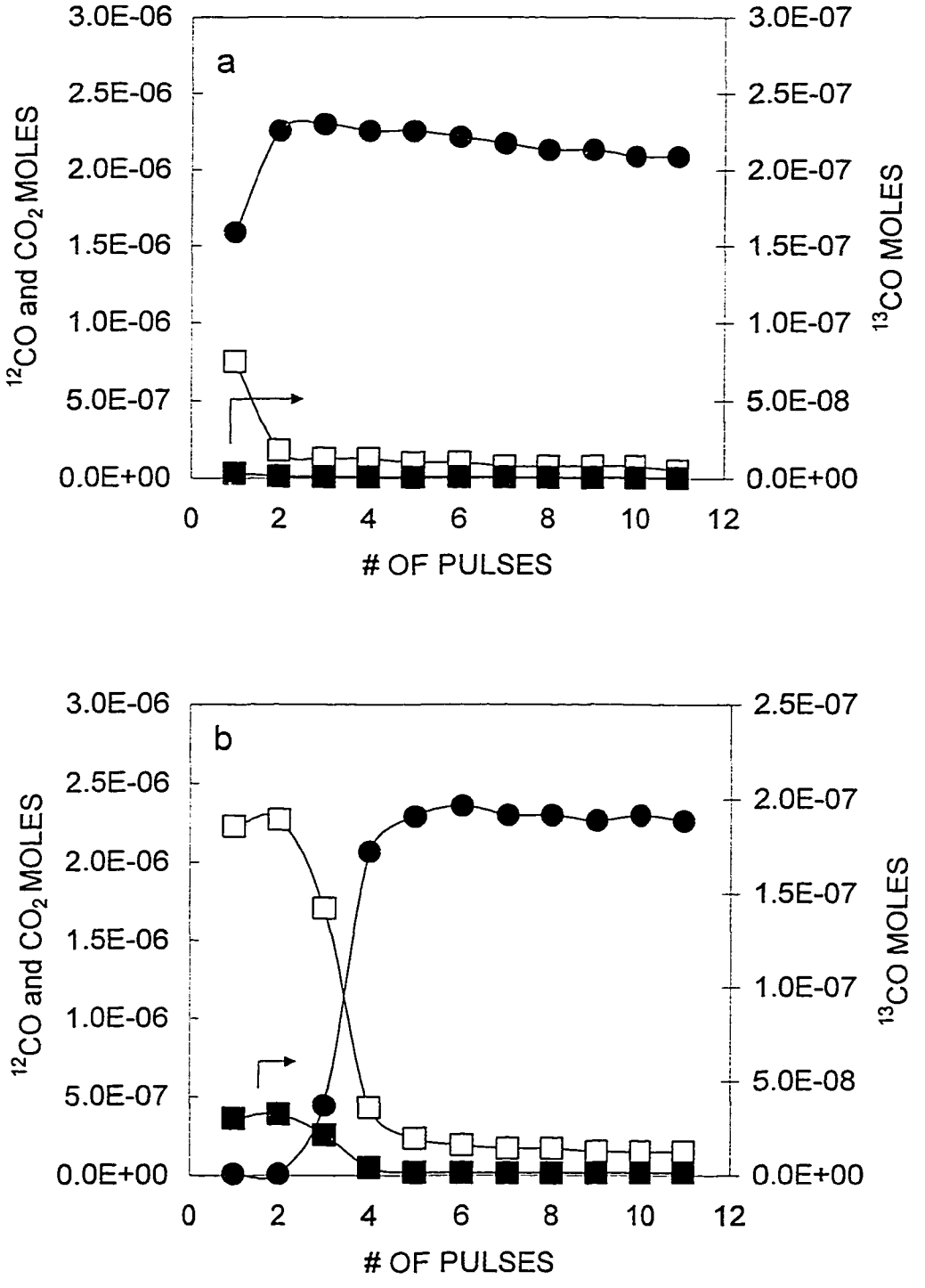

Figure 4.10: Moles of ^{13}CO (■), ^{12}CO (□), and $^{12}CO_2$ (●) produced during $^{12}CO_2$ pulses at 800°C after pulses of $^{13}CH_4$ over (a) Pt-Sn/ZrO_2 (Cl) and (b) Pt/ZrO_2.

4.3.6 XANES and EXAFS

X-ray absorption studies were performed to determine whether the state of Pt was altered during the reaction due to interaction with the promoter. Because the intensity of the white line (first peak) corresponds to the density of unoccupied *d* states, it is possible to see changes in this peak due to metal-metal interaction in an alloy. The effect of Sn on the XANES spectrum for Pt-Sn/ZrO_2 (Cl) catalyst is shown in Figure 4.11. Again, the spectra for the sample before and after exposure to the dry reforming reaction are compared to the Pt foil.

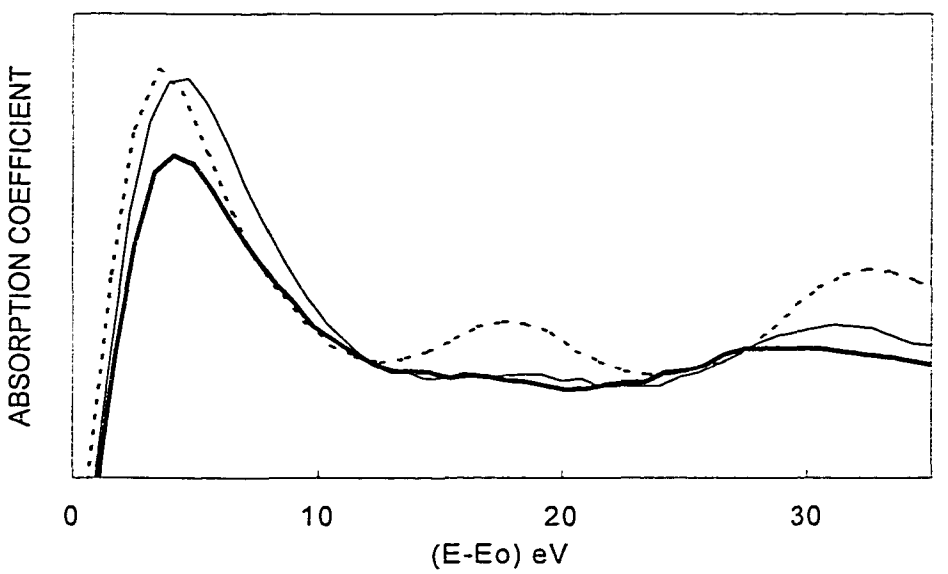

Figure 4.11: XANES spectra of Pt foil (- -), Pt-Sn/ZrO_2 (Cl) before reaction (–), and Pt-Sn/ZrO_2 (Cl) during reaction at 650°C and a 2:1 CH_4:CO_2 ratio (–).

Unlike the Pt/ZrO_2 catalyst, the intensity of the white line before reaction was much lower than that for the Pt foil. Furthermore, the addition of

Sn had a severe dampening effect, which resulted in no significant oscillations beyond the white line. After exposure to reaction conditions, the intensity of the white line of the Pt-Sn/ZrO_2 (Cl) sample was equivalent to that of the Pt foil. This increase in the white line Indicates that the Pt-Sn interaction had been disrupted.

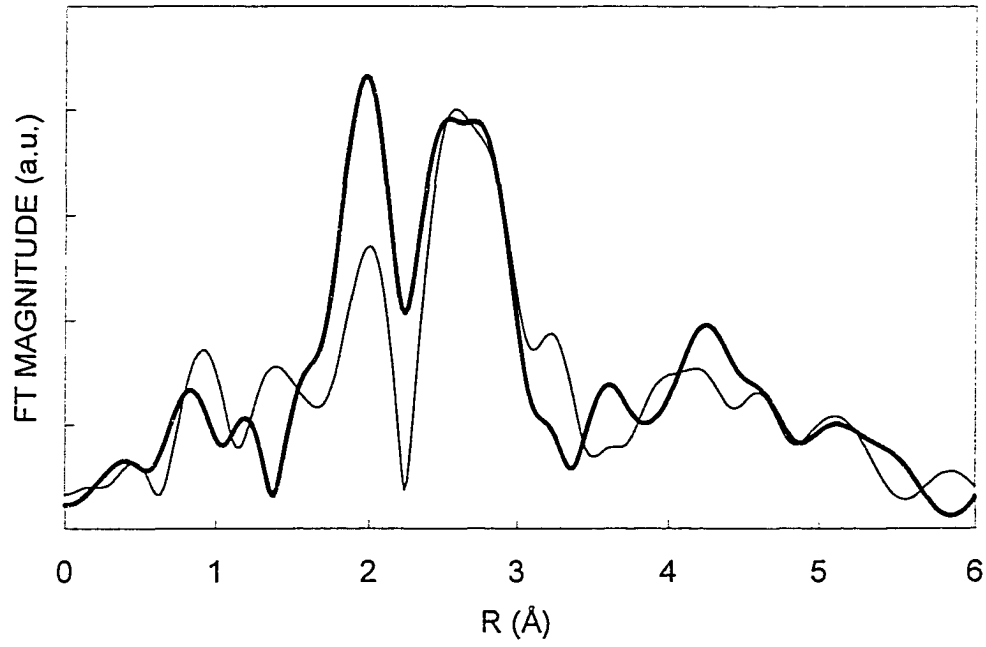

Figure 4.12: Fourier transforms of EXAFS data taken at liquid nitrogen temperatures: Pt-Sn/ZrO_2 (Cl) before reaction (–), and Pt-Sn/ZrO_2 (Cl) after reaction at 650°C and a 2:1 CH_4:CO_2 ratio (–).

The EXAFS spectra for the bimetallic sample before and after reaction are shown in Figure 4.12. The spectrum of the sample before reaction showed the presence of a peak at approximately 2-2.1 Å, which is much larger than the satellite peak observed at that region for the Pt foil (Chapter 3 - Figure 3.8). This peak has been observed by other researchers [16], and

has recently been explained as being caused by interference between the Pt-Pt and Pt-Sn bond distances [Appendix B]. After reaction, a large decrease in the intensity of this peak was observed, again indicating a loss of Pt-Sn interaction.

4.4 Discussion

It is well documented that promotion with Sn can result in significant increases in the stability of Pt catalysts [9,21-22]. Catalysts prepared by the co-impregnation of Pt and Sn on SiO_2 had less carbon deposition during dehydrogenation reactions than the unpromoted Pt/SiO_2 catalyst. Studies have shown that, in those cases, the Pt and Sn form a stable alloy and the degree of interaction can vary depending on the preparation method employed [Appendix A].

The addition of Sn to Pt/SiO_2 catalysts did reduce the amount of carbon deposited during the dry reforming reaction at 650°C and a 1:1 CH_4:CO_2 feed ratio. The bimetallic catalysts were more stable than the monometallic catalysts, and these differences became even more apparent at CH_4:CO_2 feed ratios greater than one. The results showed that CH_4 decomposition is responsible for the deactivation of the catalyst due to carbon deposition on the metal. The addition of Sn reduced the formation of carbonaceous deposits by inhibiting the decomposition of CH_4. This inhibition resulted in increased stability and a more stable product ratio. However, unlike in the case of SiO_2-supported catalysts, the co-impregnation of Sn to

the ZrO_2-supported catalyst did not improve the activity or stability of the dry reforming catalyst. Although the addition of Sn hindered the decomposition of CH_4, and decreased carbon formation by this path, the activity of the co-impregnated, bimetallic catalyst was significantly lower than that of the Pt/ZrO_2 catalyst. One explanation for the poor performance of the $Pt\text{-}Sn/ZrO_2$ (CI) catalyst could be that the presence of Sn disrupts the interaction between the Pt and support at the particle-support interface. It has been previously shown that when Pt-Sn alloys were exposed to an oxidizing atmosphere at high temperatures, the morphology of the catalyst was drastically altered [17,Appendix A]. TEM and x-ray absorption studies [23] have indicated that after oxidation of Pt-Sn catalysts in air, disruption of the alloy occurred resulting in rings of SnO_2 surrounding a metallic Pt core. It is plausible that the same effects are observed on ZrO_2, especially at temperatures of 800°C. The formation of SnO_2 rings around the Pt would completely isolate the Pt particle from the support and eliminate the cleaning mechanism.

X-ray absorption studies performed on the $Pt\text{-}Sn/ZrO_2$ (CI) catalyst after reaction provide strong evidence for the proposed disruption of the alloy and blocking of the metal-support interface. It is well known [16,18,Appendix B] that the formation of Pt-Sn alloys results in modifications of the shape of the Pt L_{III} XANES spectra, specifically a decrease in the intensity of the white line. In the case of the $Pt\text{-}Sn/ZrO_2$ (CI) catalyst, the XANES spectrum before reaction showed a decreased intensity of the white line in comparison to that of the Pt reference, indicating the presence of Pt-Sn alloys. However, this

intensity increased during the dry reforming reaction. This increase was not due to the oxidation of Pt, because the white line in this case was almost identical to that of the Pt foil reference. Instead, the change can be explained by the disruption of the alloy during the reaction, as proposed above.

At the same time, EXAFS data showed no Pt-O distance, only the two peaks that are related to the Pt-Pt and Pt-Sn bonds. We have recently shown [Appendix B] that the simultaneous presence of Pt-Sn alloys and unalloyed Pt gives rise to two peaks in the FT spectrum, one at 2.7 and other at 2-2.1 Å. The intensity of the latter is a good indication of the degree of Pt-Sn interaction. In this case, the short-distance peak greatly decreased under reaction conditions, demonstrating again the disruption of the alloy. The results of an elemental analysis performed by Galbraith laboratory on the Pt-Sn/ZrO_2 (Cl) catalyst before and after reaction eliminated the possibility that this decrease was due to volatilization and loss of Sn. These studies suggest that the Sn in the co-impregnated catalyst may become partially oxidized during the dry reforming reaction, leading to disruption of the Pt-Sn alloy.

Further evidence for the disruption of the interaction between the Pt and the ZrO_2 due to the presence of Sn is found in the results of the pulse experiments. In contrast to the Pt/ZrO_2 catalyst, which was very efficient in removing with CO_2 the ^{13}C species deposited during the $^{13}CH_4$ pulses, the Pt-Sn/ZrO_2 (Cl) catalyst only produced a small amount of ^{12}CO and almost no ^{13}CO during the $^{12}CO_2$ pulses. Even though the addition of Sn resulted in decreased carbon deposition, a negative effect of Sn is to block the

interaction of Pt with the support. The effect of this blockage can be observed in both, the less efficient reduction of the support during the $^{13}CH_4$ pulses, as well as the decreased carbon removal during the subsequent CO_2 pulses. The inability of the co-impregnated bimetallic catalyst to remove carbon from the metal is also observed in the fact that no changes in the activity of the catalyst were observed after CO_2 regeneration of the deactivated catalyst (Figure 4.8).

In order to minimize the negative effect that Sn has on the metal-support interaction, preparation methods have been used that allowed for the controlled addition of a small amount of Sn to reduce carbon deposition without disrupting the role of the support. The surface reduction deposition method results in specific placement of the Sn onto the pre-reduced Pt particle, eliminating the possibility that excess Sn is interacting with the support. This technique also allows for the position of the Sn to be controlled by varying the size of the ligand attached. The intent behind the co-impregnation of Pt and Sn onto the pre-calcined Pt catalyst was to have the alloy particles on top of Pt particles. In this case, the alloy segregation might be prevented by minimizing the contact between Sn and the support.

Figure 4.4 shows that the Pt-Sn/Pt and Pt-Sn (SR) catalysts have similar activity to the Pt/ZrO_2 catalyst, and more than twice the activity of the $Pt\text{-}Sn/ZrO_2$ (CI) sample. Furthermore, the Pt-Sn/Pt and the Pt-Sn (SR) catalysts were much more stable than the Pt/ZrO_2 and $Pt\text{-}Sn/ZrO_2$ (CI) at a CH_4:CO_2 ratio of 3:1. As mentioned in the previous chapter, the monometallic

sample experienced rapid deactivation by carbon deposition due to an imbalance between the rates of decomposition and cleaning. In contrast, the rate of deactivation on the bimetallic catalysts is greatly reduced due to the ability of Sn to inhibit the decomposition of CH_4. However, unlike the Pt-Sn/ZrO_2 (Cl) catalyst, the Pt-Sn/Pt and Pt-Sn (SR) catalyst retain the ability to dissociate CO_2 and facilitate cleaning of the carbon on the metal particle (Figure 4.6). This concept is clearly illustrated in the pulse experiments conducted on the Pt-Sn/Pt sample. This work demonstrates that the controlled deposition of Sn can result in a decrease in the carbon formation by hindering the decomposition of CH_4, without inhibiting the beneficial role of the support.

4.5 Conclusions

Although the addition of Sn to a Pt/SiO_2 catalyst results in a decrease in the initial activity of the catalyst, the stability is greatly improved. In contrast, the co-impregnation of Pt and Sn on ZrO_2 results in a decrease in the performance. Under reaction conditions, segregation of the Pt-Sn alloys can occur blocking the interaction between the metal and the support and hindering the cleaning mechanism.

In choosing the preparation technique, it is necessary to maximize the Pt-Sn interaction while minimizing the interaction between the promoter and the support. Excess Sn may act to decrease the density of CO_2 adsorption sites near the metal particle, reducing the effectiveness of the support.

Preparation techniques such as surface reduction deposition and co-impregnation of Pt and Sn onto a pre-calcined Pt catalyst result in the controlled addition of Sn. These catalyst exhibit higher activity and stability than the monometallic catalyst under severely deactivating conditions, 800°C and a 3:1 ratio of CH_4:CO_2.

4.6 References

1. Sinfelt, J. H., in "Bimetallic Catalysis: Discoveries, concepts, applications", New York, J. Wiley, (1983).
2. Adkins, S. R., and Davis, B. H., *J. Catal.*, **89**, 371 (1984).
3. Querini, . A., and Fung, S. C., *J. Catal.*, **141**, 389 (1993).
4. Sparks, D. E., Srinivasan, R., and Davis, B. H., *J. Molecular Catal.*, **88**, 359 (1994).
5. Cortright, R. D., and Dumesic, J. A., *J. Catal.*, **148**, 771 (1994).
6. Kappenstein, C., Saouabe, M., Guerin, M, Marecot, P., Uszurat, I, and Paal, Z., *Catal. Lett.*, **31,** 9 (1995).
7. Li, Y. X., Klabunde, K. J., and Davis, B. H., *J. Catal.*, **128** , 1 (1991).
8. Srinivasan, R, and Davis, B., Platinum Metals Review, **36,** 151 (1992).
9. Yarusov, I. B., Zatolokina, E. V., Shitova, N. V., Belyi, A. S., and N. M. Ostrovskii, *Catalysis Today*, **13**, 655 (1992).
10. Yang W., Lin L., Fan Y., J. Zang, *Catal. Lett.*, **12**, 267 (1992).
11. Jin, L. Y., Appl. Catal., **72**, 33 (1991).
12. Wilhem, F, US Patent 3998900 (1976).
13. Ponec, V., and Sachtler, W. M. H., *J. Catal.*, **24**, 250 (1972).
14. Dautzenberg F. M., Helle J. N., Biloen P., and Sachtler W. M. H., *J. Catal.*, **63**, 119 (1980).
15. Satterfield, C. N., "Heterogeneous Catalysis in Industrial Practice", McGraw-Hill, New York, (1991).
16. Meitzner, G., Via, G. H., Lytle, F. W., Fung, S. C., and Sinfelt, J. H., *J. Phys. Chem.* **92**, 2925 (1988).
17. Verbeek, H., and Sachtler, W. M. H., *J. Catal.*, **42**, 257 (1976)
18. Ross, P. N., *J. Vacuum Sci. Technol.*, **10**, 2546 (1992).
19. Paffett, M. T., Gebhard, S., Windham, R. G., Koel, B. E., *Surf. Sci,.* **223**, 449 (1989).
20. Xu C., Koel, B. E., and Paffett, M. T., *Langmuir*, **10**, 166 (1994).
21. Barias, O. A., Holmen, A., and Blekkan, E. A., *Catal. Today,* **24**, 361 (1995).

22. Cortright, R. D., and Dumesic, J. A., *Appl. Catal. A,* **129**, 101 (1995).
23. Chojnacki, T. P., and Schmidt, L. D., *J. Catal.,* **129**, 473 (1991).

CHAPTER 5

PROMOTION OF THE SUPPORT

5.1 Introduction

Chapter 3 discusses the role of the ZrO_2 in facilitating the cleaning of the metal particle and emphasizes the two-path mechanism. The previous chapter describes work that was performed on promotion of the metallic phase to reduce carbon deposition. The results of these studies show that traditional methods of preparation such as co-impregnation of the Pt and Sn does not enhance the performance of the catalyst. During the reaction, segregation of the Pt-Sn alloy can occur, resulting in the formation of Sn-oxide rings around a Pt metallic core. The formation of SnO blocks the interaction between the metal and the support, eliminating the cleaning mechanism responsible for the stability of the catalyst. Special preparations of bimetallic catalysts can result in a material the exhibits high activity and stability. However, these catalysts are only useful under severely deactivating conditions, high temperatures and high ratios of CH_4:CO_2.

In this chapter, promotion of the ZrO_2 support is studied with the intention of increasing the CO_2 adsorption capacity and its dissociation, which in turns increases the efficiency of the cleaning mechanism. It is well established that adding cations such as Y^{3+} or La^{3+} enhances the surface area and the thermal stability of ZrO_2 [1,2]. Similarly, recent studies [3] performed on automotive oxidation catalysts have shown that doping cerium oxide with Zr^{4+} resulted in a material that, after calcination at 800°C, had more

than six times the surface area of the unpromoted CeO_2 catalyst. Furthermore, these materials and other ceria-doped zirconia samples were shown to exhibit good oxygen storage capacities and high thermal stability [4,5]. Several studies have been performed on the redox properties of the CeO_2 doped catalyst [6,7]. Fornasiero and co-workers found that the redox properties of a $Ce_{0.5}Zr_{0.5}O_2$ mixed oxide support could be improved by sintering, that was induced by repetitive oxidation/reduction cycles [6,8]. As shown in Chapter 3, the reducibility of the support is an important factor in determining the ability of the support to adsorb CO_2 and facilitate in the dissociation at the metal-support interface.

The high reducibility and high thermal stability of the promoted ZrO_2 materials make them very attractive supports for the reforming reaction. In this chapter, a study of Pt catalysts supported on both Ce^{4+} and La^{3+} - doped ZrO_2 is reported. The activity, CO_2 adsorption capacity, thermal stability, and BET surface area of the promoted catalysts have been measured and compared to an unpromoted Pt/ZrO_2 catalyst.

5.2 Experimental

A combination of the characterization techniques described in the experimental chapter along with catalytic activity measurements have been employed to study Pt/ZrO_2, $Pt/Ce\text{-}ZrO_2$ and $Pt/La\text{-}ZrO_2$ catalysts. The specific details about the preparation method and characterization techniques can be found in Chapter 2.

5.3 Results

5.3.1 Catalytic Activity

Figure 5.1 shows the conversion of CO_2 as a function of time on stream for the Pt/ZrO_2, $Pt/Ce\text{-}ZrO_2$, and $Pt/La\text{-}ZrO_2$ catalysts after reduction at 500°C in H_2 (30 cm^3/min) for 1 hour and subsequent exposure to reaction at 800°C with a 2:1 ratio of CH_4:CO_2 (GHSV 180,000 h^{-1}). The La-doped catalyst exhibited similar activity to the unpromoted catalyst, but had higher stability than the Pt/ZrO_2 catalyst. The unpromoted catalyst had a 55% loss of activity after 18 hours of reaction, while the La and Ce-doped catalysts had only 12% and 30% activity loss, respectively. Similar trends were observed for the CH_4 conversion.

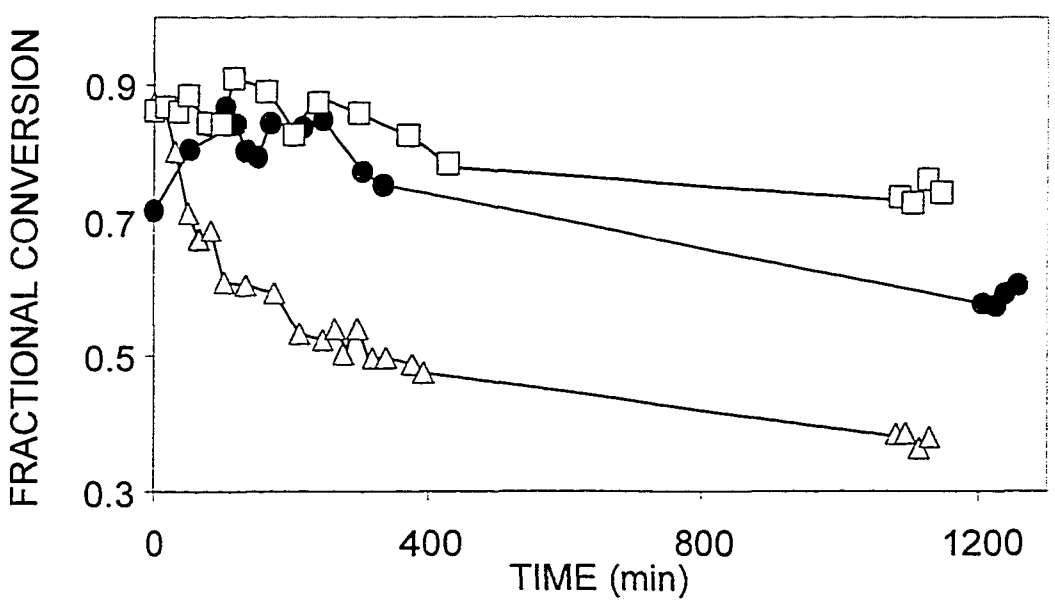

Figure 5.1: CO_2 fractional conversion for Pt/ZrO_2 (△), $Pt/Ce\text{-}ZrO_2$ (●), and $Pt/La\text{-}ZrO_2$ (□) during reaction at 800°C with a 2:1 ratio of CH_4:CO_2.

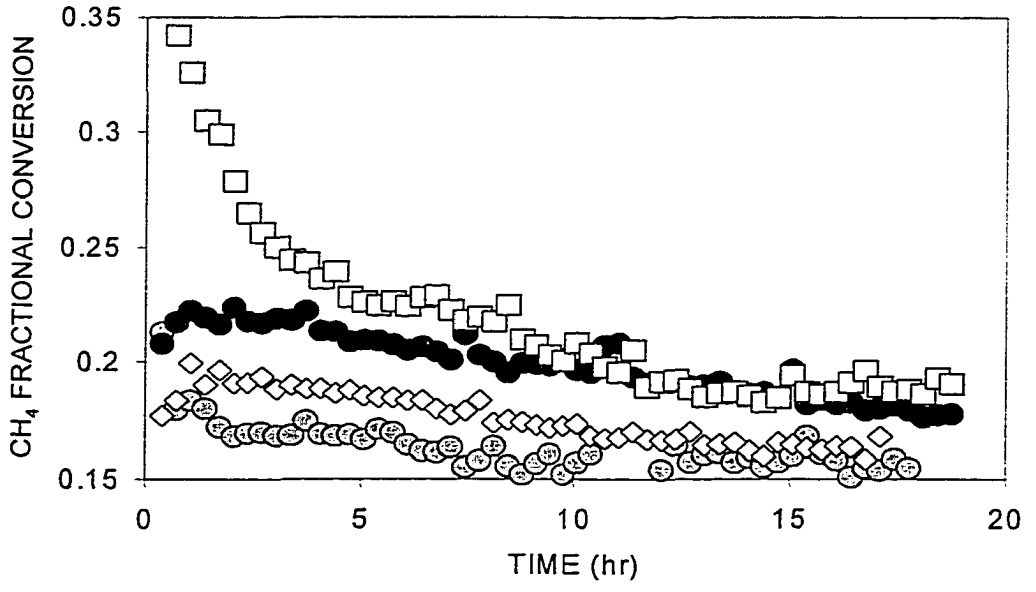

Figure 5.2: Fractional conversion of CH_4 during reaction at 800°C with a 2:1 ratio of CH_4:CO_2 over the Pt/ZrO_2 (⊙), $Pt/Ce\text{-}ZrO_2$ (●), $Pt/La\text{-}ZrO_2$, (□), and $Pt/Ce\text{-}La\text{-}ZrO_2$ (◊)after reduction at 200°C.

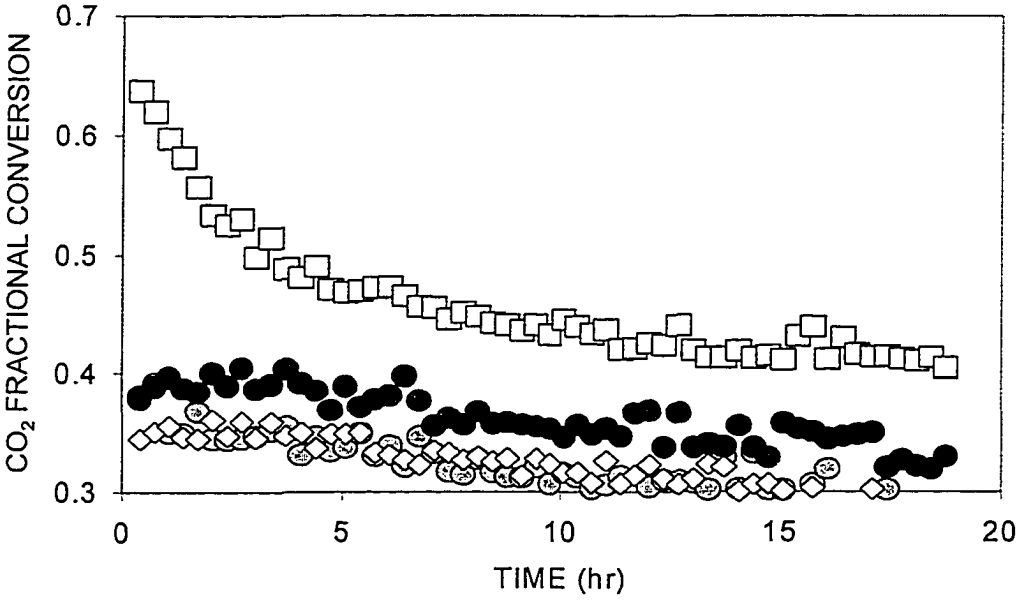

Figure 5.3: Fractional conversion of CO_2 during reaction at 800°C with a 2:1 ratio of CH_4:CO_2 over the Pt/ZrO_2 (⊙), $Pt/Ce\text{-}ZrO_2$ (●), $Pt/La\text{-}ZrO_2$, (□), and $Pt/Ce\text{-}La\text{-}ZrO_2$ (◊)after reduction at 200°C.

Figure 5.2 and 5.3 compares the CH_4 and CO_2 conversion for the three catalysts after low temperature reduction, along with the activity of a Pt/Ce-La-ZrO_2. The results of this study were very similar to the results of the experiments after high temperature reduction. The catalysts promoted with either Ce or La were more stable and active for the conversion of CH_4 than the unpromoted catalyst. Also, the La-promoted catalyst had a much higher conversion of CO_2 than the Ce-promoted and unpromoted catalyst. Surprisingly, the catalyst prepared using both Ce and La as promoters did not exhibit higher activity or stability than the catalysts that had only one promoter, exhibiting conversions similar to the unpromoted catalyst.

5.3.2 CH_4 and CO_2 Pulse Experiments

Figure 5.4 shows the H_2 production during three sets of pulses containing either CH_4 or CO_2. During the first set of CH_4 pulses, the promoted catalysts produced a significant amount H_2. The amount of H_2 produced for both the La and Ce-doped catalyst was approximately 30% more than the amount of H_2 produced on the unpromoted sample, suggesting that the amount of metal exposed for reaction is higher on the promoted samples than on the unpromoted catalyst. As expected, no H_2 was produced during the pulses of CO_2. During the subsequent set of CH_4 pulses, the Pt/La-ZrO_2 and Pt/Ce-ZrO_2 catalysts had approximately the same production of H_2 as was observed during the first set of CH_4 pulses, while the H_2 production on the Pt/ZrO_2 decreased.

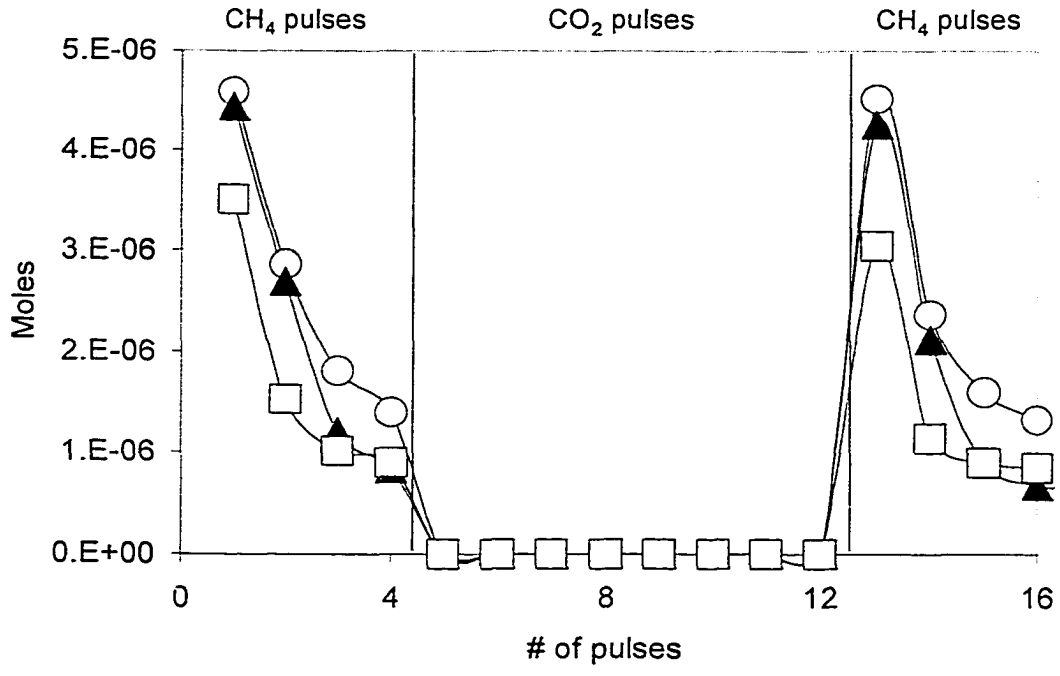

Figure 5.4: H_2 production during pulses of either CH_4 or CO_2 at 800°C over the Pt/ZrO_2 (□), $Pt/Ce\text{-}ZrO_2$ (▲), and $Pt/La\text{-}ZrO_2$ (○) catalysts.

Figure 5.5 is a graph of the CO production from the same set of pulses. During the first set of CH_4 pulses, CO production was observed with the amount of CO decreasing in the order, Ce-doped < La-doped < unpromoted catalyst. The increased production of CO on the Ce-doped catalyst can be ascribed to the ability of the promoter to facilitate the reduction of the oxide. Due to the importance of the vacancies in the dissociation of CO_2 and cleaning of the carbon on the metal, it is probable that this enhancement is partially responsible for the improved catalytic performance of the Ce-promoted catalyst.

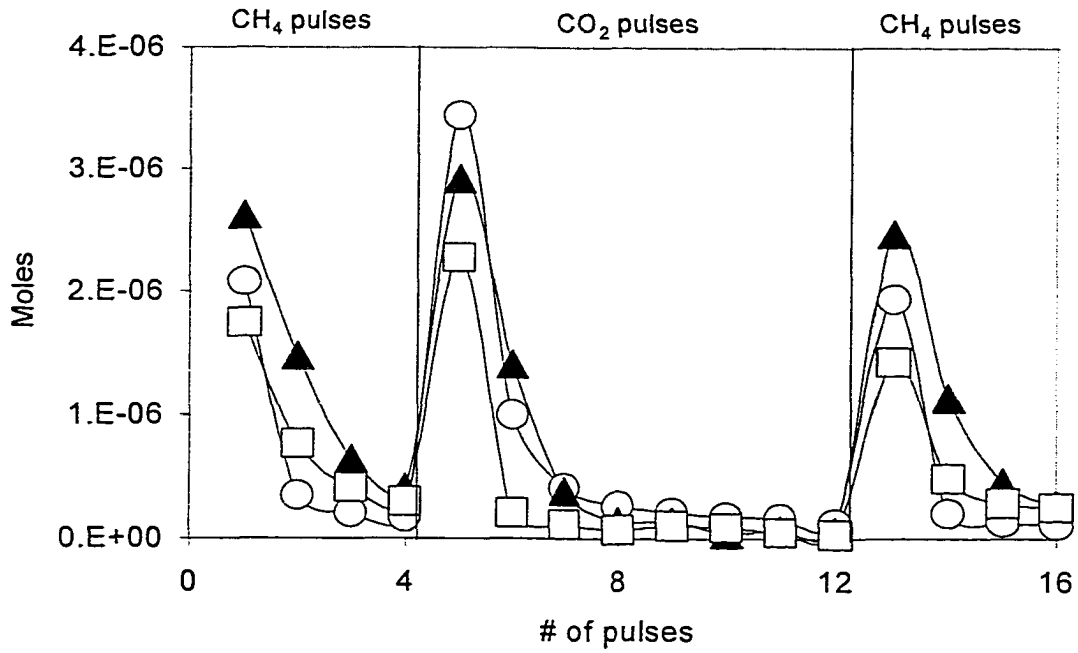

Figure 5.5: CO production during pulses of either CH_4 or CO_2 at 800°C over the Pt/ZrO_2 (□), $Pt/Ce\text{-}ZrO_2$ (▲), and $Pt/La\text{-}ZrO_2$ (○) catalysts.

The following set of pulses contained CO_2. Again, CO was observed on all three catalysts, however the order of the amount of CO produced changed. Unlike the order during the CH_4 pulses, the La-doped catalyst produced the most CO during the CO_2 pulses, followed by the Ce promoted and finally the unpromoted sample. In addition, the La- and Ce-doped catalysts produced CO during the first three pulses, while CO production on the unpromoted ZrO_2 sample ceased after the first pulse. These results suggest that the La-doped and Ce-doped catalyst have an increased ability to dissociate CO_2 and subsequently, are more effective in removing carbon deposited on the metal.

During the last set of CH_4 pulses CO was produced, indicating that the support oxygen had been partially replenished during the previous CO_2 pulses. Similar to the H_2 production during the CH_4 pulses, the promoted catalysts showed equivalent production of CO during the two sets of CH_4 pulses, while the CO production on the unpromoted Pt/ZrO_2 decreased from that observed during the first set of pulses.

Analysis of the product ratio formed during the pulses of CH_4 can reveal information about the interaction between the metal and the support. Three H_2/CO ratios are possible. If the H_2/CO ratio is equal to 2 this indicates that during the decomposition of CH_4, 2 H_2's and 1 CO are being formed. A product ratio of 2 indicates that no carbon is formed on the metal, instead the carbon reduces the support near the perimeter of the metal particle. If the ratio is less than 2, this indicates that a combination of CO, H_2, H_2O is being formed. This would occur if the Pt particle was oxidized and H_2O would be formed as a result of the reduction of the metal. Finally, if the H_2/CO ratio is greater than 2, this indicates that 2 H_2's are formed without reduction of the support. In this situation carbon deposition on the metal would occur. Figure 5.6 shows the H_2/CO production ratio observed for the same series of pulses described above. As no H_2 was observed during the CO_2 pulses, no ratio is reported for this set. The H_2/CO product ratio for the $Pt/Ce\text{-}ZrO_2$ and the Pt/ZrO_2 catalyst remains constant at approximately 2 for all of the CH_4 pulses. In contrast, the product ratio is 2 for the $Pt/La\text{-}ZrO_2$ catalyst only for the first pulse in each set. The second pulse of CH_4 results in a product ratio of 8 for

the first set and 11 for the second set. This high ratio is then observed for each of the subsequent pulses in the specific set. The high ratio for the Pt/La-ZrO_2 catalyst suggests that in the absence of CO_2, the La-doped catalyst can have significant carbon deposition. Thus, the La must have additional promotional effects, which result in increased stability.

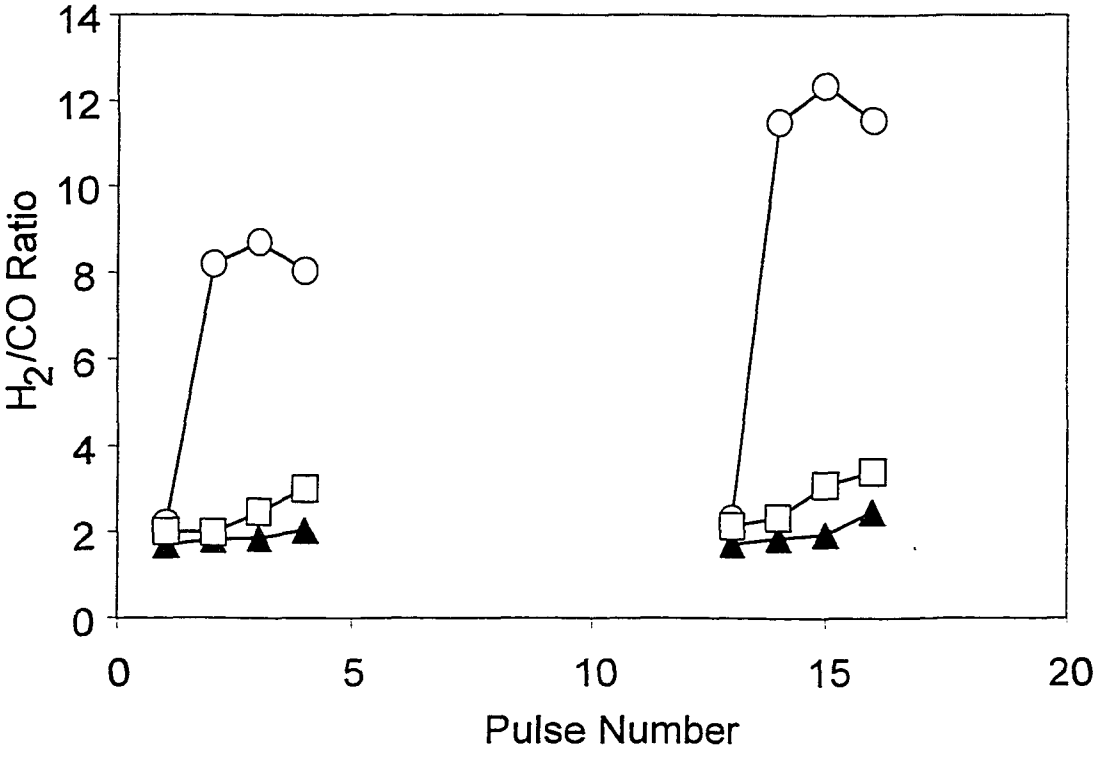

Figure 5.6: H_2/CO product ratio for pulses of CH_4 at 800°C over the Pt/ZrO_2 (□), Pt/Ce-ZrO_2 (▲), and Pt/La-ZrO_2 (○) catalysts.

Figure 5.7 shows the CO production for pulses of either CO_2 or CH_4 over the Pt/La-ZrO_2 catalyst. The experimental setup was the same as the previous set of pulses however the order of the pulses was reversed. In this experiment, pulses of CO_2 were sent to the reactor first for the purpose of probing the role of the vacancies. We intended to see if the oxygen

vacancies were necessary for the dissociation of CO_2 on the promoted catalyst, as was shown to be the case for the unpromoted sample.

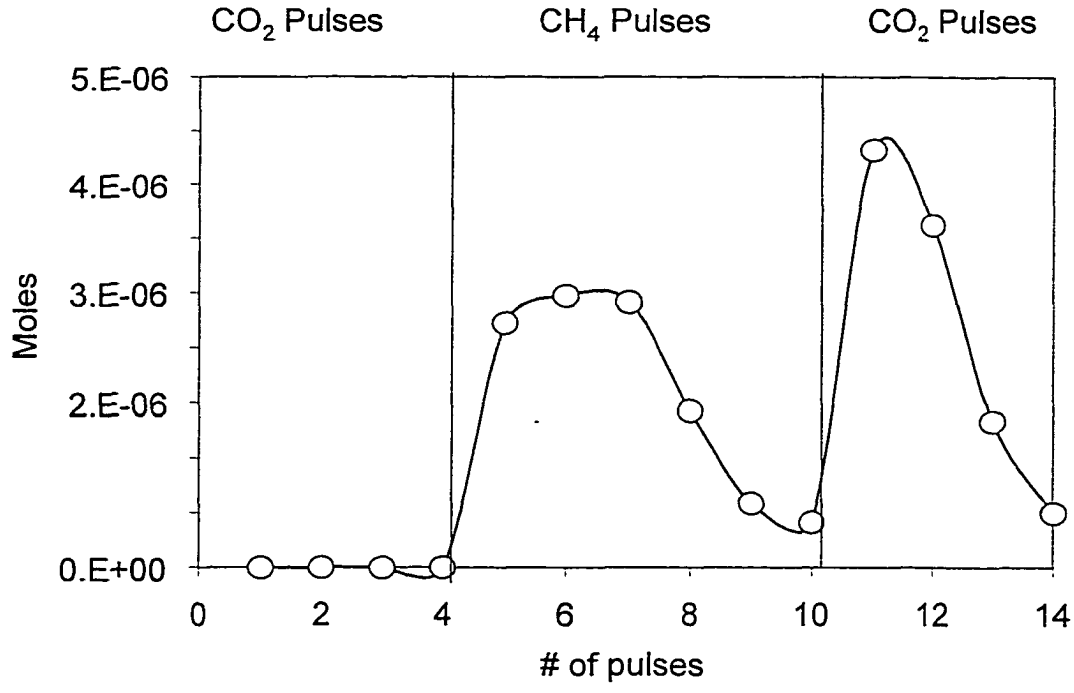

Figure 5.7: CO production during pulses of either CO_2 or CH_4 at 800°C over the Pt/La-ZrO_2 catalyst.

As is clearly shown in Figure 5.7, no CO is observed during the first set of CO_2 pulses. However, after pulses of CH_4, the subsequent CO_2 pulses resulted in a significant amount of CO produced. The CO production that occurred during the pulses of CH_4 indicates a partial reduction of the support. CO_2 dissociation occurred only after the formation of the vacancies, showing that the presence of the oxygen vacancies is required for the dissociation. These results provide evidence that the mechanism for the dry reforming reaction is the same on the promoted catalysts, and that the role of the vacancies is not altered by the presence of the promoters.

5.3.3 X-ray Diffraction

Figure 5.8 shows the XRD spectra for the Pt/ZrO_2, $Pt/Ce\text{-}ZrO_2$ and $Pt/La\text{-}ZrO_2$ catalysts after calcination at 800°C for 4 hours. The ZrO_2 in the unpromoted sample consisted primarily of the monoclinic phase, while the La-doped sample was completely tetragonal. The Ce-doped sample showed evidence of both the monoclinic and tetragonal phases. Finally, the primary phase in the sample containing both Ce and La was tetragonal.

5.3.4 BET Surface Area

Table 5.1 contains the BET surface area measurements for the various supports used in this study. The La-doped ZrO_2 had the highest surface area at 55 m^2/gram, followed by the Ce-doped ZrO_2 at 39 m^2/gram and the ZrO_2 support at 35 m^2/gram. The measured surface area of the $Ce\text{-}La/ZrO_2$ support was 49 m^2/gram.

5.3.5 TPD of CO_2

Table 5.1 also contains the amount of CO_2 desorption (moles/gram) measured during TPD of CO_2 experiments on the ZrO_2, $Ce\text{-}ZrO_2$, and $La\text{-}ZrO_2$. The corresponding TPD data is shown in Figure 5.9. Similar to the BET data, the La promoted support has the highest capacity for CO_2 adsorption with a measured CO_2 uptake of 6×10^{-4} moles/gram. The TPD of the Ce promoted and the unpromoted support were very similar showing a much small capacity for CO_2 adsorption at approximately 6 times less than the $La\text{-}ZrO_2$.

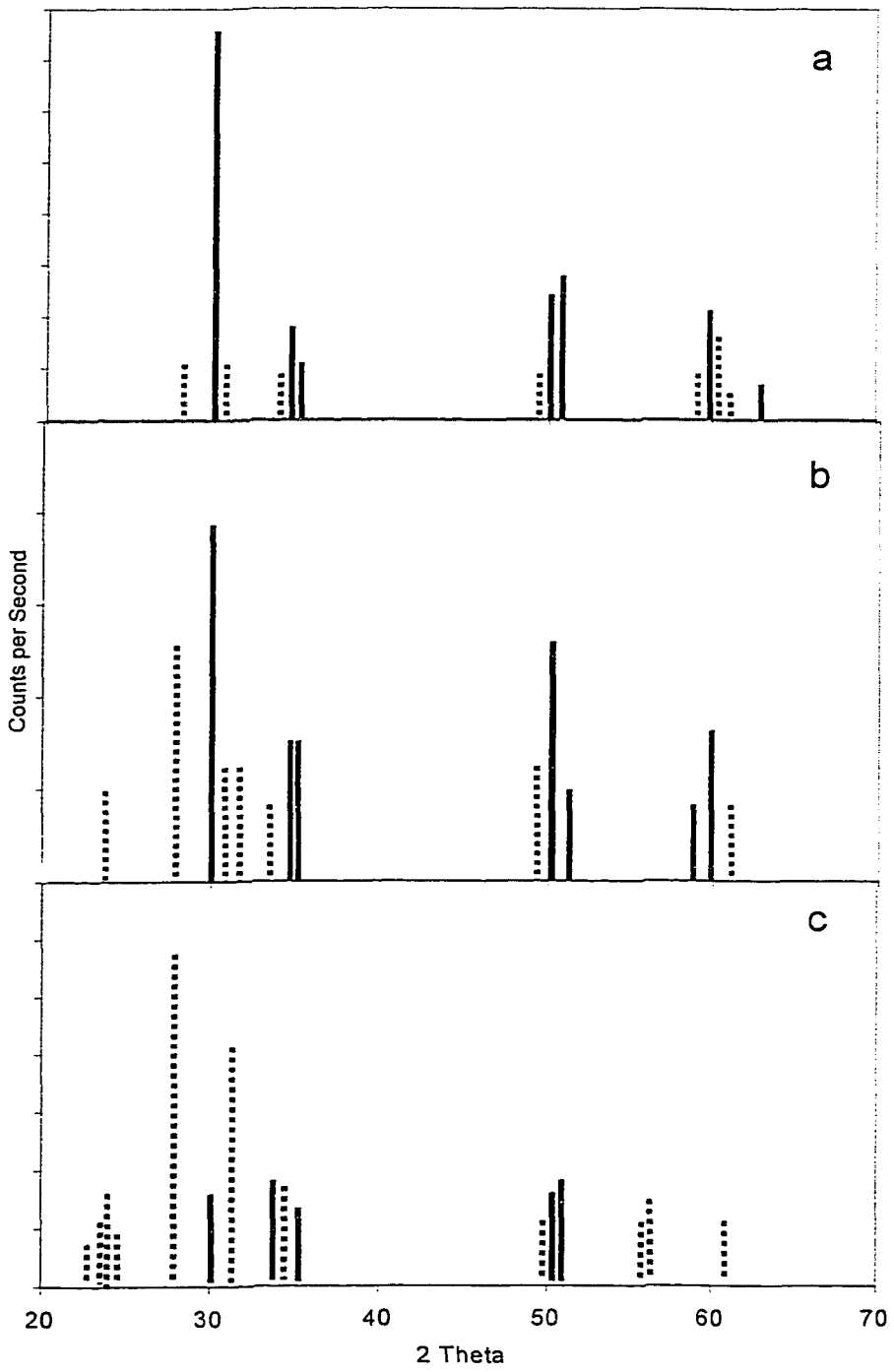

Figure 5.8: XR[illegible] erns for he ( ) P /L -ZrO_2, (b) P /Ce-ZrO_2, nd (c) P /ZrO_2 c lys s f er c lcin ion 800°C for 4 hours. (Prim ry ngles for e r gon l h se (—) nd monoclinic h se (- - -))

Support	BET Surface Area m^2/gram	CO_2 Desorption Capacity moles/gram
ZrO_2	35	$1x10^{-4}$
Ce-ZrO_2	39	$7x10^{-5}$
La-ZrO_2	55	$6x10^{-4}$
Ce-La-ZrO_2	49	----

Table 5.1: BET surface area and CO_2 desorption capacity for the supports investigated in this study.

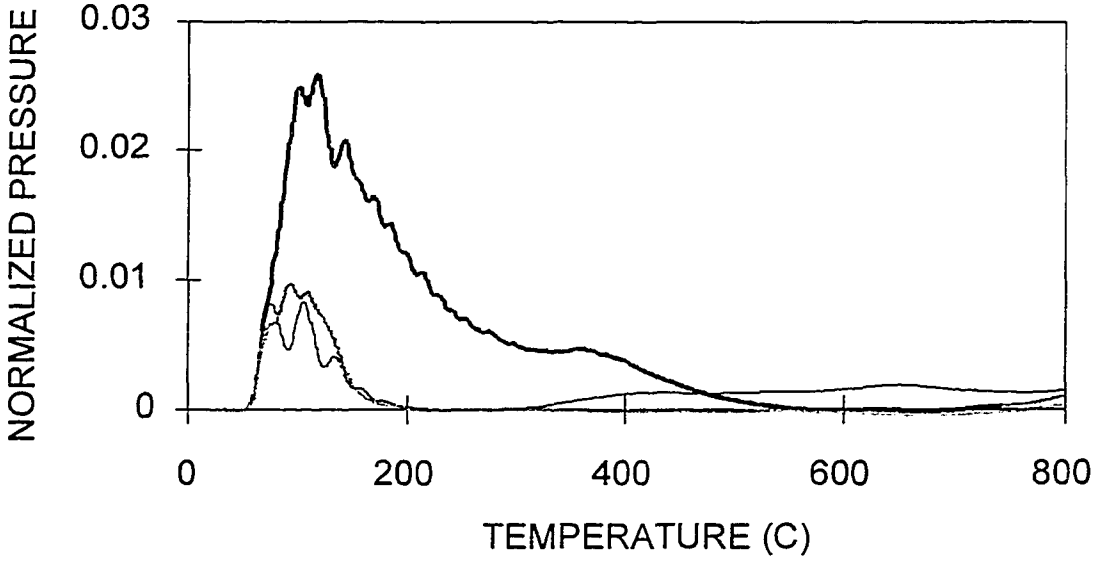

Figure 5.9: Temperature programmed desorption of CO_2 on the ZrO_2 (—), Ce-ZrO_2 (—), and La-ZrO_2 (—)supports after calcination at 800°C for 4 hours.

5.3.6 EXAFS and XANES

Figure 5.10 compares the Fourier Transform (FT) of the EXAFS functions corresponding to reduced samples of Pt/ZrO_2, Pt/Ce-ZrO_2, and Pt/La-ZrO_2 catalysts. X-ray absorption studies were performed to determine if

the promoters were altering the state of the Pt, by forming alloys or inhibiting/accelerating particle growth. The peak at approximately 2.7 is the peak that corresponds to Pt-Pt interaction before correcting for the phase and amplitude shift. Using the magnitude of the FT as an indication of the particle size, it is shown that the promoted catalysts have much larger particles after reduction than the unpromoted Pt/ZrO_2 catalyst.

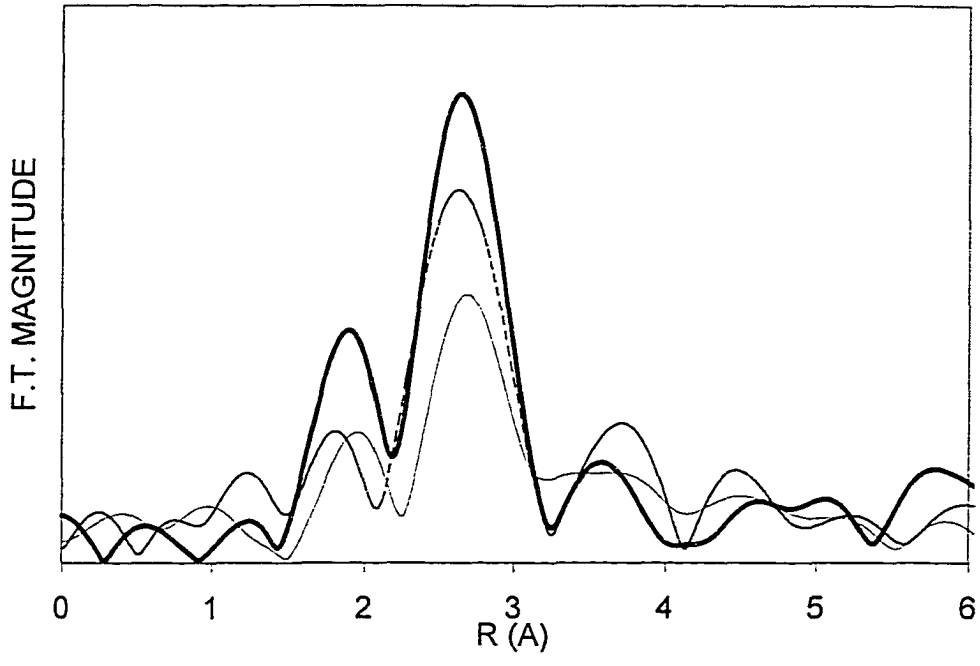

Figure 5.10: Fourier transforms of EXAFS data taken at liquid nitrogen temperatures for $Pt/La\text{-}ZrO_2$ (–), $Pt/Ce\text{-}ZrO_2$ (---), and Pt/ZrO_2 (–) catalysts after reduction at 500°C.

However, after heating to 800°C in He the magnitude of the FT peak for the Pt/ZrO_2 catalyst is much larger than the promoted samples (Figure 5.11), indicating that the presence of the promoters inhibits particle growth.

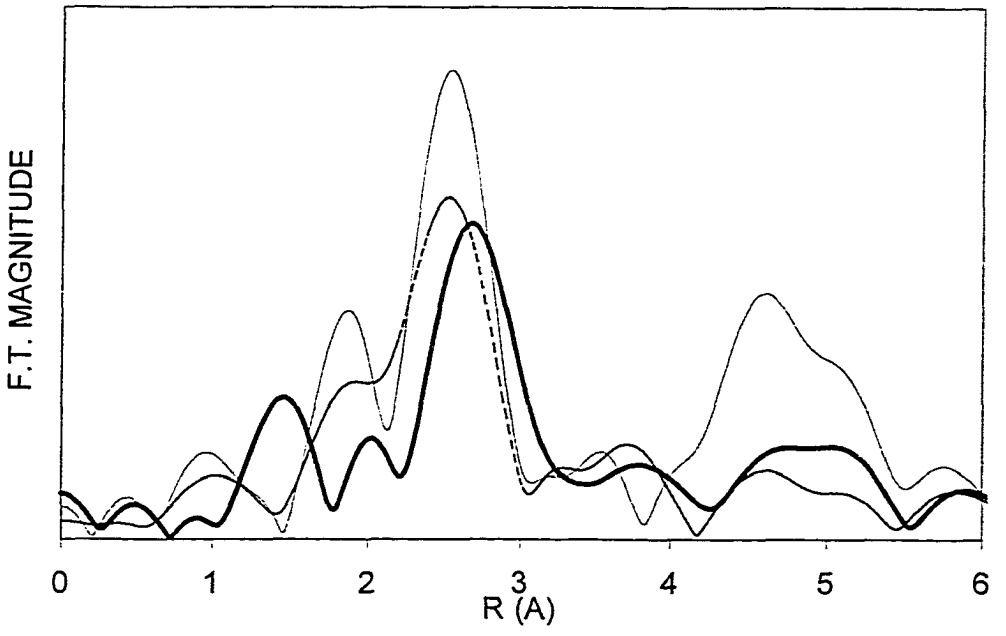

Figure 5.11: Fourier transforms of EXAFS data taken at liquid nitrogen temperatures for Pt/La-ZrO_2 (–), Pt/Ce-ZrO_2 (—), and Pt/ZrO_2 (–) catalysts after reaction at 800°C with a 2:1 ratio of CH_4:CO_2.

Figure 5.12 compares the % loss of activity with the amount of particle growth calculated from the magnitude of the FT after heating to 800°C divided by the magnitude of the FT after reduction. Because the cleaning of the metal particle is so strongly dependent upon the metal-support interaction, it is reasonable that smaller particles would be more efficient in removing the carbon on the surface of the metal. Thus, catalysts with smaller particles would exhibit higher stability than those catalysts with larger particles. The graph in Figure 5.12 shows that, as expected, the greatest percent loss in activity corresponds to the catalyst which exhibits the most severe particle

growth. The Pt/La-ZrO_2 catalyst, which experienced only moderate particle growth, was the most stable catalyst.

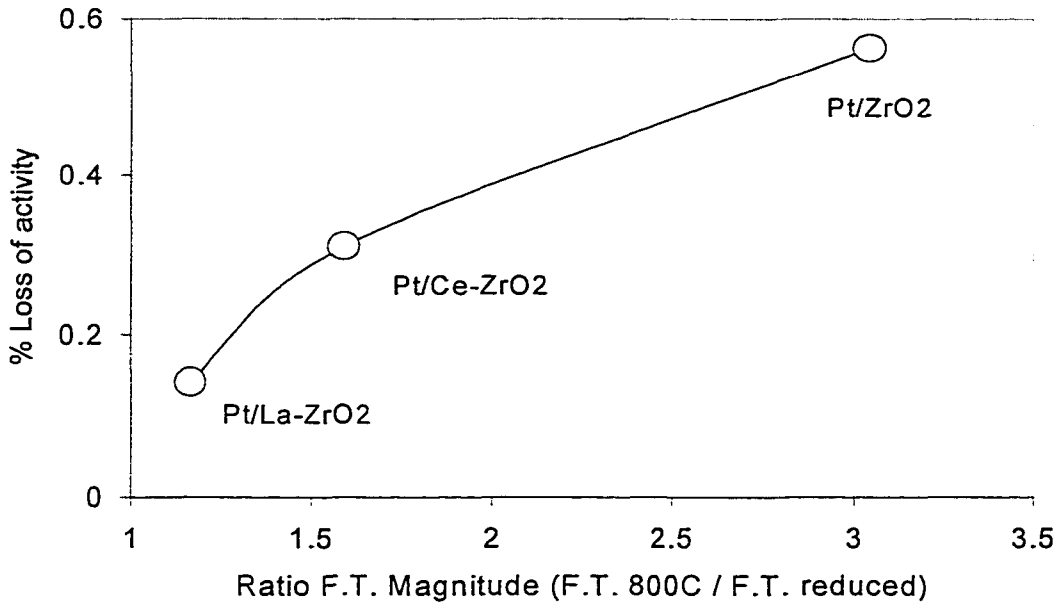

Figure 5.12: Percent loss of activity as a function of estimated particle growth for the Pt/ZrO_2, Pt/La-ZrO_2, and Pt/Ce-ZrO_2 catalyst.

5.4 Discussion

The results presented in this chapter show that the addition of either Ce^{4+} or La^{3+} results in improved catalytic performance. Both of the individually promoted catalysts exhibited higher activity and stability than the Pt/ZrO_2 catalyst. It has been suggested that the promotional effects of the lanthanum stem from the ability to increase surface area, while the cerium is successful at increasing the reducibility of the oxide [1,2,8]. Detailed characterization of the promoted catalysts indicates that the promotional

effects of the La^{3+} and Ce^{4+} include these abilities, but that they have other effects, which improve the catalytic performance.

5.4.1 Effect on Support Reduction

The DRIFTS studies presented in Chapter 3 have shown that the oxygen vacancies formed in the support during the decomposition of CH_4 play an important role in the reaction mechanism. The decomposition results in the reduction of the support near the metal particle, and it is at this vacancy site that the adsorption and dissociation of CO_2 occurs. This mechanism has been verified for the promoted catalysts by the pulse studies shown in Figure 5.7. CO_2 dissociation did not occur on the Pt/La-ZrO_2 catalyst until after the catalyst was exposed to pulses of CH_4, and the support was partially reduced. Thus, the ability of a promoter to increase the reducibility of the oxide support could have a tremendous impact on the ability to dissociate CO_2 and ultimately the stability of the catalyst.

The results of this study have shown that the addition of Ce^{4+} to the ZrO_2 did improve the reducibility of the oxide and had a beneficial effect on the long-term activity of the catalyst. The H_2/CO ratio reported in Figure 5.6 indicates that the support is readily reducible in the presence of a hydrocarbon at high temperatures. During both sets of CH_4 pulses (before and after exposure to CO_2) the Ce-doped catalyst has a H_2/CO ratio very near 2. As described previously, a ratio of 2 is observed when 2 H_2's and 1 CO are formed. The ability to reduce the support, results in a decrease in the amount

of carbon deposition that would normally occur during the decomposition of CH_4. The promotional effect of Ce^{4+} on the oxygen transfer is also shown in when comparing the amount of CO produced from the CH_4 pulses (Figure 5). During the pulses of CH_4, the Ce-doped catalyst produced the most CO indicating the highest degree of support reduction. A higher degree of reduction results in an increase in the number of oxygen vacancies formed near the metal particle and a subsequent increase in the ability to dissociate CO_2. Even though the Ce-doped catalyst does not have a higher BET surface area or CO_2 adsorption capacity, this increase in the dissociation ability and subsequent cleaning capacity results in a catalyst with enhanced activity and stability for the CO_2 reforming reaction.

5.4.2 Enhanced CO_2 Adsorption Capability

One explanation for the higher activity and stability of the promoted catalysts is that they have higher surface area and CO_2 adsorption capacity, which result in enhancement of the CO_2 dissociation and cleaning ability. The Ce-promoted support did not have a significant increase in the surface area, or an increase in the CO_2 adsorption capacity. However, as stated previously, the Ce^{4+} ability to increase the oxygen transfer resulted in an effective catalyst.

On the contrary, the results of this study provide strong evidence that the primary promotional effect of the lanthanum is increased thermal stability and CO_2 adsorption sites. Unlike the Ce-doped and unpromoted sample, the

La-doped catalyst exhibited a strong tendency for carbon formation in the absence of CO_2 (Figure 6) with the H_2/CO ratio increasing drastically after the first pulse. It is clear that the lanthanum must have promotional effects in the presence of CO_2, which result in improved activity and stability when compared to the unpromoted sample.

The XRD data shown in Figure 5.8 clearly shows that the addition of promoters, in particular lanthanum, to the ZrO_2 results in a catalyst in which the tetragonal phase of zirconia is stabilized. This stabilization of the tetragonal phase leads to a catalyst, which exhibits high thermal stability as seen in the BET surface area after high temperature calcination. The La-doped catalyst had a surface area that was 1.5 times greater than the Ce-promoted or unpromoted support, and more than 6 times the density of CO_2 adsorption sites. This increase in CO_2 adsorption capacity has a direct effect on the dissociation ability, and ultimately the long-term activity of the catalyst.

The improved dissociation and cleaning ability can be seen by analyzing the results of the pulse studies shown in Figure 5.5. The amount of CO produced during the pulses of CO_2 following the pulses of CH_4 was greater for the La-doped than the Ce-doped and unpromoted catalysts. The isotopically labeled studies from Chapter 3 have shown that the CO is produced from both the dissociation of CO_2 and from the removal of carbon that is deposited on the metal particle during the decomposition of CH_4. Therefore, promotion of ZrO_2 with La^{3+} results in a catalyst with higher thermal stability and a higher capacity for CO_2 adsorption. These promotional

effects lead to an increase in the ability to facilitate the dissociation CO_2, a more efficient mechanism for carbon removal from the catalyst, and ultimately a more stable catalyst.

5.4.3 Inhibition of Particle Growth

Another effect of the addition of promoters can be seen in the x-ray absorption studies. Figure 5.10 shows that after reduction at 500°C, the magnitude of the Fourier transform for both the promoted catalysts was much higher than that for the unpromoted catalysts. The increased magnitude in the Fourier transform indicates that after reduction at high temperature the promoted samples have larger metallic clusters than the clusters on the unpromoted ZrO_2 support. However, after 2 hours of reaction at 800°C and a 3:1 ratio of CH_4:CO_2, the Pt particles on the unpromoted catalyst are much larger than on either the Ce or La-doped catalyst (Figure 5.11). In fact, the promoted samples exhibited only moderate particle growth. Similar results were also observed using transmission electron microscopy. Figure 5.12 shows that the degree of particle growth observed follows the same order as the rate of deactivation. That is, the Pt/ZrO_2 catalysts exhibited the most growth and the fastest rate of deactivation, while the Pt/La-ZrO_2 catalyst had only minimal particle growth and exhibited the slowest rate of deactivation.

Sintering of the Pt metal might have an important role in the deactivation of the catalyst because it results in a decrease in the metal-support interaction, limiting the removal of carbon from the metal.

Furthermore, the amount of carbon required to deactivate the catalyst would be much smaller, and consequently the activity of the catalyst would decrease rapidly.

Figure 5.4 shows that the hydrogen production during the pulses of CH_4 is much lower on the unpromoted Pt/ZrO_2 catalyst as compared to the promoted samples. It is then possible that sintering is a major contributor to the lower activity and faster rate of deactivation for the Pt/ZrO_2 catalyst at 800°C. The lower activity can be ascribed to the reduction in the area of active metal exposed for reaction on the Pt/ZrO_2 catalyst. It should be noted that the sintering of the Pt particles most likely occurs during the heating to 800°C and not under reaction conditions. Figure 5.4 shows that the promoted catalysts regained nearly 100% of the hydrogen production observed during the first set of CH_4 pulses. If sintering was occurring during the reaction, it would be reasonable to observe a decrease in the activity, which could not be regained by exposure to pulses of CO_2. Although the Pt/ZrO_2 did exhibit some loss in initial activity, this loss is most likely due to less efficient cleaning on the unpromoted catalyst, which results in a reduction in the amount of exposed active metal due to carbon formation.

The results of the EXAFS and pulse studies show that agglomeration of the Pt particles does occur when the catalyst is heated to high temperatures. This sintering is detrimental to the activity of the catalyst because it decreases the area of metal exposed for reaction. However, an even greater effect is observed on the stability of the catalyst due to a reduction in the metal-

support interaction. A reduction in the interfacial area leads to a reduction in the ability of the catalyst to dissociate CO_2 and an increase in the formation of carbon on the metal. The results of this work have shown that the promoted catalysts do not experience significant sintering. Therefore, another benefit of the cerium and lanthanum is that their presence retards the Pt particle growth and the role of the support is not hindered at high temperatures, leading to increased stability.

5.5 Conclusions

The results presented in this chapter suggest that the addition of cerium and lanthanum to the support has several promotional effects. First, the promoters can increase the thermal stability of the catalyst by stabilizing the tetragonal phase of zirconia. This stabilization results in an increase in the surface area and an increase the density of CO_2 adsorption sites near the metal particle. Based on the two path mechanism described in Chapter 3, the ability of the support to provide an abundance of CO_2 near the Pt particle greatly enhances the cleaning mechanism resulting in improved stability. Second, the addition of promoters aid in retarding particle growth. This is not only beneficial for increasing the active metal surface exposed for reaction, but also maintains a high particle-support interfacial area which is crucial for efficient cleaning of the metal particle. Finally, it can not be ruled out that the addition of the promoters increases the oxygen storage capacity of the

support. It is possible that increasing the oxygen storage capacity can result in improved cleaning ability and higher catalyst stability.

5.6 References

1. Duchet, J. C., Tilliette, M. J., and Cornet, D., *Catal. Today,* **10** 507 (1991).
2. Morterra, C., Cerrato, G., and Ferroni, L., *J. Chem. Soc. Faraday Trans.,* **91(1)**, 125 (1995).
3. Trovarelli, A., de Leitenburg, C., and Dolcetti, G., *Chemtech*, **27(6)**, 32 (1997).
4. Tsukuma, K., and Shimada, M., J. *Mater. Sci.,* **10**, 1178 (1985).
5. Sato, T., and Shimada, M., *Am. Ceram. Soc. Bull.*, **64**, 1382 (1985).
6. Fornasiero, P., Balducci, G., Di Monte, R., Kaspar, J., Meriani, S., Trovarelli, A., and Graziani, M., *J. Catal.,* **151**, 168 (1995).
7. Fornasiero, P., Kaspar, and Graziani, M., *J. Catal.,* **167**, 567 (1997).
8. Balducci, G., Fornasiero, P., Di Monte, R., Kasper, J., Meriani, S., and Graziani, M., *Catal. Lett.*, **164**, 173 (1996).

CHAPTER 6

SUMMARY

The production of synthesis gas is of great interest due to the ability to further produce specialty waxes, solvents, diesel, and environmentally benign gasolines. The most widely used process for the production of synthesis gas is steam reforming, which results in a H_2:CO ratio of 3:1. This ratio is too high for applications such as methanol or oxoalcohol synthesis, which makes separation or purification necessary. Furthermore, a high steam to hydrocarbon ratio is required which increases the operating costs. In recent years, the utilization of carbon dioxide for the reforming of methane has attracted significant interest due to the advantages over steam reforming. The major obstacle preventing commercialization is the inability to find a catalyst capable of operating at the high temperatures required by industry.

Previous work has shown that supported noble metals are good catalysts for the CO_2 reforming of CH_4. Rh catalysts exhibit high activity and stability for the reforming reaction, but are not commercially feasible due to economic market fluctuations. Ni catalysts have been studied because of their low cost, but they experience rapid deactivation from carbon deposition. Pt catalysts have been shown to be very active and stable for the dry reforming reaction at 650°C, but deactivate due to carbon deposition at 800°C. Detailed studies of the reaction at 800°C are necessary because many of the concepts developed from the studies at lower temperatures are not valid at industrially relevant conditions. In this work, we have investigated

the reforming reaction over Pt/SiO_2 and Pt/ZrO_2 catalysts. Specific emphasis has been placed on studying the reaction mechanism, the role of the support, and the addition of promoters to both the metallic phase and the support to reduce carbon deposition and deactivation during the reaction.

The performance of the catalyst was shown to be strongly dependent upon the support. It was found that the Pt/ZrO_2 catalyst had much higher activity and stability than the Pt/SiO_2 catalyst due to the ability of the ZrO_2 to adsorb CO_2 near the metal particle, facilitating its dissociation. On Pt/ZrO_2 catalysts the reaction was found to occur via two independent pathways. CH_4 decomposition occurs on the metal particle resulting in the formation of H_2 and carbon deposition. When Pt is supported on ZrO_2, the carbon formed during the decomposition of CH_4 can reduce the support to form CO, creating oxygen vacancies in the support lattice near the metal particle. The adsorption and dissociation of CO_2 occurs at the vacancies, forming CO and replenishing the oxygen in the support lattice. This redox mechanism results in the cleaning of metal particles by oxygen provided by the support. The long-term activity of the catalyst is dependent upon the balance between the rate of CH_4 decomposition and the rate of dissociation of CO_2.

In an attempt to improve the stability of the catalyst by hindering the rate of CH_4 decomposition, Sn was added as a promoter to the metallic phase. This study showed that the addition of Sn to Pt/SiO_2 catalysts resulted in a catalyst that was more stable for the dry reforming reaction at moderate temperatures. However, due to the thermal instability of SiO_2, the

silica supported bimetallic catalyst did not perform well when the temperature was increased to 800°C. When Sn and Pt were co-impregnated on ZrO_2 the catalytic performance was not improved with the catalyst exhibiting lower activity and stability than the monometallic catalysts. X-ray absorption studies have shown that under oxidizing conditions, segregation of the Pt-Sn alloys occurred, resulting in the formation of tin oxide around the Pt metal. The formation of tin oxide blocks the interaction between the metal and support, inhibiting the role of the ZrO_2.

Surface reduction deposition and other preparation methods resulted in the controlled placement of Sn on the Pt particle, minimizing the promoter-support interaction. These catalysts exhibited higher activity and stability than the monometallic catalyst under severely deactivating conditions, 800°C and a 3:1 ratio of CH_4:CO_2. One application for these bimetallic catalysts could be at natural gas reservoirs where the supply of CO_2 is limited. Although some natural gas reservoirs have an abundance of CO_2 many reservoirs consist primarily of CH_4. The ability of these catalysts to operate in an excess of CH_4 and be regenerated in CO_2 without destruction of the alloy could make the recovery of the natural gas at these reservoirs feasible. In short, these Pt-Sn catalysts allow for the dry reforming reaction to be carried out over a broader range of feed ratios and temperatures.

The second method that was employed to reduce carbon deposition and increase the stability of the catalyst was to add promoters to the support to improve the CO_2 adsorption capacity and dissociation rate. Promotion of

the ZrO_2 support with cerium and lanthanum, prior to the addition of the Pt, resulted in increased activity and stability of the catalyst. The cerium and lanthanum effectively enhanced the cleaning mechanism and reduced carbon deposition on the metal. The improved performance of the promoted catalyst can be attributed to multiple effects including stabilizing the surface area for high temperature operation, increasing the density of CO_2 adsorption sites near the metal particle, and retarding particle growth under reaction conditions. All of these promotional effects result in a catalyst, which is very active and stable for the dry reforming reaction under severely deactivating conditions. Because cerium and lanthanum promoted catalysts operate very efficiently at various ratios of CH_4:CO_2 and at the high temperatures required by industry, these catalysts appear very promising for commercial application.

APPENDIX A

CHARACTERIZATION OF Pt-Sn INTERACTION IN BIMETALLIC CATALYSTS

A.1 Introduction

Pt containing bimetallic catalysts have been of interest for many years because of the enhanced stability towards deactivation by carbon deposition. Promoters such as Re, Ir, and Sn are commonly used in industrial reforming reactions resulting in high activities and selectivities without substantial formation of carbonaceous deposits [1]. Of these three promoters, Sn has been widely studied because of the ability to achieve high catalytic activity for alkane dehydrogenation [2-5]. One explanation for the enhanced properties of the promoted catalysts is formation of alloys between the Pt and the Sn, which reduces the size of Pt ensembles [6, 7], decreasing coke formation and increasing selectivity. It has also been suggested that Sn may modify the catalytic properties of Pt by electronic or ligand effects [8, 9]. This modification may be responsible for changes in the heat of adsorption of different adsorbates participating in the reaction [10, 11].

Even though Sn is one of the most efficient promoters employed in commercial processes [12, 13], deactivation due to coke formation is not completely eliminated and the catalysts still exhibit short lifetimes and must undergo continuous or frequent regenerations to maintain activity [14]. The regeneration typically consists of exposing the spent catalyst to oxygen or air at high temperatures to burn off any carbon produced during the reaction,

followed by a reduction step that brings the catalyst back to the active (metallic) form.

One of the main problems concerning regeneration is the possibility that the exposure to such reduction / oxidation cycles can cause important changes in the catalyst morphology that negatively alter the catalytic properties of the bimetallic catalyst. For example, studies have shown that Pt-Rh alloys, when heated in air, form particles with Pt rich centers and Rh_2O_3 outer surface [15, 16]. Subsequent reduction results in a metallic Rh layer covering a Pt core [17]. On the other hand, Pt-Pd supported alloys behave differently when heated in air at high temperatures. Oxidation causes the Pt-Pd alloy to form two separate crystallites of metal and PdO, both in contact with the silica support [18]. When reduced at high temperatures, the Pd forms metal particles on the edges of the Pt particle. Work has also been done on Pt-Ir alloys, and it has been shown that the alloy is completely destroyed when heated in air [19, 20]. For the particular case of Pt-Sn, Verbeek and Sachtler [7] proposed that, after exposure to air and subsequent reduction, the unsupported Pt-Sn alloys become surface enriched in Sn at the expense of the subsurface zone, with the center of the particle getting rich in Pt. More recently, Chojnacki and Schmidt [21] studied Pt-Sn films supported on planar amorphous silica films and found that exposure to O_2 at 550°C for 1 hr. resulted in destruction of the intermetallic species leaving metallic Pt cores surrounded by a ring of SnO_2 in contact with the silica. However, after

subsequent reduction for long periods of time (18 hrs at 650°C), complete recombination of the alloys was obtained.

In this chapter the interaction between the active metal (Pt) and the promoter (Sn) following different preparation methods is explored, as well as the effects of regeneration treatments on catalytic properties.

A.2 Experimental

A combination of the characterization techniques described in the experimental chapter along with catalytic activity measurements have been employed to study three different Pt-Sn bimetallic catalysts and analyzed the extent of metal-metal interaction. It is widely recognized that the support can strongly affect the metal-metal interaction [22], and if it contains acidity, it can greatly promote the rate of coke formation under isobutane dehydrogenation conditions [23]. Therefore, we have used a silica support which interacts very weakly with Pt or Sn and does not contain acidity. The details about the preparation method and characterization techniques can be found in Chapter 2. A summary of the precursors used, the metal loading, and the nomenclature to be used throughout this appendix can be found in Table A.1.

All catalysts were exposed to cycles of reduction / oxidation before characterization and activity tests. The treatments and nomenclature, summarized in Table A.2, are as follows. The term "fresh" is applied to impregnated samples, which were calcined in air at 400°C for 2 hours.

Catalyst Nomenclature	Pt Weight %	Molar Pt:Sn ratio	Preparation Techniques	Solvent	Precursor
Pt (1.0)	1.0	1:0	Impregnation	HCl	H_2PtCl_6
Pt (1.5)	1.5	1:0	Impregnation	Water	H_2PtCl_6
Pt-Sn (CI)	1.5	1:1	Co-impregnation	Water	H_2PtCl_6
Pt-Sn (CIC)	1.0	1:1.65	Co-impregnation	HCl	H_2PtCl_6
Pt-Sn (SI0.3)	0.3	1:1.65	Sequential Impregnation	Acetone	$Pt(NH_3)_4(NO_3)_2$
Pt-Sn (SI1)	1.0	1:1.65	Sequential Impregnation	Acetone	$Pt(NH_3)_4(NO_3)_2$

Table A.1: Characteristics of the catalysts investigated

Pretreatment Nomenclature	Conditions
Fresh	Calcined in air at 400C for 2 hours
REG300, REG400, REG500	Fresh sample reduced in H2 at 500C for 1h, exposed to reaction conditions at 500C for 1 h, then exposed to air at 300C, 400C, and 500C respectively for 1 hour
OX300, OX400, OX500	Fresh sample reduced in H2 at 500C for 1h, exposed to air at 300C, 400C, and 500C respectively for 1 hour

Table A.2: Summary of pretreatments performed on the catalysts.

Regenerated samples had initially the same pretreatment as the fresh ones, but then were reduced in H_2 at 500°C for 1 hour, exposed to isobutane at 500°C, and treated in air for 1 hour at either 300°C, 400°C, or 500°C to burn any carbonaceous deposits that formed during reaction. These catalysts will be referred to as REG300, REG400, and REG500, respectively. Some fresh samples were reduced and then oxidized in air for 1 hour at 300°C,

400°C, and 500°C without exposure to isobutane. These samples will be referred to as OX300, OX400, and OX500, respectively

A.3 Results

A.3.1 H_2 and CO Chemisorption

Table A.3 gives the H_2 chemisorption data obtained for fresh samples of Pt (1.5), Pt-Sn (Cl) and Pt-Sn (CIC) catalysts, as well as OX300, OX400, and OX500 Pt (1.5) and Pt-Sn (Cl) catalysts. As shown in the table, the bimetallic catalysts Pt-Sn (Cl) and, particularly Pt-Sn (CIC), exhibited significantly lower chemisorption capacities than the monometallic catalysts. For the pure Pt (1.5) sample, varying the oxidation temperature resulted in only a small variation in the fraction of Pt exposed. The Pt-Sn (Cl) sample showed an initial decrease in the fraction exposed with oxidation at 300 °C followed by little variation in adsorption capacity with increasing oxidation temperature. Chemisorption values on the fresh samples were within the range of values reported in the literature [15, 24, 25].

The CO adsorption studies were performed on fresh and spent Pt (1.5 and 1.0), Pt-Sn (Cl), and Pt-Sn (CIC) catalysts. Table A.3 also shows the amount of CO adsorbed by each catalyst. As in the case of H_2 chemisorption, the monometallic Pt catalyst was found to adsorb much more CO than the bimetallic samples. The Pt-Sn (CIC) catalyst showed slightly less CO adsorption than the Pt-Sn (Cl) sample.

Catalyst	Pretreatment	Chemisorption		Turnover Frequencies (sec-1)		
		H/Pt	CO/Pt	based on H/Pt	based on CO/Pt	per total Pt
Pt (1.5)	Fresh	0.51	0.38	2.2	3.6	1.12
	OX300	0.58	-	2.3	-	-
	OX400	0.56	-	-	-	-
	OX500	0.49	-	2.4	-	-
	Spent	-	0.13	-	-	-
Pt(1.0)	Fresh	-	0.3	-	-	-
	Spent	-	0.03	-	-	-
Pt-Sn (Cl)	Fresh	0.30	0.1	6.2	20.6	1.86
	OX300	0.21	-	7.9	-	-
	OX400	0.24	-	7.1	-	-
	OX500	0.22	-	4.5	-	-
	Spent	-	0.02	-	-	-
Pt-Sn (ClC)	Fresh	0.09	0.06	30.9	46.3	2.78
	Spent	-	<0.01	-	-	-

Table A-3: Hydrogen and CO chemisorption and initial turnover frequencies.

An interesting result was observed on the spent catalysts. After 1 hour under reaction conditions (500°C, pure isobutane, 30 WHSV) the samples were cooled in pure He and tested in the dynamic CO adsorption. As shown in Table A.3, the adsorption capacity of the bimetallic samples, particularly Pt-Sn (CIC), became exceedingly low. It is important to note that, despite losing their chemisorption capacity, these samples still retained most of their original activity.

A.3.2 Transmission Electron Microscopy

Figures A.1a and A.1b show the TEM images of a co-impregnated 1:1 Pt:Sn catalyst. The micrograph shown in 1a and 1b are for the fresh and OX500 samples after reduction in H_2 at 500°C for 1 hour. The fresh sample showed two types of particles. The first range from 25Å-50Å in size and were very light in contrast. The second type were much larger (150Å-250Å) and much darker in contrast. After treatment in air at 500°C for 1 hour and reduction for 1 hour, both types of particles underwent changes. The small particles experienced growth so that the average particle size became 50Å-100Å. At the same time, the number of smaller particles (<30Å) became much greater. The larger particles also experienced morphological changes so that the contrast of the particles was no longer homogenous. The particles consisted of surfaces of light contrast with distinct particles of darker contrast. The monometallic Pt catalyst exhibited smaller particles (20-30Å), consistent with the dispersion determined by the chemisorption measurements.

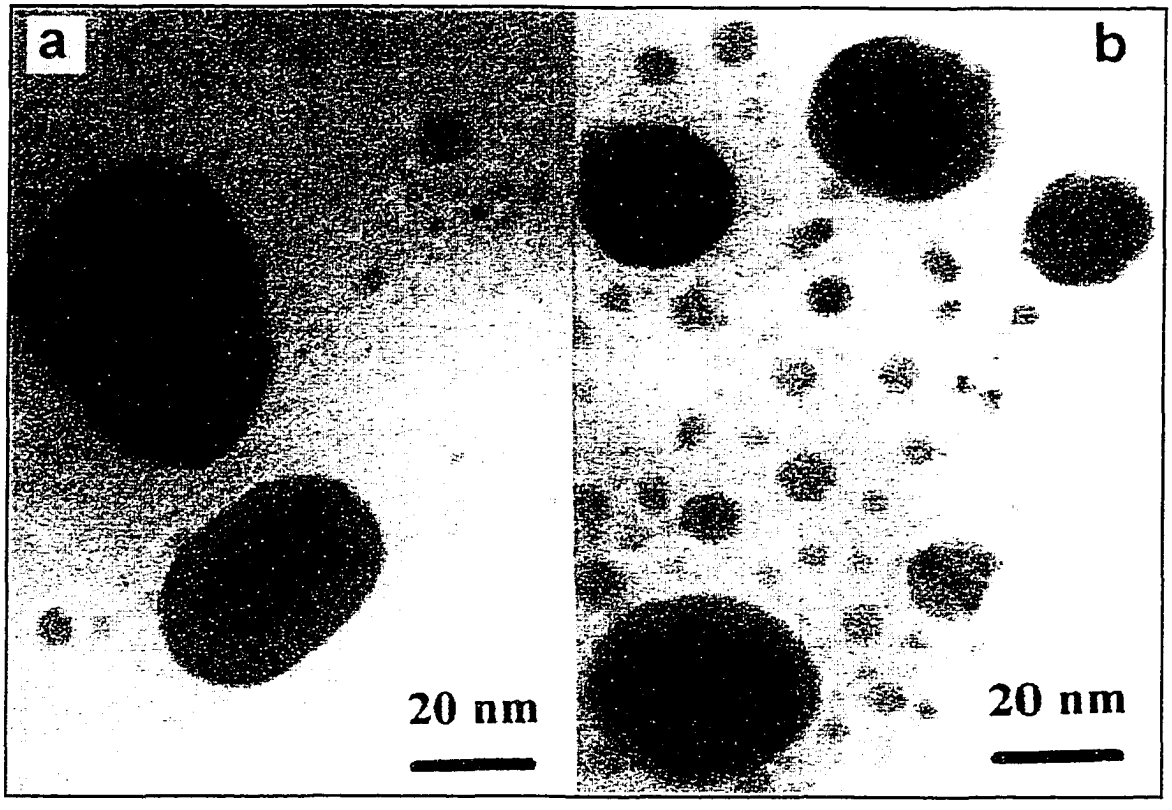

Figure A.1: TEM micrographs of Pt-Sn/SiO_2 (a) fresh after reduction and (b) OX500 after reduction.

A.3.3 Temperature Programmed Reduction

Figure A.2 shows the results of the TPR studies done on the pure Pt (1.5) and Pt-Sn (CIC) catalysts after calcination at 350°C. The TPR for the pure Pt catalyst shows that the H_2 consumption has a maximum at about 125°C and ends at about 200°C. This profile also shows some H_2 consumption at about 400°C. However, this is not due to the reduction of Pt species, but rather to the removal of impregnation precursors which were not totally eliminated during the initial calcination step. The profile for the Pt-Sn (CIC) catalyst has two H_2 consumption peaks. The first appears in the same

position as that for pure Pt (125°C), while the second has a maximum at 200°C. Unlike the catalysts prepared by sequential impregnation, the Pt-Sn (CIC) shows no reduction peak at high temperatures, characteristic of unalloyed Sn.

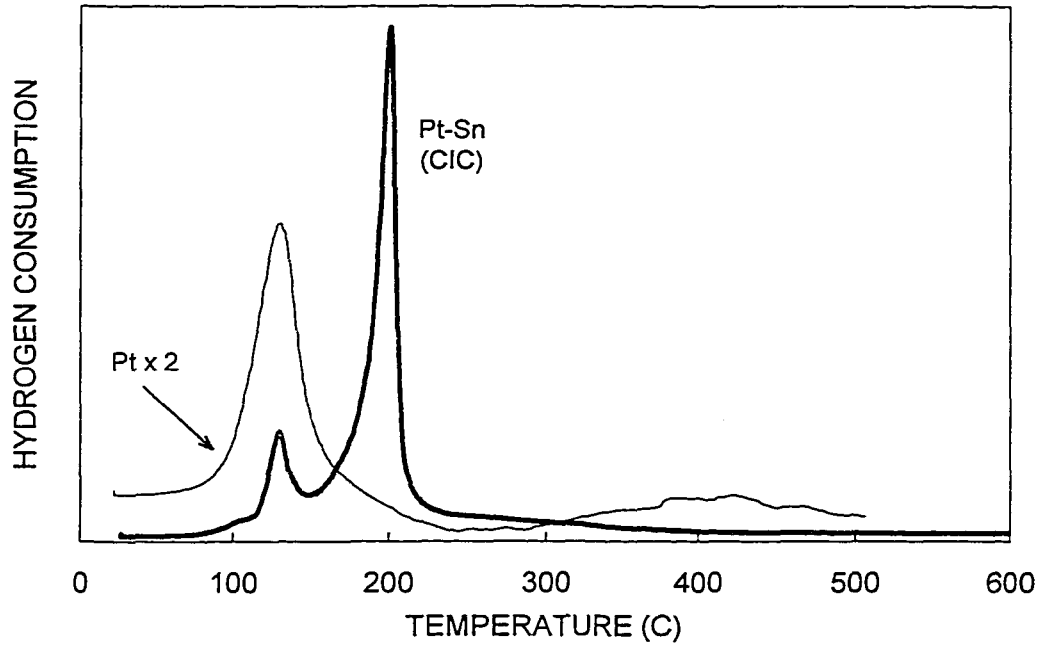

Figure A.2: Temperature Programmed Reduction (TPR) profiles of silica-supported Pt (1.5) and Pt-Sn (CIC) catalysts after calcination at 350°C.

The profiles for the Pt-Sn (SI) catalysts are shown in Figure A.3. They contain peaks that are broader and extend to much higher temperatures than those shown in Figure A.2. Calcination of the sample at 400°C resulted in three H_2 consumption regions. The first peak again appears at the same position as that for pure Pt (125 °C) and has the smallest intensity of the three peaks. The second consumption region is the largest, and has a maximum

near 250 °C. The last region spans from approximately 400 °C to 600 °C with the greatest intensity at about 525 °C.

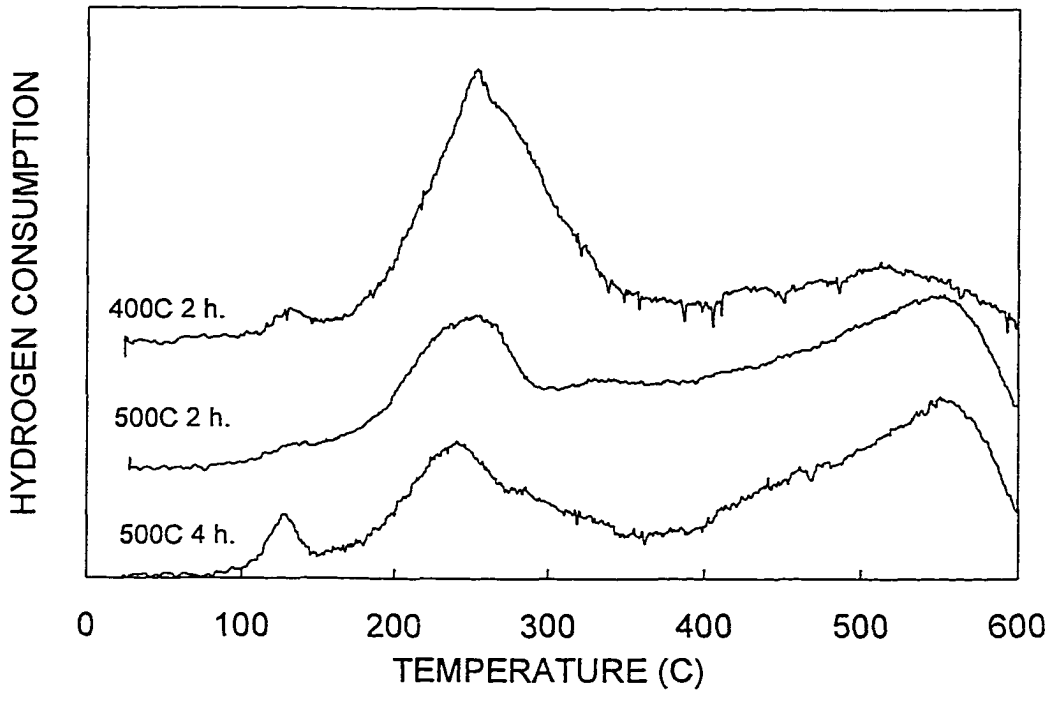

Figure A.3: TPR profiles of silica-supported Pt-Sn (SI) catalyst after calcination at various temperatures and times

Figure A.3 also shows the consequences of increasing the calcination temperature on the TPR profile. When the calcination was done at 500°C for 2 hours, the peak at 125°C did not change much, but the peak at 250°C decreased in intensity while the higher temperature peak became dominant. Also, the position of the third region shifted slightly so that the maximum occurred at 575°C. When the calcination time increased to 4 hours, the low temperature region showed a large increase in intensity.

The TPR profiles for the Pt-Sn (Cl) catalyst after oxidation at different temperatures are shown in Figure A.4. The fresh Pt-Sn (Cl) sample showed three hydrogen consumption peaks centered at 146°C, 186°C, and 375°C. The first two peaks appeared as a large broad region with the highest intensity at 186°C, and a shoulder at lower temperatures. The third peak was much smaller.

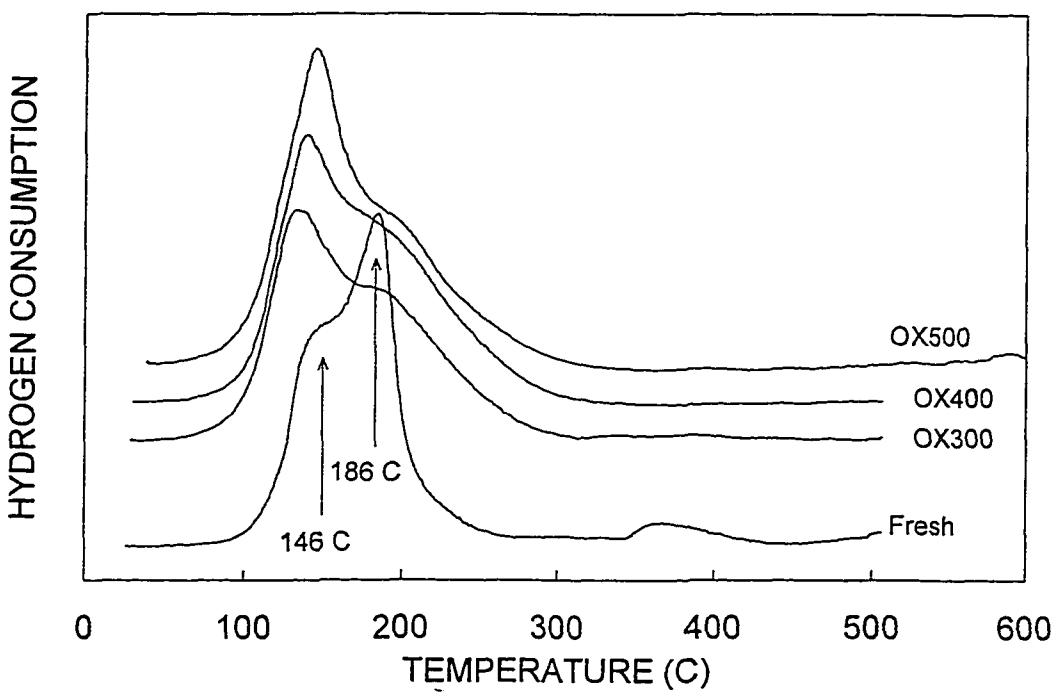

Figure A.4: TPR profiles of the Pt-Sn (Cl) catalyst after various pretreatments: Fresh, OX300, OX400, and OX500 (see Table A.2 for details of each pretreatment)

Subsequent oxidation of the reduced sample at 300°C, 400°C, and 500°C resulted in the removal of the high temperature peak and, more relevant to the succeeding discussion, a significant decrease in the intensity

of the peak at 186°C. This decrease in intensity was accompanied by the appearance of a shoulder between 200 and 300°C that made the peak broader. Finally, the peak that appeared at 146°C on the fresh sample slightly changed position as the oxidation temperature increased.

A comparable set of experiments was done for the pure Pt (1.5) catalyst (not shown). These runs exhibited a single consumption peak at about 125°C, which did not change much after the various oxidation pretreatments. These runs confirmed that the peak at about 400°C in the fresh monometallic catalyst was due to the removal of residues from the impregnation precursors. They were eliminated during the reduction / oxidation cycles and the H_2 consumption at 400°C did not appear for these samples.

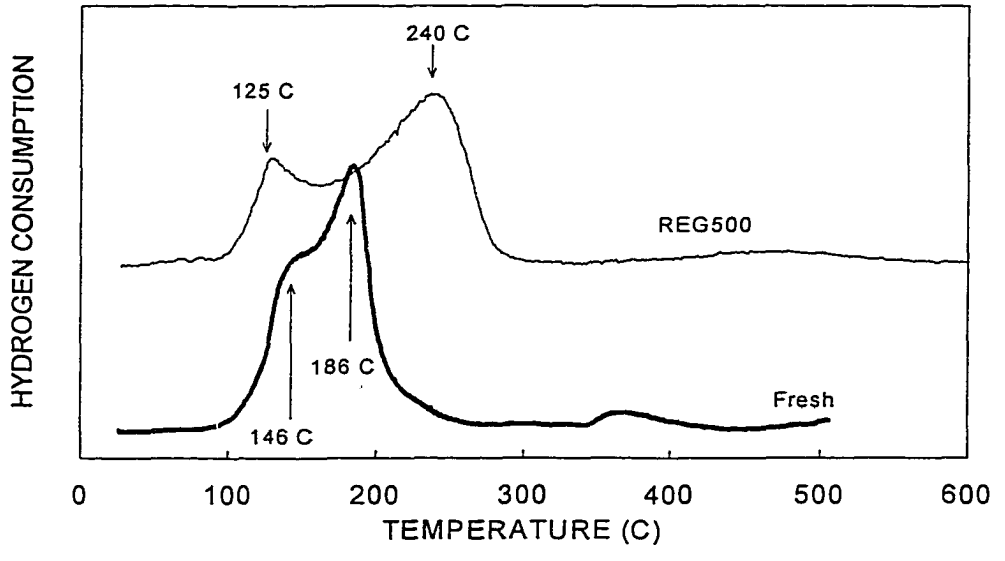

Figure A.5: TPR profiles of the Pt-Sn (Cl) catalyst after various pretreatments: Fresh, and REG500 (see Table A.2 for details of each pretreatment)

Figure A.5 shows the TPR results for the regenerated Pt-Sn (Cl) sample, REG500, in comparison to the fresh catalyst. The result is similar to that observed for the series of oxidized samples, although in this case the effects were more pronounced. The low temperature peak shifted to the position that is typical of unalloyed Pt, 125°C, while the conversion of the 186°C peak into a broad peak at about 240°C was more evident for this sample than for the oxidized samples.

A.3.4 Temperature Programmed Oxidation of Carbonaceous Deposits

TPO studies were performed on the catalysts after exposure to isobutane for 15 minutes. Figure A.6 shows that the addition of Sn decreased the intensity of the CO_2 evolution in all three oxidation regions.

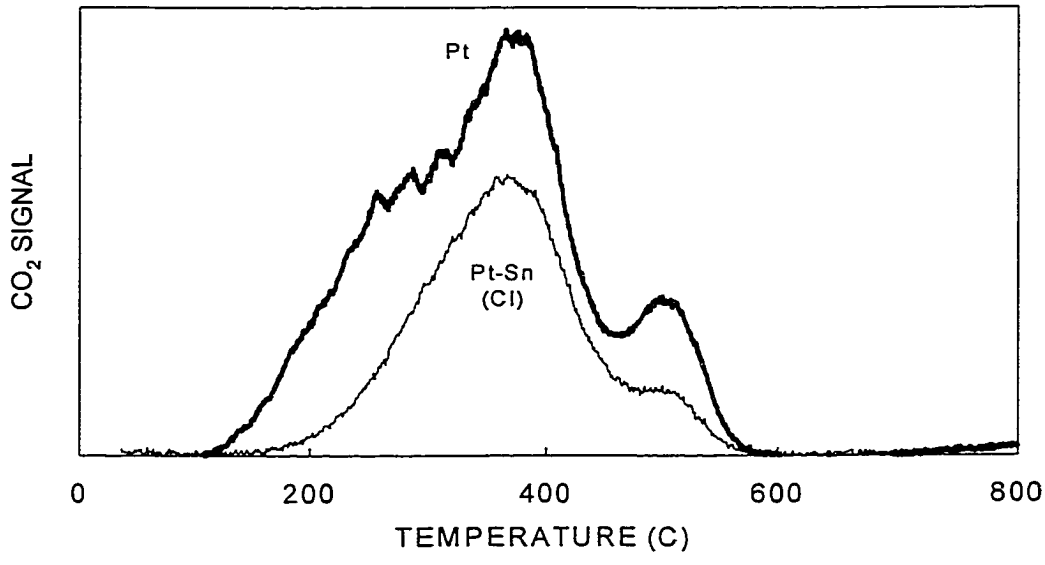

Figure A.6: Temperature Programmed Oxidation (TPO) profiles of carbonaceous deposits left on the monometallic Pt (1.5) and the bimetallic Pt-Sn (Cl) catalysts after exposure to isobutane at 500°C for 15 minutes.

The position of the peaks are the same for the pure Pt and bimetallic Pt-Sn samples, however, the amount of coke formed on the bimetallic sample was approximately 50 % less than that on the monometallic Pt catalyst. The amount of carbon formed on the Pt (1.5) catalyst after 15 minutes was 0.31 wt %, which corresponds to about 4 C atoms per Pt atom.

Figures A.7a and A.7b show the results of diluting the isobutane feed with He on the Pt (1.5) and Pt-Sn (Cl) samples, respectively. On the Pt catalyst, dilution with He had almost no influence on the amount of coke measured after 15 minutes of reaction. However, on the Pt-Sn (Cl) dilution with He resulted in the reduction of the largest TPO peak (375 °C) by about 50 % and almost complete elimination of the high temperature oxidation peak (510 °C). Dilution with He did not affect the position of any of the three oxidation peaks for either the Pt (1.5) or Pt-Sn (Cl) catalysts.

Changing the partial pressure of isobutane with the addition of H_2 modified the coke formation for both the Pt (1.5) and Pt-Sn (Cl) catalysts. Figures A.8a and A.8b show that the intensity of all of the peaks decreased by about 50 % when the ratio of H_2 to isobutane approached 1. Also, the high temperature peak showed a slight shift in temperature from a maximum of 500 °C with no H_2 flow to 525 °C at a H_2 flow of 50 cc/minute.. The Pt-Sn (Cl) catalyst showed changes in both the intensity and positions of the peaks with the addition of H_2. The largest peak shifted from approximately 375 °C with no H_2 flow to 325 °C with H_2 flow of 50 cc/minute..

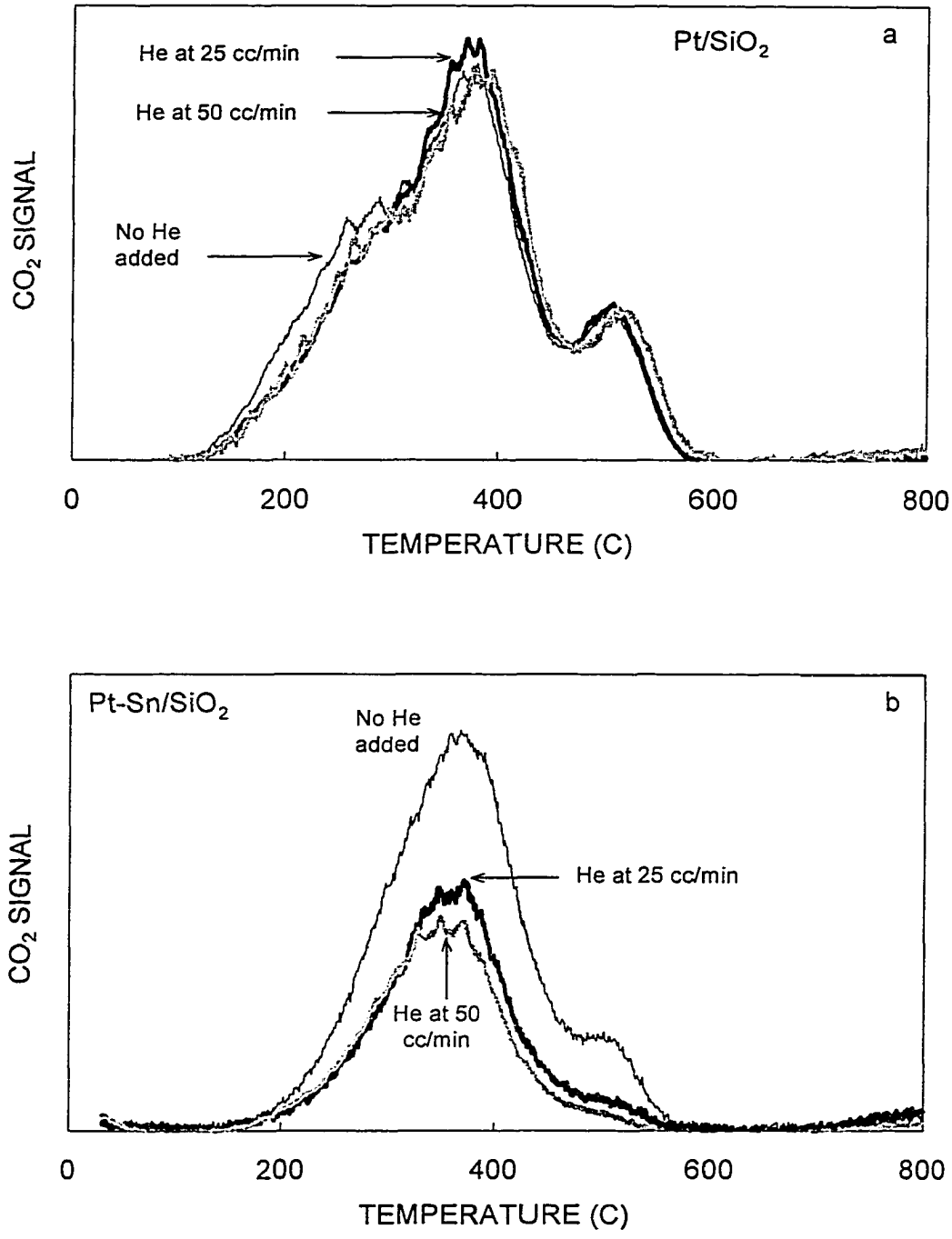

Figure A.7: TPO profiles of carbonaceous deposits left on the catalysts after exposure to isobutane at 500°C for 15 minutes at a constant isobutane flow rate of 54 cc/min (83 WHSV) and He flow rates of 0, 25 and 50 cc/minute. (a) $Pt(1.5)/SiO_2$ catalyst; (b) Pt-Sn (Cl)/ SiO_2 catalyst.

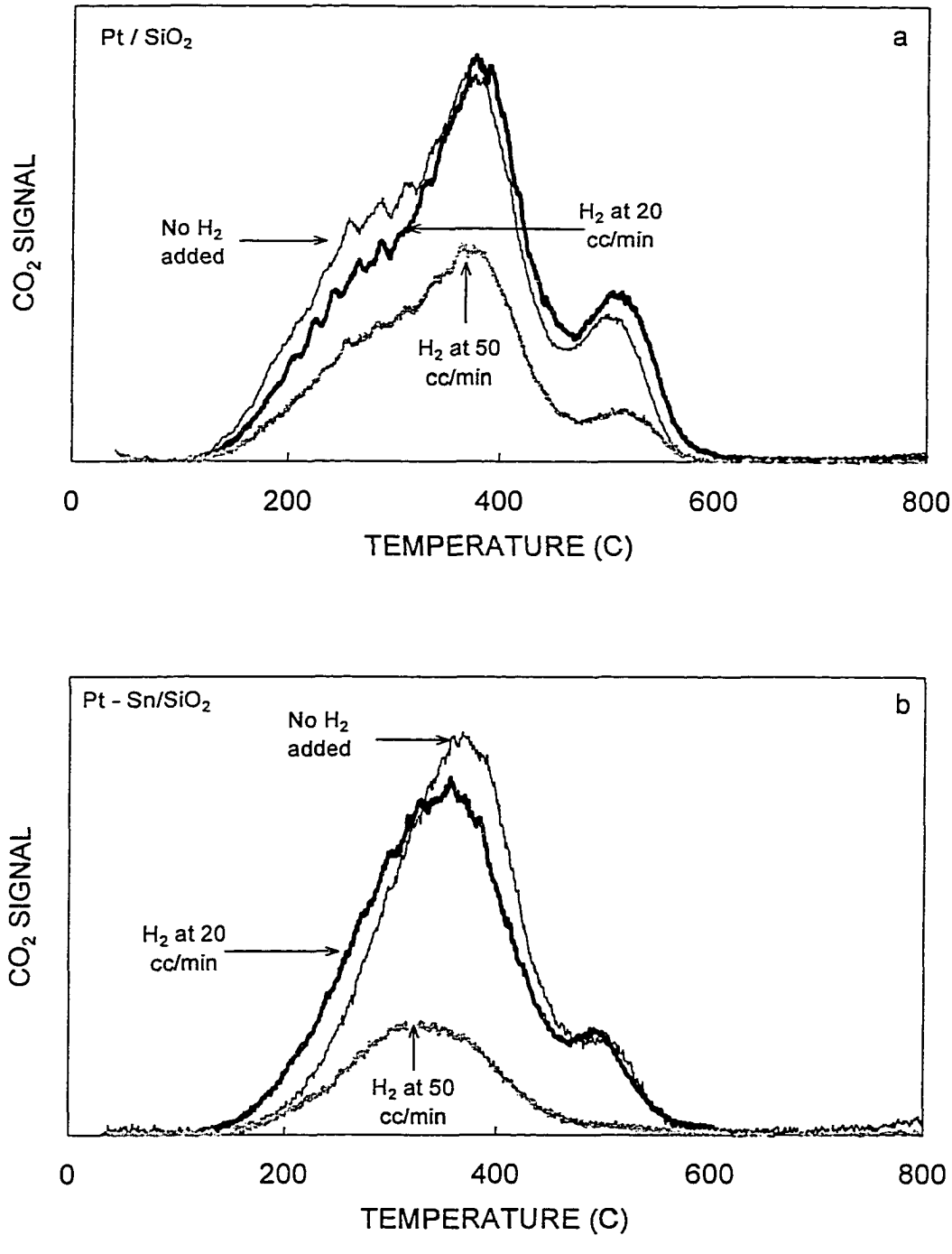

Figure A.8: TPO profiles of carbonaceous deposits left on the catalysts after exposure to isobutane at 500°C for 15 minutes at a constant isobutane flow rate of 54 cc/min (83 WHSV) and H_2 flow rates of 0, 25 and 50 cc/minute. (a) Pt (1.5)/SiO_2 catalyst; (b) Pt-Sn (Cl)/ SiO_2 catalyst.

The high temperature peak was not affected with a H_2 flow of 20 cc/minute, but was completely removed at the higher flow rate of H_2. Figure A.9 compares the amount of carbon deposited on each catalyst for the various conditions described above.

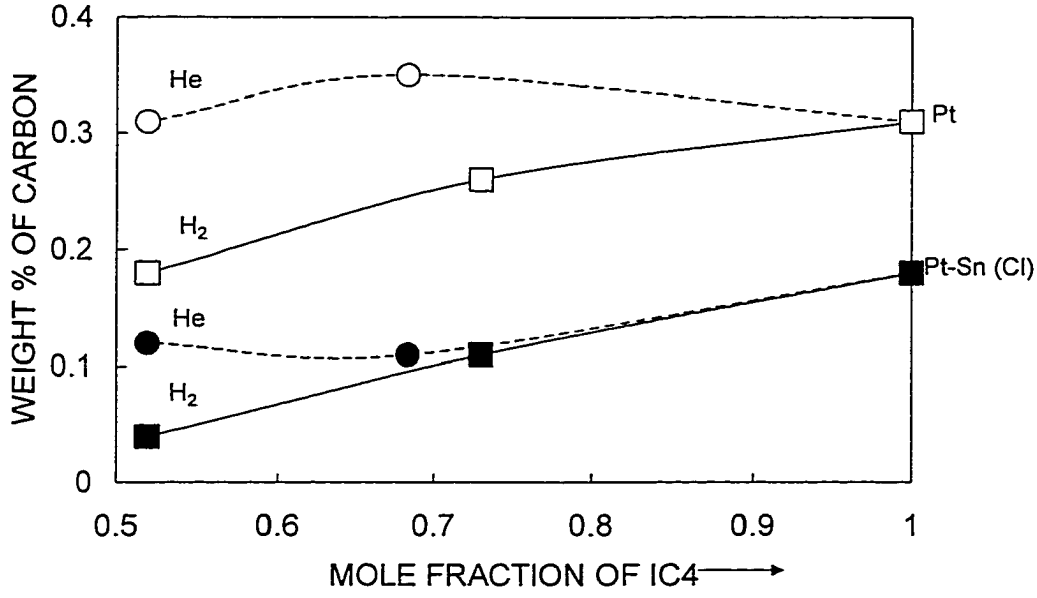

Figure A.9: Amount of carbon deposited on the Pt (1.5) (open symbols) and Pt-Sn/SiO_2 (Cl) (filled symbols) catalysts, after 15 minutes exposure to isobutane at 500°C and at a space velocity of 83 WHSV, as a function of isobutane concentration in He (circles) and H_2 (squares).

The trend lines clearly show the effects of adding H_2 and He to the feed stream along with the reduction in coke formation with the addition of Sn. It is observed that dilution with He does not affect the amount of coke deposited on the monometallic catalyst. Deactivation of the Pt catalyst occurs so rapidly that saturation of the surface by carbon deposits has occurred after

only a few minutes on stream. However, dilution with hydrogen results in a marked decrease in the amount of carbon when the H_2:hydrocarbon ratio approaches 1:1 due to hydrogenation of coke precursors.

Figure A.10 shows the TPO profiles for three Pt (1.5) samples after exposure to pure isobutane for 2 minutes. The first is a fresh sample exposed to isobutane at 500°C for 2 minutes. The second is OX500, which has been exposed to isobutane for 2 minutes at 500°C. The third is a fresh sample which has been exposed to isobutane for 2 minutes at 500°C, regenerated in air at 500°C for 1 hour, reduced in H_2 at 500°C for 1 hour, and then exposed to isobutane a second time for 2 minutes (REG500). Since the amount of coke is a strong function of the olefin concentration in the gas phase and, consequently, the level of conversion, we have normalized the TPO signal to the steady state conversion obtained on each of the samples. All comparisons will be made on this basis.

The TPO profile for the fresh sample of the monometallic Pt (1.5) catalyst after 2 minutes of reaction is similar to the one obtained after 15 minutes of reaction. Oxidation at 500°C before exposure to reaction caused the position of the CO_2 peaks to shift to higher temperatures. The appearance of a high temperature oxidation peak was seen on the oxidized catalyst, but this peak was not present on the regenerated sample. This high temperature peak started at approximately 550°C and spanned up to 800°C. The two peaks at lower temperatures shifted from approximately 275°C and

400°C to 350°C and 425°C, respectively. The amount of coke formed on the oxidized catalyst was slightly less than that of the fresh sample. Regeneration of the catalyst resulted in a 45 % decrease in the coke formed during the second exposure to isobutane. The positions of all three oxidation peaks were identical to that of the fresh sample, however the intensity of each of the peaks, especially the one at 400°C was significantly reduced.

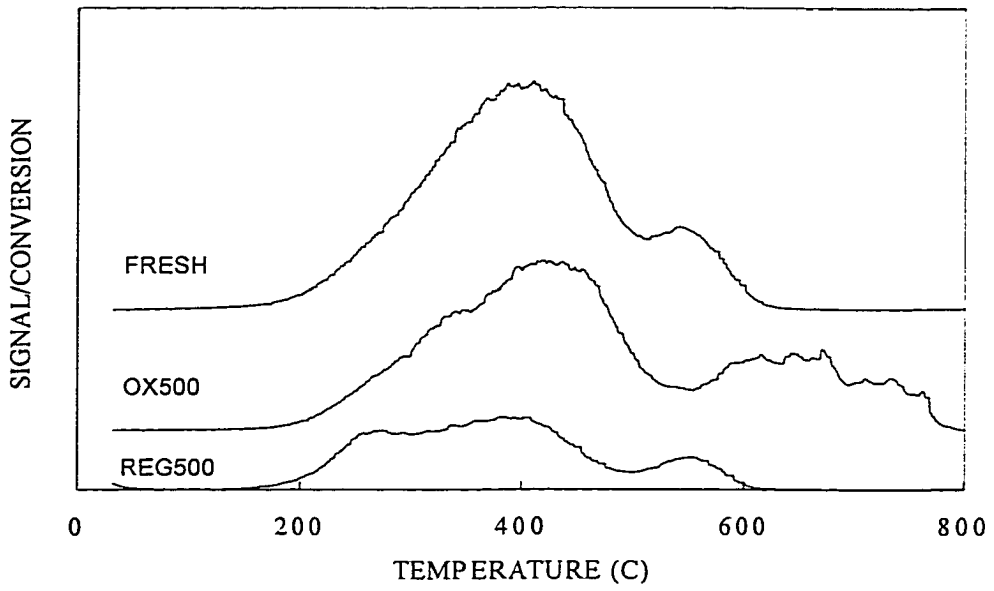

Figure A.10: TPO profiles of Fresh, OX500, and REG500 samples of pure Pt (1.5)/SiO_2 catalysts after exposure to isobutane at 500°C (248 WHSV) for 2 minutes.

As will be explained below, we ascribe the reduced rate of coke formation observed on the regenerated catalysts to the presence of coke deposits that were not removed by the regeneration process. These remaining deposits modify the Pt surface making it more resistant to coking. To prove this, we conducted TPO measurements on a regenerated catalyst

without further exposure to the isobutane feed. Indeed, this experiment showed that about 25 % of the carbon initially deposited still remained on the catalyst after the regeneration step.

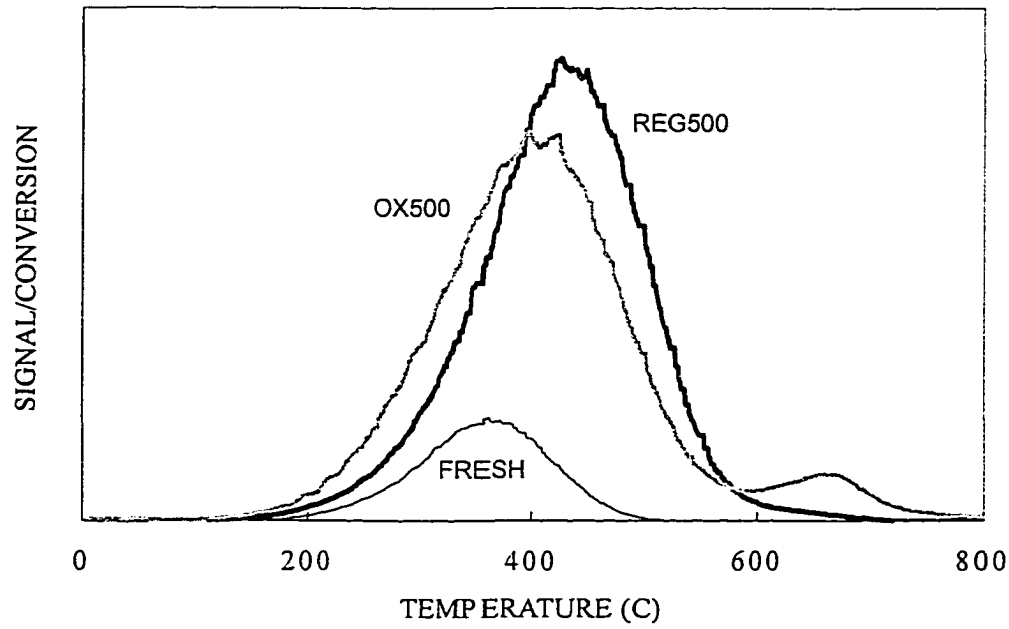

Figure A.11: TPO profiles of Fresh, OX500, and REG500 sample of Pt-Sn (Cl)/SiO_2 catalysts after exposure to isobutane 500°C (248 WHSV) for 2 minutes.

Contrary to the monometallic catalyst, the bimetallic Pt-Sn (Cl) showed an increase in the rate of coke formation after the regeneration and oxidation pretreatments. As shown in Figure A.11, the fresh sample formed a very low amount of coke during exposure to isobutane for 2 minutes. Only one broad oxidation peak was observed at approximately 375°C. The OX500 catalyst formed a much larger amount of coke and the subsequent TPO profile looked very similar to that of the oxidized monometallic Pt (1.5) sample. The main

peak shifted to temperatures near 410°C and a new high temperature peak appeared near 650°C. Like the oxidized Pt-Sn catalyst, the regenerated sample (REG500) resulted in a much higher rate of coke formation than the fresh bimetallic catalyst and the TPO of this sample exhibited a single broad peak centered at around 410°C.

In summary, the reduction / oxidation (500°C) cycle on the monometallic Pt catalyst did not have a great effect on the amount of coke formed during the following reaction period but significantly altered its oxidation characteristics, i.e., the coke became more refractory. The regeneration of the Pt catalyst did not completely eliminate the coke deposits, but these deposits hindered further formation of coke. The bimetallic catalysts exhibited a very different behavior. Both, the oxidation and regeneration procedures caused a large increase in the amount of coke that was formed during the subsequent 2 minute cycles under reaction conditions.

A.3.5 Isobutane Dehydrogenation Activity

Isobutane dehydrogenation reaction studies were performed on the monometallic Pt, and bimetallic Pt-Sn (CI), Pt-Sn (CIC), and Pt-Sn (SI) catalysts. Figure A.12 (a and b) compares the dehydrogenation activity and selectivity of the Pt (1.5), Pt-Sn (CI), Pt-Sn (CIC), and Pt-Sn (SI1) catalysts in a flow of isobutane:He, 2:1, at a space velocity of 248 WHSV. Although all bimetallic catalysts showed greater activity and selectivity than the unpromoted catalyst, the co-impregnated catalysts exhibited a significantly

better performance than the sequentially impregnated catalyst. This superior performance was evident in the activity, selectivity and stability.

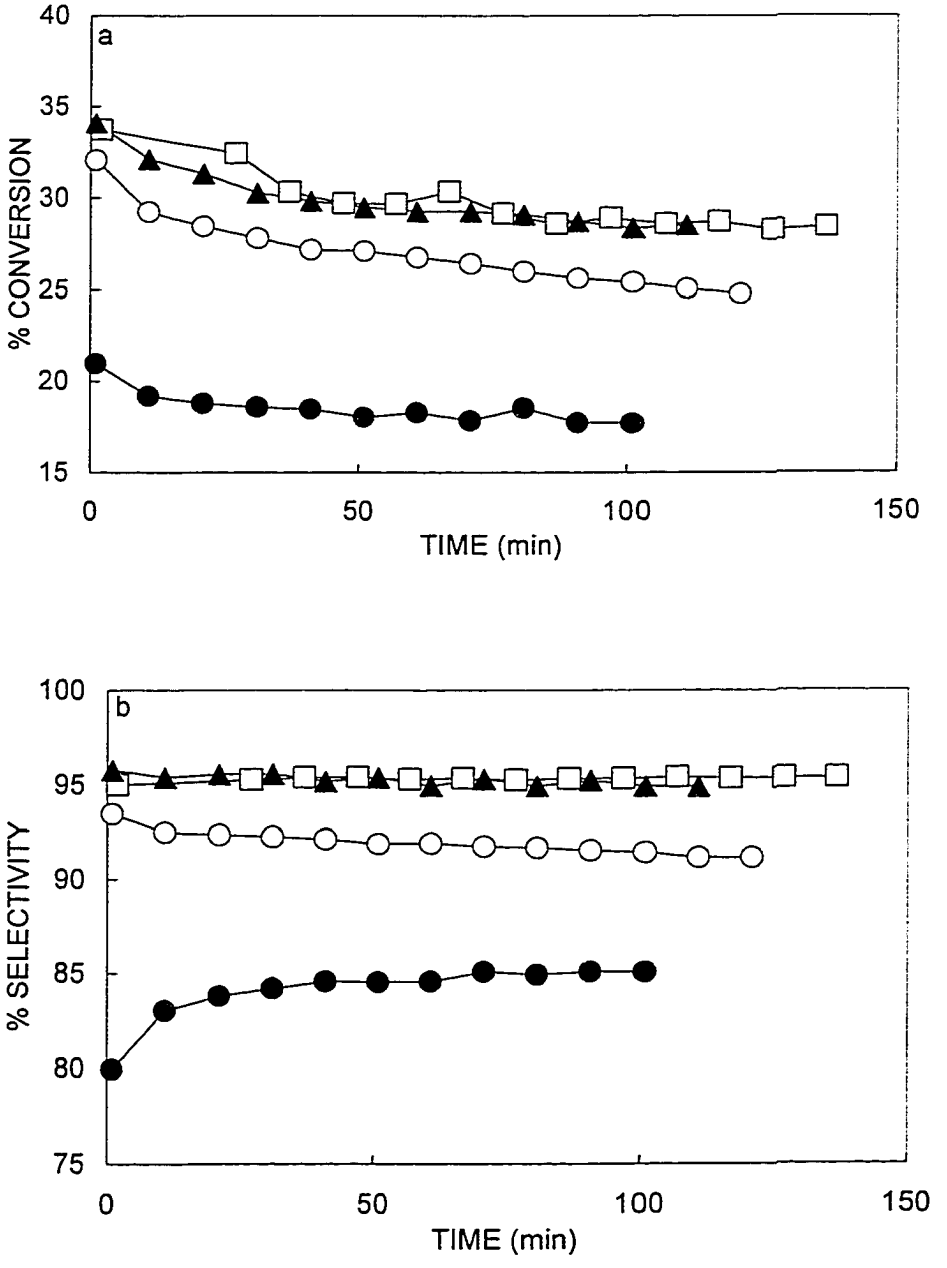

Figure A.12: Isobutane dehydrogenation as a function of time on stream over Pt (1.5) (●), Pt-Sn (CI) (□), Pt-Sn (CIC) (▲), and Pt-Sn (SI) (○) catalysts in a flow of 2:1 isobutane:He at 500°C (248 WHSV). (a) conversion (%); (b) selectivity to isobutene (%)

The selectivity of the co-impregnated bimetallics remained near 96 % throughout the duration of the experiment, while the Pt (1.5) catalyst selectivity started at 80 % and increased to reach a maximum of 84 % after 100 minutes on stream. The sequentially impregnated catalyst presented a selectivity higher than the monometallic, but substantially lower than the co-impregnated catalysts.

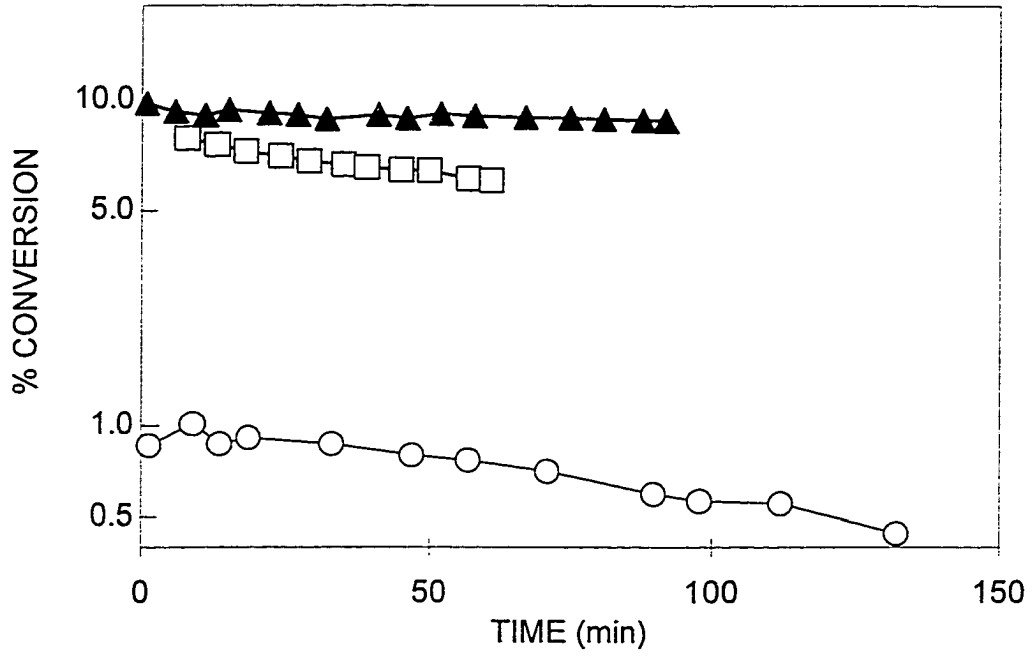

Figure A.13: Logarithmic comparison of the variation of the isobutane conversion as a function of time for the Pt-Sn (CI) (□), Pt-Sn (CIC) (▲), and Pt-Sn (SI) (○) in a low of isobutane at 500°C (300 WHSV).

The most dramatic differences displayed among the bimetallic catalysts prepared by the different procedures was observed when the samples were tested under pure isobutane at 500°C and a space velocity of 300 WHSV. Under these conditions the deactivation of the monometallic

catalysts was very fast and the conversion after a few minutes was below the detectable limit. By contrast, no deactivation was observed on the Pt-Sn (CIC) catalyst which, under these conditions, maintained a 10 % conversion for several hours and 100 % selectivity to isobutylene. As illustrated in Figure A.13, the other co-impregnated CI catalyst, exhibited similarly high conversion and selectivity. However, the rate of deactivation was significantly higher than that observed on the CIC sample. Finally, the sequentially impregnated catalyst exhibited a much poorer performance, with a conversion about one order of magnitude lower and, even at these low conversions, a high rate of deactivation.

Figure A.14 shows the results of an experiment performed to analyze the effects of the presence of H_2 on the activity and selectivity of the bimetallic Pt-Sn (CIC) catalyst. In the first run, we exposed the sample to a flow of 10 cc/minute isobutane and 110 cc/minute He at a space velocity of 245 WHSV. Under these conditions, the catalyst exhibited a high initial activity but deactivated rapidly. A subsequent run was performed in the presence of H_2 keeping the same space velocity. In this run we used a flow of 10 cc/minute isobutane, 100 cc/minute He, and 10 cc/minute H_2. In this case, the initial activity was much lower than that in the absence of H_2 but the deactivation was much less severe. After 90 minutes on stream, the flow was switched to the conditions of the first run, and the conversion increased to values even greater than that on the catalyst that was not exposed to H_2. Similar experiments were also performed on the pure Pt (1.0) catalyst, however, in

this case, the initial activity in the presence of H_2 was higher than that for the runs diluted only with He.

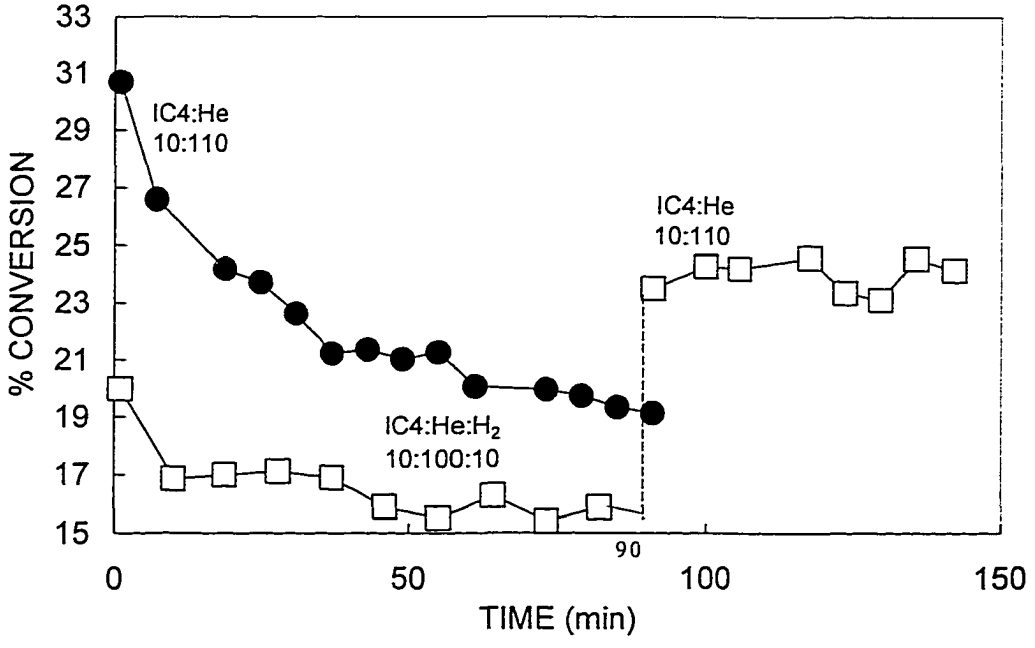

Figure A.14: Effect of hydrogen addition on the time evolution of the isobutane dehydrogenation activity of a fresh Pt-Sn (CIC) sample at 500°C. (●): run in an isobutane:He mixture at a 10:110 flow ratio and a space velocity of 245 WHSV. (□): run in isobutane:He:H_2 at flow of 10:100:10 (245 WHSV) for 90 minutes, then return to the conditions of the first run, that is, flow of isobutane:He at 10:110 (245 WHSV).

To study the effect of regeneration on the monometallic and bimetallic catalysts, the spent Pt (1.5) catalyst after a reaction period of 100 minutes at 500°C (2:1 isobutane:He, 248 WHSV) was regenerated by carbon burning in air for 1 hour at 300 °C and 500 °C with subsequent reduction for 1 hour in H_2 at 500 °C.

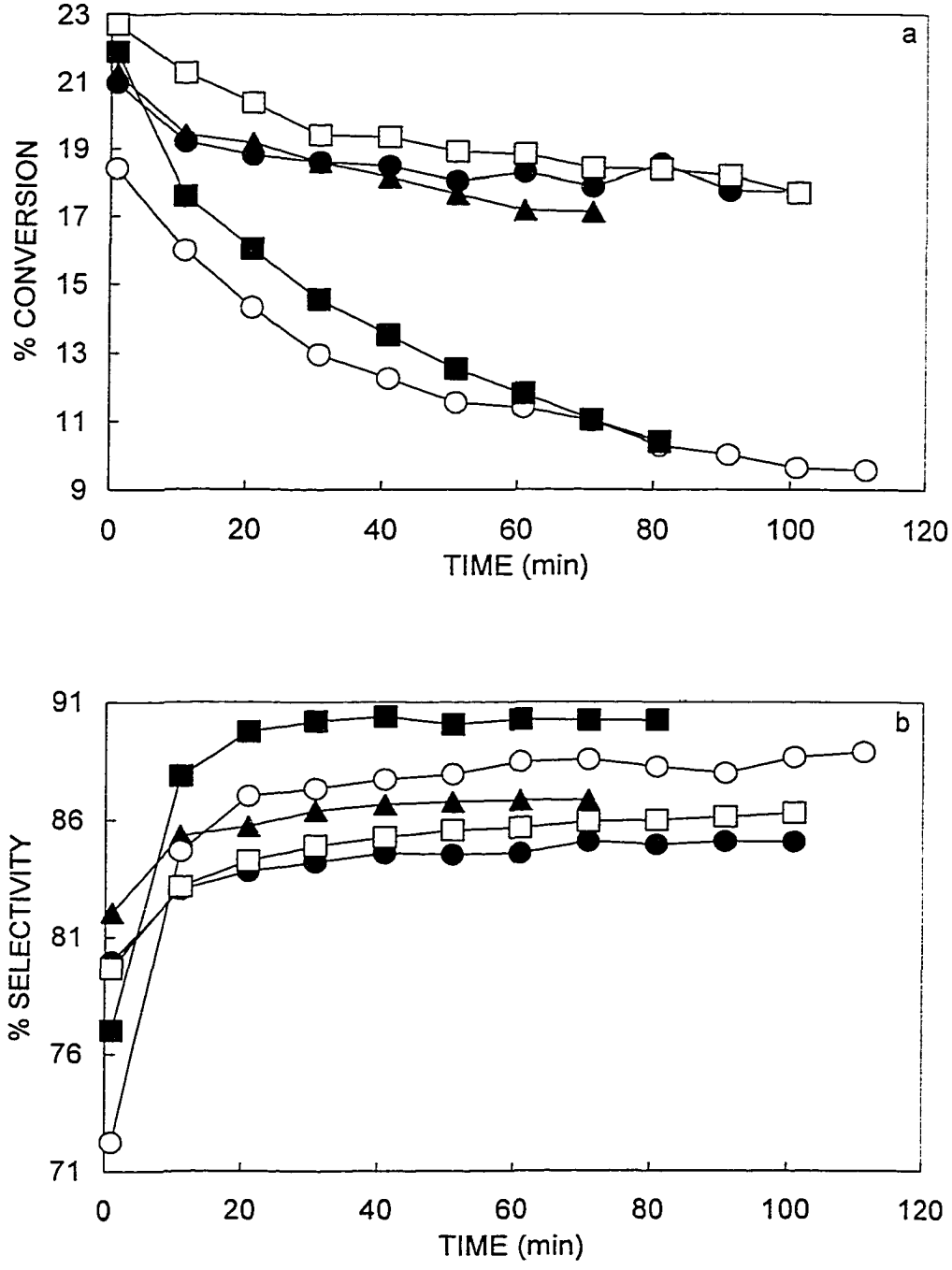

Figure A.15: Isobutane dehydrogenation as a function of time on stream over Fresh (●), REG300 (□), REG500 (▲), OX300 (○), and OX500 (■) samples of pure Pt (1.5) in a flow of 2:1 isobutane:He at 500°C (248 WHSV). (a) conversion (%); (b) selectivity to isobutene (%)

Figure A.15a shows that, in the case of the monometallic Pt (1.5) catalyst, the regeneration at 300°C and 500°C resulted in a catalytic behavior similar to that of the fresh Pt (1.5) catalyst. Figure A.15a also shows the activity data for the pure Pt sample after reduction followed by oxidation at 300°C and 500°C (OX300 and OX500), and subsequent reduction at 500°C. On these samples, the level of activity after 2 minutes was about the same as that of the fresh or regenerated samples, but, as opposed to the regenerated catalysts, these samples exhibited a dramatic increase in the rate of deactivation. After 90 minutes on stream, the catalysts had lost approximately 50 % of their respective activities at 2 minutes.

The corresponding selectivity data for the same series of samples are shown in Figure A.15b. The fresh Pt sample had the lowest selectivity to isobutene when compared to the regenerated and oxidized catalysts. The regenerated catalysts had selectivities at 2 minutes near that of the fresh Pt, but then increased with time on stream to approximately 85 %. Oxidation at 300°C and 500°C resulted in an initial decrease in the selectivity, but after 10 minutes on stream the selectivity already reached 85 %, and continued to increase to values near 90 %.

Figure A.16 shows the effects of regeneration on the bimetallic Pt-Sn (Cl) catalyst. The catalyst regenerated at 300 °C regained almost all of the activity of the fresh. On the other hand, regeneration at 500 °C resulted in a

large loss of activity. The selectivity of the Pt-Sn (Cl) catalyst showed only a slight decrease with regeneration.

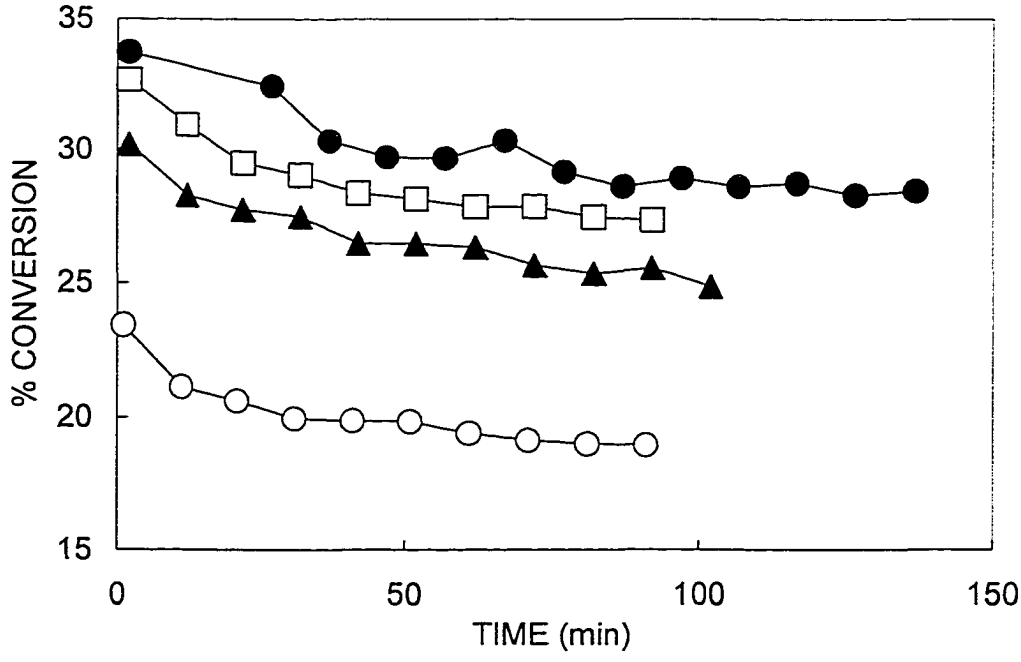

Figure A.16: Isobutane dehydrogenation activity for Fresh (●), REG300 (□), REG400 (▲), REG500 (○) samples of Pt-Sn (Cl) in a flow of 2:1 isobutane:He at 500°C (248 WHSV).

Figure A.17 depicts the effects of the reduction / oxidation cycles on the Pt-Sn (Cl) catalysts. The activity observed on the OX300 and OX500 samples was lower than the activity of the catalyst regenerated under the same conditions. Also, the selectivities of all of the oxidized samples were lower than those of the regenerated samples at the equivalent temperatures. The catalytic behavior of the Pt-Sn (ClC) sample (not shown) did not differ much from that of the Pt-Sn (Cl) sample described above. The main

difference was a more pronounced drop in activity and selectivity after the regeneration treatment at 500°C.

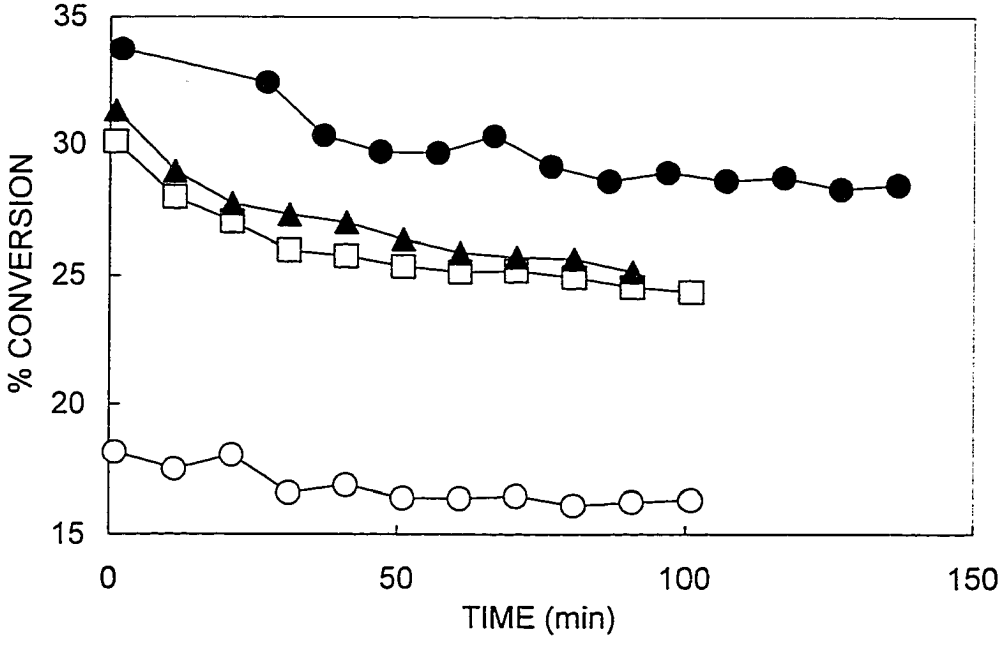

Figure A.17: Isobutane dehydrogenation activity for Fresh (●), OXD300 (□), OXD400 (▲), OXD500 (○) samples of Pt-Sn (Cl) in a flow of 2:1 isobutane:He at 500°C (248 WHSV).

In summary, although the bimetallic catalysts exhibited higher activity and selectivity than the monometallic ones, these differences became less pronounced after reduction / oxidation treatments at high temperatures. The high temperature oxidation treatment had adverse effects on both monometallic and bimetallic catalysts, while the high temperature regeneration only affected the catalytic behavior of the bimetallic samples.

A.4 Discussion

The results of these experiments show the importance of the type of impregnation procedure used in the preparation of Pt-Sn/SiO_2 catalysts and demonstrate that the regeneration process may result in deterioration of the catalytic performance due to a decreased interaction between the active metal and the promoter.

A.4.1 Effect of the impregnation method employed

The composition of the bimetallic clusters in Pt-Sn catalysts has been a matter of study for several years [26]. The presence of bimetallic alloys has often been reported. For example, from their EXAFS and x-ray diffraction data, Meitzner et al. [6] have proposed that PtSn and Pt_3Sn alloys are present in reduced Pt-Sn catalysts. Similarly, Li et al. [27] used Mossbauer studies to show that PtSn is the most prevalent alloy formed on the bimetallic catalyst. Chojnacki and Schmidt [19] used TEM and electron diffraction to show that Pt and Sn supported on planar amorphous silica films consisted of several intermetallic species including PtSn, Pt_3Sn, and $PtSn_4$. Reduction of the films for 18 hrs. at 650°C in H_2 resulted in particles with the major phase being PtSn but with a surface layer of $PtSn_4$. No FCC Pt was found on these films, possibly due to the long reduction times and high reduction temperatures. Although the oxidation state of Sn has been a matter of discussion, it is now widely accepted that the fraction of tin alloyed with Pt is metallic Sn^o [28] and this fraction is much larger on SiO_2 than on Al_2O_3 [27, 29]. Therefore, we

could expect than on our SiO_2 support, depending on the initial distribution of the precursors on the surface, a relatively large amount of Sn should be alloyed with Pt.

In fact, the different TPR results obtained for the various preparations can be explained in terms of the presence of Pt-Sn alloys of different compositions [19, 30]. The position of the reduction peaks can be expected to shift to higher temperatures as the concentration of Sn, more difficult to reduce than Pt, increases. For example, the Pt-Sn (CIC) sample showed two distinct hydrogen consumption peaks. The low temperature reduction peak at around 125°C is characteristic of unalloyed Pt and was also seen on the monometallic Pt catalyst. The dominant peak at about 200 °C can be ascribed to a Pt-Sn alloy with a higher concentration of Sn than those observed on the Pt-Sn (CI) sample, which had H_2 consumption peaks appearing at lower temperatures. In both cases, however, peaks indicative of unalloyed Sn, which should appear at much higher temperatures, were not observed. By contrast, the sequentially impregnated catalyst, Pt-Sn (SI), exhibited high temperature consumption peaks. In this case, the Pt species are much less effective in catalyzing the reduction of Sn, indicating that a large fraction of Sn is physically separated from Pt. These results demonstrate that, among the preparation methods studied here, the co-impregnation methods are clearly superior to the sequential impregnation method. Preparations based on sequential impregnation methods may result in low extents of Pt-Sn interaction. For example, in agreement with our data,

Barias et al. (15) have reported TPR profiles of Pt-Sn catalysts prepared by sequential impregnation that show large H_2 consumptions at high temperatures, indicating a large fraction of unalloyed Sn. If, as discussed below, the catalytic performance is a strong function of the extent of metal-metal interaction, the sequential impregnation method is not recommended.

The hydrogen and CO chemisorption data also support the conclusion that on the CIC sample there is a larger extent of Pt-Sn interaction than on the CI sample. Even though both bimetallic catalysts showed a decrease in the ability to adsorb hydrogen and CO when compared to the monometallic sample, the Pt-Sn (CIC) sample had a much lower adsorption capacity, corresponding to a higher degree of Pt-Sn interaction. A similar drop in chemisorption capacity has been observed by Cortright and Dumesic [31], who found that increasing the Sn loading resulted in a decrease in the fraction of exposed sites and a weakening of the hydrogen adsorption strength.

A.4.2 Effect of the Pt-Sn interaction on dehydrogenation activity

The extent of metal-metal interaction resulting from the different preparations greatly affects the catalytic performance. One of the most obvious effects that we observed when adding Sn was an improvement in selectivity and stability as compared to those of the monometallic Pt catalyst, even in the absence of H_2 in the feed.

These increases in stability and selectivity have been generally explained [4, 5] in terms of dilution of Pt ensembles by Sn, which greatly

reduces the activity towards reactions that require a large ensemble of Pt atoms to constitute the active sites, such as hydrogenolysis and coking. Also, the increase in selectivity of the pure Pt sample with time on stream can be explained by the same geometric arguments. The carbon deposits play the role of the inactive species that inhibit further undesired reactions. This explanation accounts for two observations on the pure Pt catalyst. Both, the selectivity and the stability of the catalyst improve as a function of time on stream as the number of large ensembles is reduced by the presence of carbon.

On the pure Pt catalyst the initial deactivation is very fast. Thus, it is difficult to measure the "true" initial activity and determine whether the initial dehydrogenation rate on Pt is higher or lower than on the bimetallic catalyst. Some authors have reported that pure Pt is initially more active but after a short time it deactivates while the bimetallic retains its activity [32]. Other authors, have reported lower activities for the monometallic catalyst. It is conceivable that, in the catalysts prepared by sequential impregnation, the fraction of unalloyed Pt that rapidly deactivates is large enough to show a much lower initial rate than those prepared by co-impregnation. For the latter, the fraction of unalloyed Pt would be less and, as a consequence, they would present a lower extent of rapid deactivation.

The TEM micrographs in Figures A.1a and A.1b show that the bimetallic catalyst contains large (250Å) particles. As stated before, we believe that these particles are a combination of several Pt-Sn alloys. Even

though the bimetallic catalysts, which have a high degree of interaction, are composed of these large particles, they still exhibited higher initial activity than the pure Pt catalyst which had much smaller particles (see Figure A.12). It is then clear that the catalytic activity that will result after the first few minutes on stream is not determined by the fraction of Pt exposed, i.e., the metal particle size, but rather by the degree of interaction between the metal and the promoter. The catalysts which have less interaction have a higher fraction of unalloyed Pt. As shown in Figure A.13, the Pt-Sn (SI) catalyst, which had the lowest extent of Pt-Sn interaction, exhibited a very high rate of deactivation, much greater than that of the Pt-Sn (CI) or (CIC) catalysts.

The notion that rapid deactivation is responsible for the apparent increase in initial activity with the addition of Sn, is supported by the results of activity studies performed in the presence of hydrogen. Figure A.14 clearly shows that the presence of hydrogen decreases the initial activity of the bimetallic catalyst. However, even though the initial activity of the catalyst decreases, the stability of the catalyst is increased because the presence of hydrogen increases the resilience to coke formation by cleaning the Pt surface (see Figure A.9). On the other hand, the results for the pure Pt catalyst show that the addition of H_2 resulted in increases in both, initial activity and stability. On this catalyst, the coke removal capacity of hydrogen overcomes the decrease in activity by adsorption site competition. As a result, the reduction in deactivation rate manifests itself as an apparent increase in initial activity.

Although the geometric modification of the Pt ensembles by addition of Sn may explain most of the observed changes in catalytic properties, there are some indications that more subtle ligand effects may also be present. For example, the shape of the white line in the Pt L_{III} XANES spectra, representing allowed transitions from occupied *2p* orbitals to unoccupied *5d* orbitals is significantly altered by addition of Sn. This modification has been explained in terms of a transfer of electrons from Sn to Pt which would reduce the number of unfilled *d* states in Pt and could have an effect on the intrinsic catalytic properties. More recently, on the basis of a comparison of several intermetallic compounds (Pt_3M, where M = Ti, Co, or Sn), Ross [33] postulated that the intermetallic interaction is predominantly through *sp* orbitals rather than through *d* orbitals. In the case of Pt_3Sn alloys, the Pt-Sn bonding would involve the occupied Sn *5p* and the unoccupied Pt *6p*. The resulting donation of *p* electrons from Sn to Pt would only have an indirect effect on the *d* states of Pt, which would shift to lower energies and become narrower. Even though the Pt-Sn interaction is relatively subtle, it can result in a decrease in the heat of CO adsorption as large as 20 kJ/mol [34]. This energy difference would cause dramatic changes in the adsorption equilibrium constants at 298 K and, consequently, in the observed adsorption capacity. For example, a simple calculation can be done assuming that, at room temperature and under the dynamic adsorption conditions, the CO surface coverage should be significantly less than 1. Accordingly, a lowering

of 20 kJ/mol in heat of adsorption represents a drop in coverage by a factor of 3.2×10^3.

If we analyze the CO adsorption data in Table A.3, we can see that although the spent catalysts were still active after 1 hour on stream, their CO adsorption capacity approached zero. As discussed above, the unalloyed Pt should be rapidly covered by coke while the Pt-Sn alloys remain more or less free of coke. We can conclude that the alloyed Pt does not adsorb significant amounts of CO and, therefore, the CO/Pt measured on the fresh catalyst is mainly due to the fraction of unalloyed Pt. The situation may be similar for the H_2 chemisorption. In fact, Verbeek and Sachtler [7] have shown that Pt-Sn alloys adsorb very little hydrogen and have ascribed this decrease to a lowering of the heat of adsorption. Recent microcalorimetry studies [5, 28, 29] showed that, even though the addition of Sn resulted in a large decrease in the saturation H or CO adsorption coverages, the heats of adsorption at zero coverage on Pt:Sn (1:1) samples were similar to those on pure Pt. However, it must be noted that these SiO_2-supported samples were prepared by sequential impregnation and, as shown above, this technique leads to a large fraction of unalloyed Pt. The adsorption that is measured under the conditions of those studies occurs primarily on the Pt sites which are not forming an alloy with Sn. For changes in the initial heats of adsorption to be seen, a large fraction of Pt would need to be alloyed with Sn. When higher Sn concentrations were used in those studies, the heats of adsorption at zero coverage decreased significantly, as expected.

This conclusion has important consequences on the meaning of turnover frequencies on Pt-Sn catalysts. For example, if we compare the TOF based on both CO and hydrogen chemisorption for the pure Pt and bimetallic Pt-Sn catalysts we observe that these values significantly increase in the order Pt < Pt-Sn(Cl) < Pt-Sn(ClC). Being dehydrogenation a structure insensitive reaction, geometric arguments alone would predict that the TOF should be about the same on the three catalysts. As explained above, it is difficult to determine the "true" initial activity because, even after only a couple of minutes under reaction conditions the catalyst is already partially deactivated. Using a H_2/hydrocarbon ratio of 6:1, Cortright and Dumesic [5] have found TOF values for a 1:1 Pt/Sn catalyst that are very similar to that of the pure Pt catalyst. However, at those high H_2/hydrocarbon ratios, the initial deactivation should be much less severe than in our case.

If, as proposed above, the initial deactivation increases with the amount of unalloyed Pt, we might expect that deactivation should follow the opposite order to that of the observed TOF, i. e., Pt > Pt-Sn(Cl) > Pt-Sn(ClC), even when the "true" initial TOF was the same on the three samples. The unalloyed Pt in the sample, due to rapid deactivation, is not the species responsible for sustained activity. However, CO and H_2 chemisorption primarily occurs on the unalloyed Pt. Therefore, for bimetallic Pt-Sn catalysts, TOF values based on CO or H_2 chemisorption have no practical significance.

A.4.3 Effect of regeneration procedures

As mentioned above, lower alkane dehydrogenation catalysts require frequent regenerations in air at high temperatures. These treatments can be detrimental to the dispersion of the metal and the interaction between the metal and promoter [35]. In this work, we have investigated the effects of such treatments on the performance of Pt-Sn/SiO_2 catalysts.

As shown in the TPRs of Figure A.3, when the SI sample was treated in air at 500°C for increasing periods of time, the H_2 consumption peak associated with Pt-Sn alloy significantly decreased while those ascribed to unalloyed Pt and unalloyed Sn increased. This segregation was also observed in the co-impregnated catalysts, which started with a much higher extent of Pt-Sn interaction. As shown in Figure A.4, the TPR peak at intermediate temperatures decreased with increasing oxidation temperature while the consumption at lower (Pt-rich) and higher (Sn-rich) temperatures gradually increased. Finally, a similar segregation phenomenon was observed when the coked catalyst was regenerated at 500°C in air. In this case, the splitting of the peaks was even more pronounced (see Figure A.5). It is interesting to consider the important differences observed in the TPR profiles of the samples of the OX (and REG) series with those that we call "fresh". One can note that, even though the fresh samples were oxidized at 400°C and then reduced at 500°C, they were clearly different from those of the OX and REG series which had an extra oxidation and reduction cycle.

TEM can also be used to support the segregation theory. Previous TEM studies on Pt-Sn (19), have found that oxidation at 550°C for 1hour resulted in severe morphological changes in the intermetallic particles. The Sn in the alloys formed an oxide and migrated to the surface of the particle. SnO_2 formed a ring around the edge of the particle in contact with the SiO_2 support. The Pt did not form an oxide but went to FCC Pt at the core of the particle. Subsequent 18hour reduction (650°C) resulted in complete recombination of the alloys. In our case, the TEM of OX500 after reduction for 1hour shows heterogeneous particles that are not present in the TEM of the fresh sample. We postulate that some recombination of the alloy may have occurred but that short reduction times after oxidation are not sufficient for total recombination of the alloy, leaving a particle with segregated Pt and Sn regions.

It is important to determine whether the proposed disruption of the alloys and metal segregation phenomena have an important effect on the catalytic properties. In fact, as demonstrated in this work, the effects may certainly be dramatic. Figure A.11 shows that the reduction / oxidation treatment resulted in a large increase in the amount of coke deposited on the Pt-Sn (CI) sample. At the same time, the alloy disruption caused by the oxidation treatment resulted in an important drop in conversion as illustrated in Figure A.17 for the co-impregnated Pt-Sn (CI) sample.

The oxidation and regeneration treatments also altered the monometallic Pt catalyst, but the effects were different from those on the Pt-

Sn samples. For example, the amount of coke deposited during 2 minutes in isobutane on the oxidized Pt catalyst was about the same as that deposited on the fresh catalyst. However, the TPO shows that on the former, the carbon deposits are more refractory. This change could be due to an increase in the Pt particle size, which are typically observed when Pt is heated in oxygen at high temperatures [36]. However, as shown in Table A.3 the change in chemisorption capacity was not very pronounced. It is possible that even though the overall metallic area did not change much upon the reduction / oxidation cycle, the type of exposed crystallographic planes changed, causing a change in the coking process. Studies on model Pt catalysts [37] have shown that graphitic carbon deposition occurs much more readily on flat terraces than on edges and corners. Therefore, if the reduction / oxidation cycle results in an increase in the density of fat planes, we might expect an increase in deposition of graphitic carbon.

As opposed to the reduced / oxidized samples, the regenerated monometallic Pt catalysts showed less coke than the corresponding fresh samples. This result can again be explained in terms of the presence of refractory carbon deposits left on the surface after the regeneration which can act as diluting species breaking up Pt ensembles and reducing the rate of coke formation.

The observed trend in coke formation on the monometallic catalysts was paralleled by that of the rates of deactivation. The oxidized monometallic samples, which exhibited a high rate of coke formation, showed a much

higher rate of deactivation than the fresh and regenerated catalysts and a more pronounced variation in selectivity. Also, the initial selectivity was lower for the OX500 sample than for the other two samples, which is consistent with the presence of flat Pt planes, more active for hydrogenolysis and coke formation. This sample rapidly formed coke so it deactivated and increased selectivity more rapidly than the other two samples.

The activity studies showed that both, the oxidation and regeneration of the bimetallic Pt-Sn catalysts at 500°C, resulted in a great loss of activity and selectivity. The decrease in activity can be due to segregation or partial destruction of the Pt-Sn alloy which results in an increase in the deactivation due to coking. Comparison of the TPO profiles for the fresh and OX500 Pt-Sn (Cl) with that for the fresh and OX500 Pt samples show that after oxidation at 500°C a high temperature carbon peak forms as in the case of OX500 Pt. This could indicate that some of the alloy has been destroyed leaving behind patches of unalloyed Pt, on which the formation of the graphitic carbon is more favorable. The OX500 and REG500 bimetallic Pt-Sn (Cl) samples still form less carbon than the pure Pt sample, but almost four times the amount found on the fresh bimetallic sample. Comparison of Figures A.16 and A.17 shows that the REG500 bimetallic sample Pt-Sn (Cl) retained more of its initial activity than the OX500 sample. This difference can be explained by the same argument used above for the monometallic catalyst, the carbon not removed during the regeneration hinders the coke formation on the unalloyed Pt regions.

To explain the changes in catalytic activities and properties experienced by the Pt-Sn (Cl) and Pt-Sn (ClC) catalysts after reduction / oxidation cycles and regeneration at 500°C we may not need to postulate the complete segregation of the metals in separate particles. Based on the surface enrichment model observed on the Pt-Sn and the Pt-Rh alloys and the TEM evidence of Chojnacki and Schmidt (19), we can speculate that, after reduction and before the treatment in air, the particle is composed of a Pt-Sn alloy. Under oxidizing conditions at high temperatures, the Sn forms an oxide and, at the expense of the subsurface layer, the exterior becomes rich in Sn. The Pt, which does not form an oxide, is metallic and becomes the core of the particle. Reduction at high temperatures results in the destruction of the oxide and possibly redistribution of the Sn, opening patches of pure Pt. Although the thermodynamically most stable configuration would be the complete recombination of the alloy [7, 19], short reduction times do not allow for this to occur. Consequently, after reduction, the bimetallic particles have become heterogeneous, with Sn-rich regions interdispersed with Pt-rich regions. It is even possible that pure Pt ensembles are present allowing for the formation of more refractory carbon to form on the surface under subsequent exposure to reaction conditions. The dramatic consequences of the reduction / oxidation treatments on the catalytic properties of silica-supported Pt-Sn catalysts demonstrated in this work should be taken into account when the regenerability of a dehydrogenation catalyst is considered for practical applications.

A.5 Conclusions

The addition of Sn can significantly improve the catalytic behavior of Pt/SiO_2 catalysts for reactions such as the dehydrogenation of isobutane. The results of this work have shown that the promoting effect of Sn strongly depends on the method employed in the preparation. Catalysts prepared by co-impregnation, particularly when the solvent is an aqueous solution containing HCl, result in a high extent of Pt-Sn interaction. By contrast, sequential impregnation results in a large fraction of unalloyed Pt. When H_2 is not added to the feed during the dehydrogenation reaction, this fraction of unalloyed Pt rapidly deactivates due to carbon deposition. In choosing a preparation method, it is important to maximize the degree of Pt-Sn interaction rather than maximize the metal dispersion because it is the fraction of alloyed Pt that is responsible for the sustained activity.

This work has also shown that high temperature treatments in air or previously reduced Pt-Sn samples are detrimental for the catalytic properties. After these treatments, the rate of deactivation due to Pt-Sn segregation resulting in disruption of the alloy structure is responsible for this effect. Reduction after oxidation results in some recombination of the alloy, but long times and high temperatures are necessary for the complete recombination.

Finally, CO and hydrogen adsorption does not take place to a great extent on the Pt-Sn alloys, the small amount measured occurs mostly on unalloyed Pt. Since, in the absence of added H_2, this fraction of the catalyst is rapidly deactivated, TOF values based on H/Pt or CO/Pt values have no

practical significance. Therefore, for the rest of the experiments performed in this study, activity will be reported and compared only in terms of conversion, not in terms of TOF.

A.6 References

1. Balakrishnan K., and Schwank J., *J. Catal.*, **127**, 287 (1991).
2. Yarusov, I. B., Zatolokina, E. V., Shitova, N. V., Belyi, A. S., and N. M. Ostrovskii, *Catalysis Today*, **13**, 655 (1992).
3. Yang W., Lin L., Fan Y., J. Zang, *Catal. Lett.*, **12**, 267 (1992).
4. Jin, L. Y., Appl. Catal., **72**, 33 (1991).
5. Wilhem, F, US Patent 3998900 (1976).
6. Dautzenberg F. M., Helle J. N., Biloen P., and Sachtler W. M. H., *J. Catal.*, **63**, 119 (1980)
7. Cortright, R. D., and Dumesic, J. A., *J. Catal.*, **148**, 771 (1994)
8. Meitzner, G., Via, G. H., Lytle, F. W., Fung, S. C., and Sinfelt, J. H., *J. Phys. Chem,.* **92**, 2925 (1988)
9. Verbeek, H., and Sachtler, W. M. H., *J. Catal.*, **42**, 257 (1976)
10. Paffett, M. T., Gebhard, S., Windham, R. G., Koel, B. E., *Surf. Sci.*, **223**, 449 (1989)
11. Xu C., Koel, B. E., and Paffett, M. T., *Langmuir*, **10**, 166 (1994)
12. Antos, G. J., U. S. Pat. 4,216,346 (1980).
13. Olbrich M. E., McKay D. L., and Montgomery D. P., U. S. Pat. 4,926,005 (1986).
14. Catalytica Studies Division, in "Catalytic Dehydrogenation and Oxidative Dehydrogenation" (1991), Cat. Stud. No. 4190 DH
15. Chojnacki, T. P., and Schmidt, L. D., *J. Catal.*, **115**, 473 (1989)
16. Wang, T., and Schmidt, L. D., *J. Catal.*, **70**, 187 (1981)
17. Barias, O. A., Holmen, A., and Blekkan, E., *Catalysis Today,* **24**, 361 (1995)
18. Chen, M., and Schmidt, L. D., *J. Catal.*, **56**, 198 (1979)
19. Foger, K., and Jaeger, H., *J. Catal.*, **70**, 53 (1981)
20. Sinfelt, J. H., and Via, G. H., *J. Catal.*, **56**, 1 (1979)
21. Chojnacki, T. P., and Schmidt, L. D. *J Catal.*, **129**, 473 (1991)
22. Nuñez G. M. and Rouco A. J., *J. Catal.*, **111**, 41 (1988)
23. Resasco D. E., Marcus B. K., Huang C. S., and Durante V. A., *J. Catal.* **146**, 40 (1994)
24. Balakrishnan K., and Schwank J., *J. Catal.*, **127**, 287 (1991)
25. Afonso J. C., Aranda D. A. G., Schmal D., Frety R., *Fuel Proc. Tech.*, **42**, 3 (1995)

26. Srinivasan R. and Davis B. H., *Platinum Metals Rev.*, **36**, 151 (1992)
27. Li, Y. X., Klabunde, K. J., and Davis, B. H., *J. Catal.*, **128**, 1 (1991)
28. Lieske, H and Volter, J., *J. Catal.* **90**, 46 (1984)
29. Zhou, Y. Davis S. M., *Catal. Lett.*, **15**, 51 (1992)
30. Chang T.-H., Leu F. C., *J. Chin. Inst. Chem. Eng.*, **26**, 393 (1995)
31. Cortright, R. D., and Dumesic, J. A., *Appl. Catal. A,* **12**, 101 (1995)
32. Cortright, R. D., and Dumesic, J. A., *J. Catal.,* **157**, 576 (1995)
33. Ross, P. N., *J. Vac. Sci. Tech.,* **10**, 2546 (1992)
34. Haner A. H., Ross, P. N., Bardi U., and Atrei A., *J. Vac. Sci. Tech.,* **10**, 2719 (1992)
35. Fan Y., Xu Z., Zang J., and Lin L., in "Catalyst Deactivation 1991", Elsevier Sci. Publ., *Stud. Surf. Sci. Catal.* **68**, 683 (1991)
36. Chen, M., and Schmidt, L. D., *J. Catal.*, **55**, 348 (1978)
37. Somorjai G. A., and Blakely D. W. , *Nature*, **258**, 580 (1975)

APPENDIX B

INTERFERENCE PHENOMENA in the EXAFS SPECTRA of Pt-Sn BIMETALLIC CATALYSTS

B.1 Introduction

The ability of a promoter to alter the catalytic properties of supported transition metal catalysts has been known for decades [1]. The addition of promoters such as Re, Sn, and Ir to Pt/Al_2O_3 reforming catalysts has a profound effect on the stability of the catalyst by substantially reducing carbon deposition [2-4]. More recently, the interest for bimetallic catalysts has grown further [5, 6], especially for Pt catalysts promoted with Sn. These catalysts do not require complex activation procedures, which makes them the preferred catalyst for continuous regeneration processes [7, 8]. They have also proven to be beneficial in many other reactions involving hydrocarbons such as dehydrogenation of lower alkanes [9, 10].

Recent studies have shown that the preparation method employed can have a large effect on the degree of Pt-Sn interaction [Appendix A]. Catalysts prepared by co-impregnation of Pt and Sn in an aqueous solution of HCl resulted in a large fraction of the Pt alloyed with Sn. When co-impregnation was performed using only water as the solvent, the degree of Pt-Sn interaction decreased and some unalloyed Pt was observed. Finally, the catalysts prepared by sequential impregnation of the two metals resulted in minimal alloy formation with large amounts of unalloyed Pt and Sn. Studies have also shown that the degree of Pt-Sn interaction has a significant effect

on the activity and stability of the catalyst. When the fraction of Pt alloyed with Sn increased, the stability of the dehydrogenation catalyst increased, due to decreased carbon deposition. These results indicate that alloy formation is necessary for the production of an effective catalyst, and that maximizing the degree of interaction should be of primary importance when choosing a preparation method.

A variety of characterization techniques have been employed to unveil the structural details of these bimetallic systems. Among them, Extended X-ray Absorption Fine Structure (EXAFS) has been widely recognized as a powerful tool since it can be used to determine the local environment around metal atoms and, consequently, demonstrate the existence of bimetallic clusters. However, in the case of Pt-Sn bimetallic catalysts, the analysis and the detailed interpretation of EXAFS spectra are very complex [11]. The main difficulty in using EXAFS to characterize the formation of Pt-Sn alloys arises from the fact that Pt-Pt and Pt-Sn distances are not sufficiently different, which greatly complicates the analysis. Despite the very similar bond lengths of the components (2.77 and 2.75), the Fourier transforms of Pt-Sn EXAFS spectra reported in the literature frequently show an unexpected short-distance peak around 2.1-2.2 Å. The appearance of this peak has perplexed some authors [8], and its origin has not yet been determined. The results of this study are intended to explain the observed EXAFS spectra and to determine the local structure of the metallic phase in a typical Pt-Sn/SiO_2 catalyst.

B.2 Experimental

The details about the catalyst preparation method and characterization techniques can be found in Chapter 2. The loading of Pt was 1 wt% with a molar ratio of Pt:Sn of 1:1. The raw EXAFS data was extracted from the absorption spectra and normalized by dividing the absorption spectra by the height of the edge jump. Pre-edge background subtraction was done with either a power series curve fit. Post-edge background subtraction was done with a cubic spline with 7 knots, starting 50 eV past the edge jump. To avoid overemphasizing the low energy region [12], the χ data for the reduced samples, which contain Pt or Sn in the first coordination sphere, were k^3-weighted. Theoretical standards were generated by the program FEFF from the University of Washington [13-15] for metallic Pt and several Pt-Sn alloys. In all cases, cluster sizes of 8 Å were used to determine the possible scattering paths. These paths were subsequently used to fit the experimental EXAFS data. In the fitting, the bond distances, coordination numbers, and Debye-Waller factors for each atomic pair were allowed to vary independently, together with the parameters E_o and S_o^2. The atomic pairs considered were Pt-Pt in a Pt cluster, and Pt-Sn and Pt-Pt in the alloys.

B.3 Results and Discussion

The k^3-weighted EXAFS spectrum taken at the Pt L_{III} edge and the corresponding Fourier Transform (FT) are shown in Figures B.1a and B.1b, respectively. The FT plot, which has not yet been corrected for the amplitude

and phase shift, shows the presence of two main peaks, one at approximately 2.15 Å and the other at 2.75 Å. Similar radial distributions were obtained on several other Pt-Sn/SiO_2 catalysts prepared in our laboratory and have been previously observed by others authors [8,16]. This spectrum exhibits two features that have not been previously explained. The first is the appearance of a short-distance peak at 2.15 Å, which is too long for any metallic coordination. The second feature is the position of the main peak at 2.75 Å, which appears slightly shifted from the typical uncorrected Pt-Pt distance (2.62 -2.68 Å).

Comparison of the uncorrected Pt-Sn/SiO_2 FT with the uncorrected pure Pt FT shows that the short-distance peak coincides with the position of a satellite peak from the Pt-Pt bond distance. However, inspection of the data after correction for the amplitude and phase shift according to the method proposed by Marques et al. [17], indicates that the two peaks do not have the same origin. Figure B.2 includes the corrected Fourier transforms for the experimental data of the Pt foil and Pt-Sn catalyst as well as the theoretical data for a Pt cluster. It is clear that the correction of the FT for the two pure Pt systems resulted in complete elimination of the satellite peak at 2.1 Å, while for the Pt-Sn catalyst, the short-distance peak was still present.

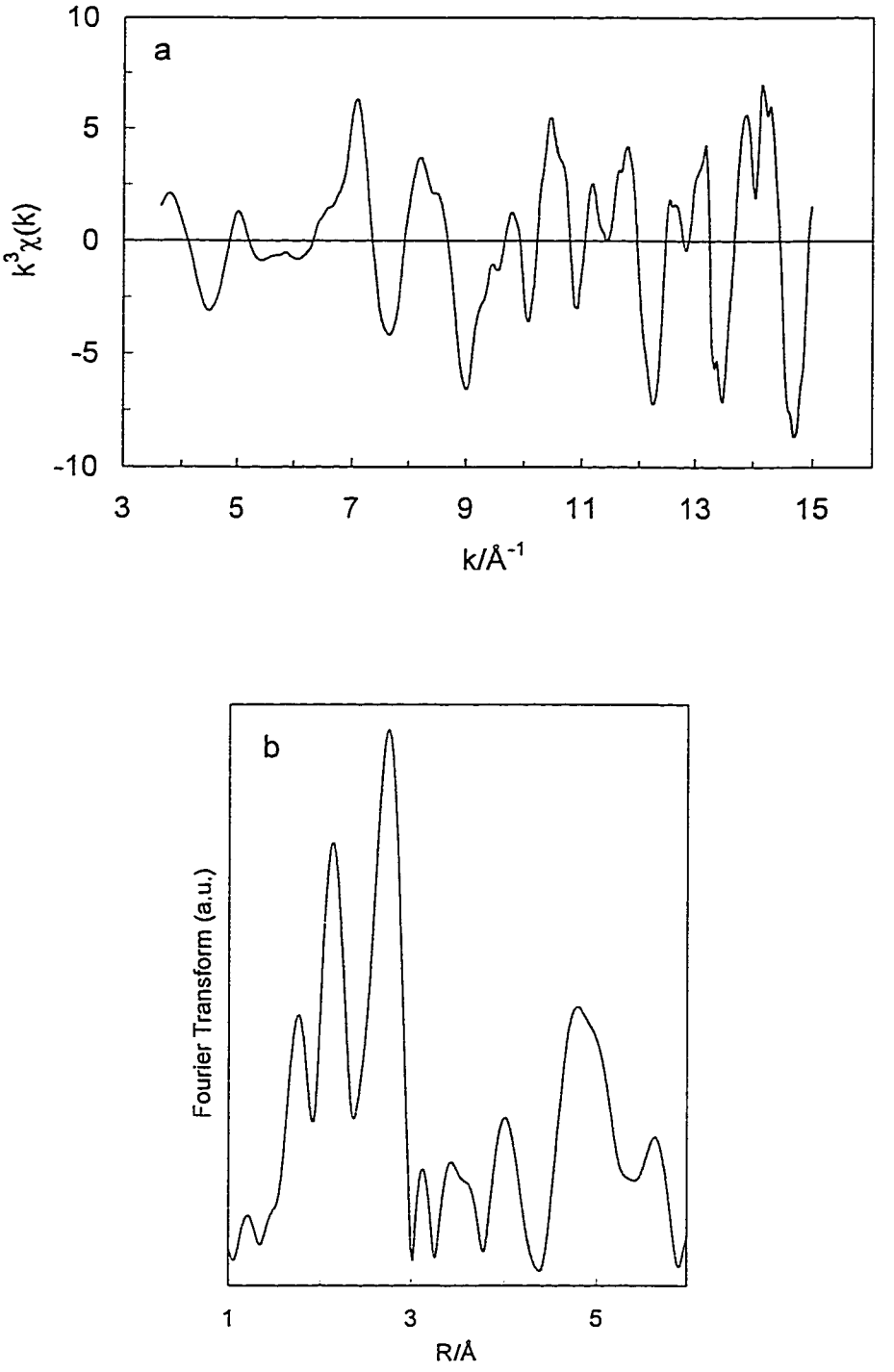

Figure B.1: (a) EXAFS spectrum of the bimetallic Pt-Sn/SiO_2 catalyst. k^3-weighted, Δk = 3.6-15 Å^{-1}. (b) Fourier transform corresponding to the EXAFS spectrum of the bimetallic Pt-Sn/SiO_2 catalyst.

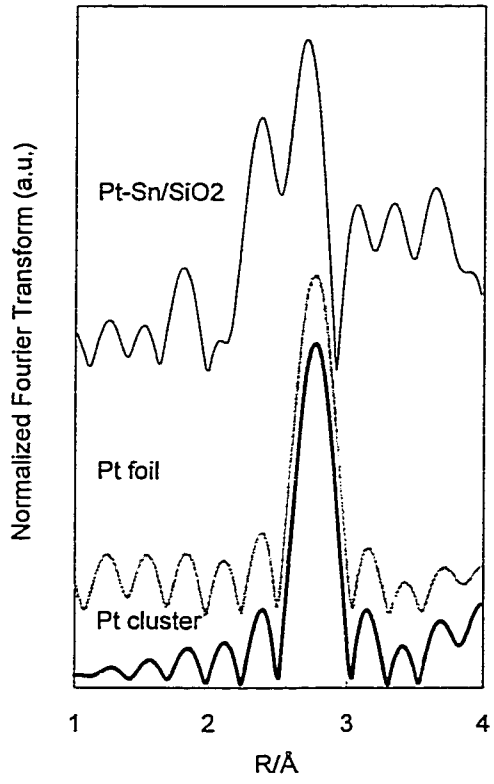

Figure B.2: Amplitude and phase shift corrected Fourier transforms for the Pt-Sn/SiO_2 catalyst, the standard Pt foil, and the theoretical Pt cluster.

In addition, new features at long distances appeared in the corrected FT for the bimetallic catalyst. These features do not correspond to real distances in the system but are probably generated by applying phase and amplitude corrections that are only correct for Pt backscattering atoms. Therefore, these corrections could distort the spectrum when applied to backscattering atoms other than Pt. This analysis indicates that Pt atoms are not the only constituents of the environment around Pt in the bimetallic catalyst. Rather, two types of backscattering atoms can be present in the first

coordination sphere. It should be noted that EXAFS represents the sum of all possible environments in which Pt may exist, therefore, some of the Pt may be unalloyed and some in the form of Pt-Sn alloys.

It has been proposed that the short-distance peak observed in the FT of Pt-Sn catalysts corresponds to the presence of oxidized species and/or Pt species coordinated to chlorine left on the catalyst from the preparation [8]. However, the results of the XANES studies (not shown) performed on the bimetallic catalyst indicate that these species are not present. It is well known that if Pt were oxidized or coordinated to electron withdrawing elements such as Cl, the intensity of the white line would have increased [18]. Contrarily, the addition of Sn resulted in a decrease in the intensity of the white line, in agreement with previous observations [16]. These results demonstrate that Pt is not coordinated to oxygen or chlorine and eliminates the possibility that these species are responsible for the short distance peak.

In order to elucidate the origin of the 2.15 Å-peak, a theoretical analysis of the structure of Pt-Sn alloys was performed using the FEFF software package from the University of Washington [13-15]. Clusters up to a maximum radial distance of 8 Å were generated for pure Pt and the most common Pt-Sn alloys. The corresponding radial distributions obtained from the theoretical EXAFS functions showed that all of the Pt-Sn alloys, except for Pt_2Sn_3, exhibited a single peak between 2.5 and 2.74 Å. The Pt_2Sn_3 alloy had two peaks; however, the first peak was around 2.40 Å, which is significantly different from the position of the short-distance peak at 2.15 Å. Therefore, it

is concluded that considering Pt-Sn alloys alone can not satisfactorily fit the experimental data. Comparison of the theoretical FT for the Pt and Pt-Sn alloys showed that the main peak of the alloys is very near that of the pure Pt cluster. Modeling the system with EXAFS functions for Pt and Pt-Sn alloys independently will not account for the appearance of a peak at 2.15 Å and, would result in unreasonable Pt-Pt distances. Therefore, another technique should be used in order obtain a good fit.

In previous XRD studies [16], it was reported that PtSn and Pt_3Sn are the most abundant alloys in Pt-Sn bimetallic catalysts. Hence in the following analysis, these will be the primary alloys considered. By adding the individual theoretical EXAFS functions of the pure Pt cluster and the PtSn alloy, a new EXAFS spectrum was obtained (Pt+PtSn). Similarly, the sum of the pure Pt cluster and the Pt_3Sn alloy generated a new spectrum (Pt+Pt_3Sn). The radial distribution functions were obtained by performing Fourier analysis on the (Pt+PtSn) and (Pt+Pt_3Sn) EXAFS spectra, and the FT for both are shown in Figures B.3 and B.4, respectively. An interesting result was obtained with the addition of the individual Pt and PtSn EXAFS functions. As mentioned before, each individual contribution only exhibited a single peak at positions not largely different from each other. However, the combination of the two resulted in two main peaks at 2.18 and 2.78 Å. Qualitatively, this theoretical FT and the experimental FT obtained from the bimetallic Pt-Sn/SiO_2 catalyst are very similar. Moreover, the positions of the main peaks are nearly the same.

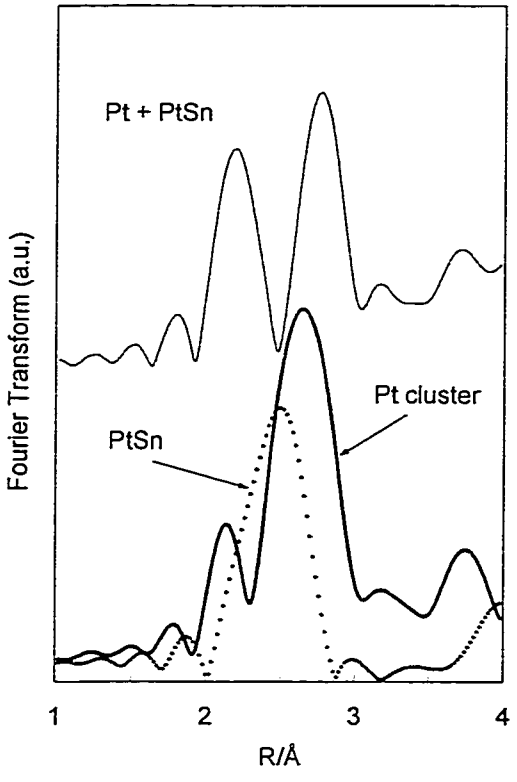

Figure B.3: Fourier transform of the combined Pt + PtSn EXAFS function compared to the Fourier transforms of the individual components derived from the theoretical EXAFS functions.

In contrast, when the individual EXAFS functions of pure Pt and the Pt_3Sn alloy were added, a Fourier transform with a single main peak was obtained. Similar results were obtained when the individual EXAFS functions for pure Pt and the other Pt-Sn alloy phases were added together. From these results it can be concluded that only the combination of Pt and specific alloy structures, such as the PtSn alloy, gives rise to the appearance of the short-distance peak at about 2.15 Å and the shift of the main peak to near 2.75 Å.

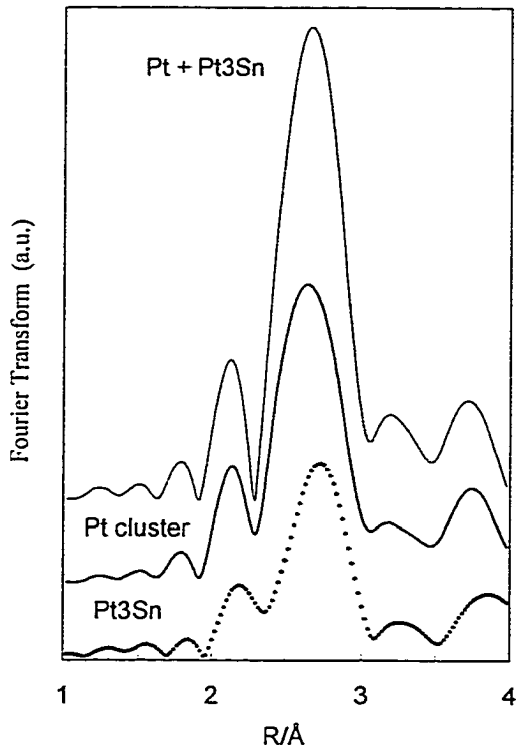

Figure B.4: Fourier transform of the combined Pt + Pt_3Sn EXAFS function compared to the Fourier transforms of the individual components derived from the theoretical EXAFS functions.

To obtain a more detailed picture of the origin of these peaks, an inverse Fourier transform was applied over a restricted range of R, 1.5-3.5 Å, isolating the EXAFS contribution of the first coordination sphere of Pt. The resultant EXAFS contribution shown in Figure B.5 for the combined Pt + PtSn EXAFS function is very different from those of the individual components, pure Pt clusters and PtSn alloy. Due to a significant phase difference between the two components, an interference occurs generating nodes in the envelope curve that are not present in the individual EXAFS functions. Although the presence of other alloy phases cannot be rule out, it is important

to note that this interference was not observed for the other theoretical Pt-Sn clusters we analyzed.

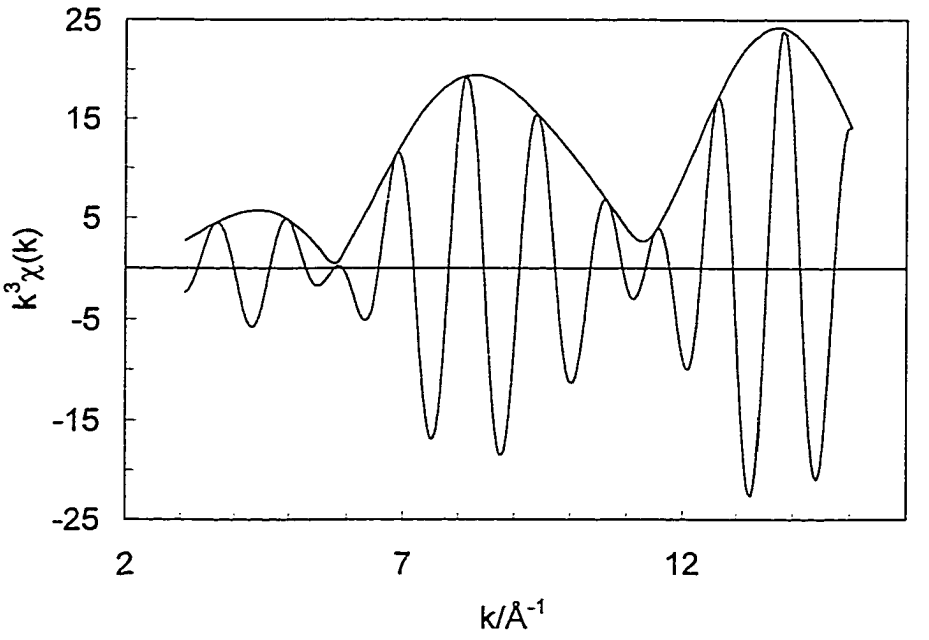

Figure B.5: EXAFS contribution and amplitude envelope of the first coordination sphere of Pt corresponding to the addition of Pt cluster and Pt-Sn alloy. Range of R, 1.5-3.5 Å.

These results suggest that the appearance of the short-distance peak and the shift of the main peak to longer distances are an indication of the simultaneous presence of unalloyed Pt and the alloy phase PtSn in the catalysts. The origin of the short distance peak can then be ascribed to the interference phenomenon discussed above and is not due to the existence of a true metallic distance Pt-X at 2.15 Å. The fact that a combination of the individual pure Pt and Pt-Sn EXAFS functions were required to qualitatively explain the experimental EXAFS data obtained for the bimetallic sample

indicates that the catalyst's metallic fraction is a mixture of Pt clusters and a PtSn alloy phases. From these results alone it is not possible to discriminate the case in which the catalyst is composed of pure Pt particles and PtSn particles from that in which the particles contain both Pt and PtSn phases.

To further verify that the combination of Pt clusters and PtSn alloy accurately represents the real Pt-Sn/SiO_2 catalyst, the same phase shift and amplitude correction was done on the theoretical (Pt+PtSn) EXAFS function as was performed on the experimental EXAFS data. The result of this correction on both the theoretical and experimental functions is illustrated in Figure B.6. In both cases the short-distance peak is clearly seen as well as the long distance features resulting from the distortion mentioned above.

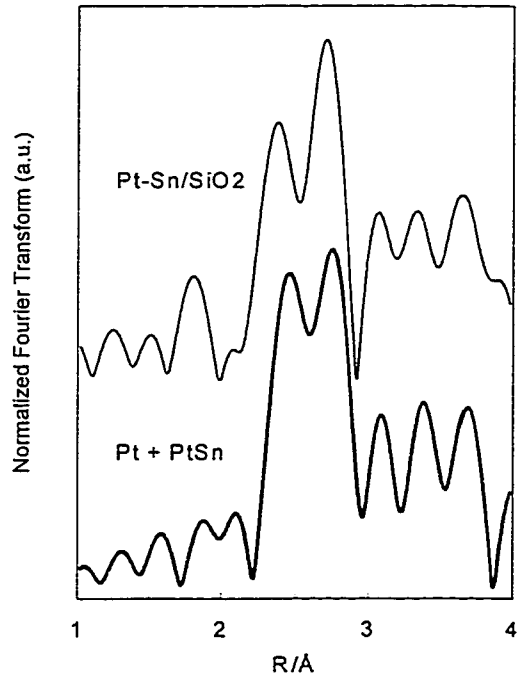

Figure B.6: Amplitude and phase shift corrected Fourier transforms for the combined Pt + PtSn and for the Pt-Sn/SiO_2 catalyst.

In order to obtain a more quantitative description of the metallic phases in the catalyst, the experimental data was fitted using the FEFFIT program [13-15]. Poor fits were obtained for the bimetallic Pt-Sn/SiO_2 catalyst when only a single metallic phase (i.e. pure Pt or Pt-Sn alloys) was used to fit the data. However, when both Pt clusters and PtSn alloy were used simultaneously, the quality of the fit was excellent. Figures B.7a and B.7b show the results of the best fit in k-space and R-space, respectively.

The structural parameters resulting from this fit are summarized in Table B.1. The computed interatomic distances for both PtSn alloy and Pt cluster are slightly lower than the corresponding theoretical values; however, small distance contraction for small metallic particles has been previously reported and discussed in the literature [19,20].

Table B.1 shows that the analysis of the EXAFS data resulted in a total Pt coordination number of 2.5 for the alloy. Using the pure PtSn alloy as a model, it is possible to approximate the individual contribution of the Pt-Pt and Pt-Sn bonds to the total coordination number calculated. In the first shell of pure PtSn alloy, each Pt is coordinated to two Pt atoms and six Sn atoms (1), or 25 % of the bonds correspond to Pt-Pt bonds and the remaining 75 % to Pt-Sn bonds. Thus, the coordination number of 2.5 for the alloy would correspond to 0.6 Pt-Pt and 1.9 Pt-Sn bonds.

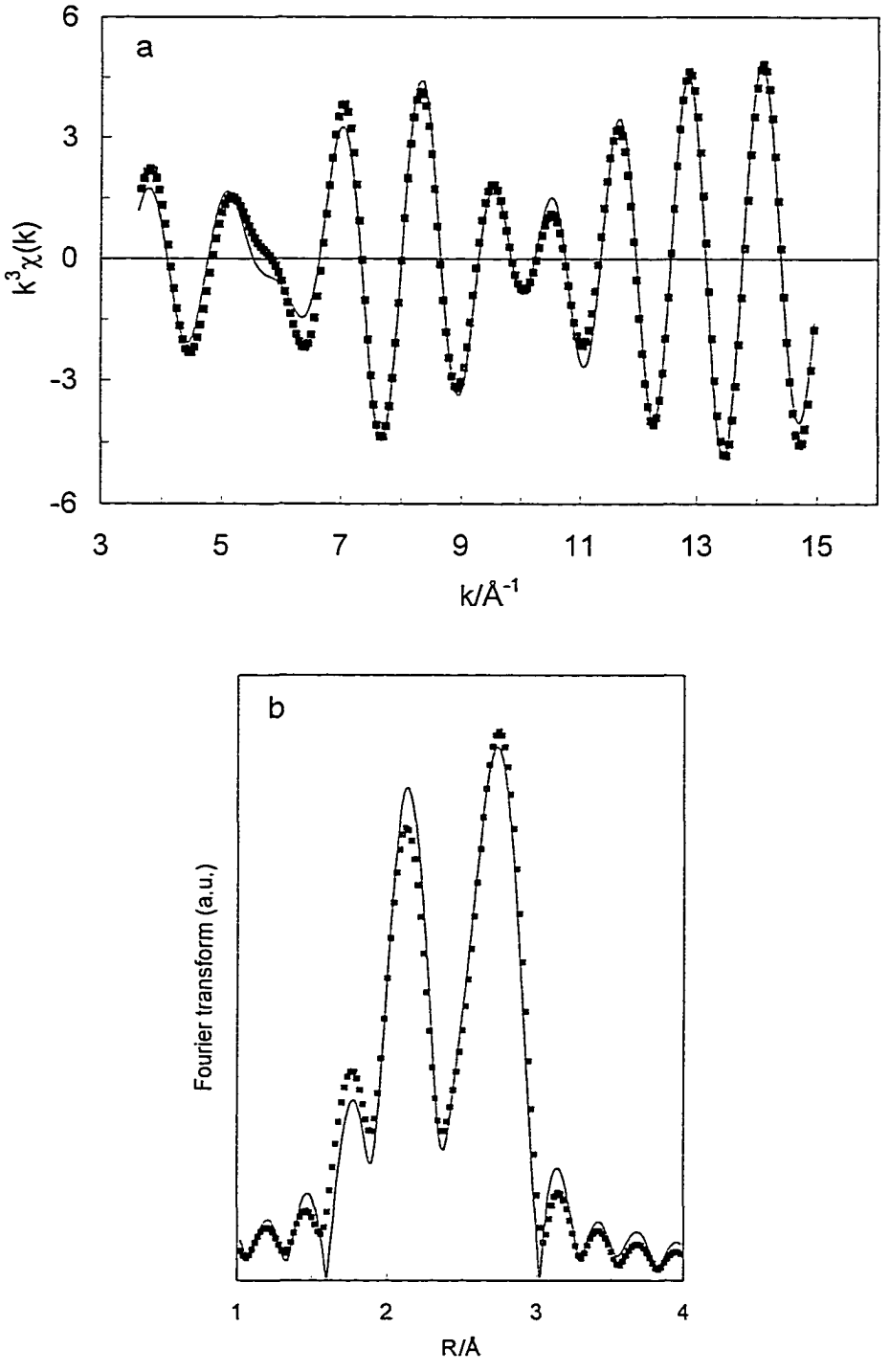

Figure B.7: (a) Fit in k-space for the Pt-Sn/SiO_2 catalyst. Experimental (square) and modeled (full line) EXAFS contributions around Pt. (b) Fit in R-space for the Pt-Sn/SiO_2 catalyst. Experimental (square) and modeled (full line) radial distributions around Pt.

Catalyst	Fitted Experimental Data			Theoretical Data		
	Pt-Sn (alloy)		Pt Cluster	Pt-Sn (alloy)		Pt Cluster
$Pt\text{-}Sn/SiO_2$	Pt-Pt	Pt-Sn	Pt-Pt	Pt-Pt	Pt-Sn	Pt-Pt
N (± 0.5)	2.5		7.2	2	6	12
R (Å) (± 0.01)	2.63	2.65	2.74	2.77	2.75	2.77
σ^2 $(Å)^2$ (± 0.001)	0.005		0.005	----		----
ΔE_o (eV) (± 1.0)	0.3		0.3	----		----

Table B.1: Structural parameters determined from EXAFS analysis of the bimetallic $Pt\text{-}Sn/SiO_2$ catalyst.

Using the calculated coordination numbers shown in Table B.1 and the known coordination numbers for the perfect Pt and PtSn alloy crystals, an estimation of the fraction of alloyed and unalloyed Pt can be obtained. Assuming that the pure Pt and bimetallic alloy phases have similar degree of dispersion, the following expression can be used to estimate the fraction of Pt in the alloy:

$$\frac{(N_a/N^o_a)}{(N_p/N^o_p) + (N_a/N^o_a)} \qquad \text{(B-1)}$$

where N_a and N_p are the experimental coordination numbers of Pt in the alloy and in the Pt cluster, respectively, while N^o_p and N^o_a are the corresponding numbers for the perfect Pt (N^o_p = 12) and PtSn alloy (N^o_a = 8), respectively. Accordingly, for the Pt-Sn catalyst used in this work, the fraction of Pt in the

alloy would be close to 35 %. It must be noted that this is a minimum limit since this estimation does not take into account that the alloy may be forming a thin layer over a Pt core [21]. In a structure like that, the fraction of alloy exposed to the surface would be much larger than that of the unalloyed Pt, which would greatly reduce the coordination number of the alloy. The large fraction of PtSn alloys present is in good agreement with previous TPR studies performed on the same bimetallic catalyst. The results of the TPR analysis indicated the presence of both a reduction peak at 200°C due to the PtSn alloy and one at much lower temperatures (125°C) due to reduction of unalloyed Pt [Appendix A].

Finally, it must be noted that although other combinations of Pt-Sn pairs could also produce the interference phenomenon, the best fits were obtained with the pure Pt cluster and PtSn alloy. For instance, the addition of the individual EXAFS functions of the two bimetallic alloys PtSn and Pt_3Sn also produced two peaks in the R-space. However, the quality of the fit was much lower than that obtained with Pt and PtSn. Moreover, when three contributions were considered, (Pt, PtSn and Pt_3Sn), the quality of the fit was not improved. In all cases, the Pt_3Sn fraction incorporated by the optimization program in the fit was very low and it could be neglected.

B.4 Conclusions

The results of this work have demonstrated that interference between the EXAFS data coming from different pairs of atoms with comparable

distances may result in the appearance of peaks, which would not appear if the individual contributions were studied separately. These effects have been shown here for the case of the Pt-Sn system but may be a general phenomenon present in other bimetallic systems. For example, in a recent work [22] done on Pt-Pd bimetallic catalysts, a short-distance peak near the main Pt-Pt peak was observed in the FT despite the fact that the Pt-Pd distance is almost the same as that of Pt-Pt. A similar analysis might indicate the presence of the same interference shown in this work. The results of this study also show that EXAFS is a powerful technique that can be used to identify the presence of bimetallic alloys. In addition, fitting of the experimental data using theoretical references provides the opportunity to obtain an estimate of the fraction of alloy present in bimetallic catalysts. Therefore, analysis of EXAFS data obtained under reaction conditions can provide a quantitative picture of the structure of the catalyst during the reaction and a better understanding of the catalytic properties of the material.

B.5 References

1. Sinfelt, J.H., in "Bimetallic Catalysis: Discoveries, concepts, applications", New York, J. Wiley, (1983).
2. Adkins, S. R., and Davis, B. H., *J. Catal.*, **89**, 371 (1984).
3. Querini, C. A., and Fung, S. C., *J. Catal.*, **141**, 389 (1993).
4. Sparks, D. E., Srinivasan, R., and Davis, B. H., *J. Molecular Catal.*, **88**, 359 (1994).
5. Cortright, R. D., and Dumesic, J. A., *J. Catal.*, **148**, 771 (1994).
6. Kappenstein, C., Saouabe, M., Guerin, M, Marecot, P., Uszurat, I, and Paal, Z., *Catal. Lett.*, **31**, 9 (1995).
7. Li, Y. X., Klabunde, K. J., and Davis, B. H., *J. Catal.*, **128**, 1 (1991).

8. Srinivasan, R, and Davis, B., *Platinum Metals Review*, **36**, 151 (1992).
9. Antos, G. J., U.S. Patent 4,216,346, 1980.
10. Olbrich, M. E., McKay, D. L., and Montgomery, D. P., U.S. Patent 4,926,005, 1986.
11. Wang, H. and Haller, G. L., Proc. 15th North Amer. Meet. Catal. Society, Chicago, May 1997, paper C16, p 73.
12. Sayers, D. E. and Bunker, B. A., in "X-ray Absorption: Principles, Applications, Techniques of EXAFS, SEXAFS, and XANES". (D. Koningsberger and R. Prins, editors), J. Wiley, 1988, p. 211
13. Rehr, J. J., Zabinsky, S. I. and Albers, R. C., *Phys. Rev. Lett.*, 69, 3397 (1992).
14. Rehr, J. J., Mustre de Leon, J., Zabinsky, S. I. and Albers, R. C., *J. Amer. Chem. Soc.*, **113**, 5135 (1991).
15. Mustre de Leon, J., Rehr, J. J., Zabinsky, S. I. and Albers, R. C., *Phys. Rev.*, **B44**, 4146 (1991).
16. Meitzner, G., Via, G. H., Lytle, F. W., Fung, S. C., and Sinfelt, J. H., *J. Phys. Chem.*, **92**, 2925 (1988).
17. Marques, E.C., Sandstroem, D.R., Lytle, F.W. and Greegor, R.B.J., *J. Chem. Phys.*, **77**, 1027 (1982).
18. Lytle, F.W., Wei, P.S.P., Gregor, R.B., Via, G.H. and Sinfelt, J.H., *J. Chem. Phys.*, **70**, 4849 (1979).
19. Guyot-Sionnest, N.S., Villain, F., Bazin, D., Dexpert, H., LePeltier, F., Lynch, J. and Bournonville, J.P., *Catal. Lett.*, **8**, 283 (1991).
20. Borgna, A., LeNormand, F., Garetto, T., Apesteguía C. R. and Moraweck, B., *Catal. Lett.*, **13**, 175 (1992).
21. Chojnacki, T.P. and Schmidt, L.D., *J. Catal.*, **129**, 413 (1991).
22. Bazin, D., Triconnet, A. and Moreaux, P., Nuclear Instruments and Methods in Physics Research, **B 97**, 42 (1995).

IMAGE EVALUATION TEST TARGET (QA-3)

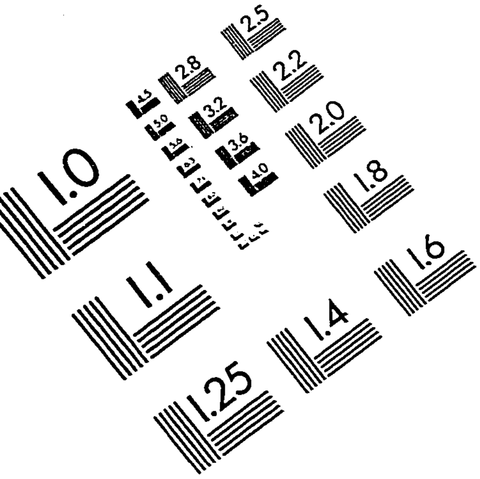

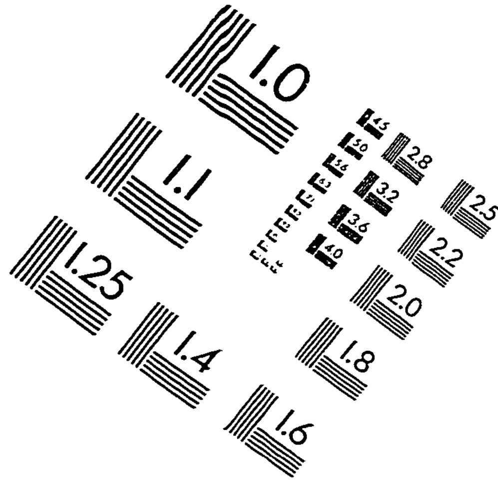

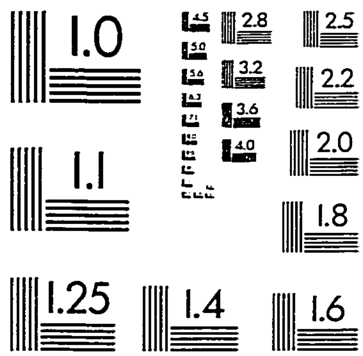

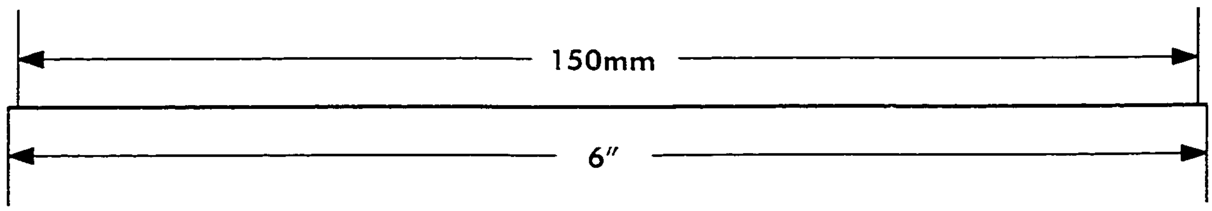

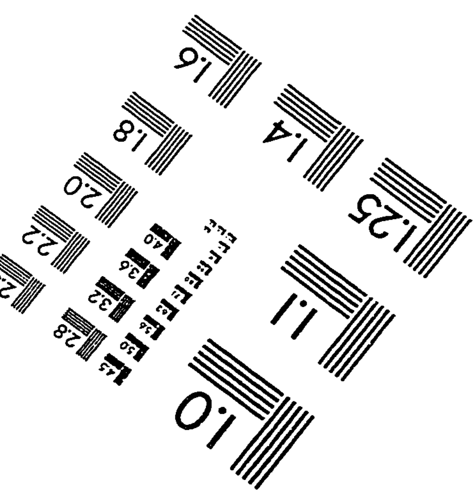

APPLIED IMAGE . Inc
1653 East Main Street
Rochester, NY 14609 USA
Phone: 716/482-0300
Fax: 716/288-5989